The Role of the Fibronectin Synergy Site in Skin Wound Healing

Irene Gimeno Lluch

Directores de tesi: Mercedes Costell Rosselló i María Benito

FACULTAT DE CIÈNCIES BIOLÒGIQUES

Departament de Bioquímica i Biologia Molecular- Institut Universitari BioTECMED

Programa de Doctorat en Biomedicina i Biotecnologia

València, Juliol 2022

A ma mare i a mon pare, per tant

Agraïments

Més important, si cap, que el propi contingut de la tesi, és la gent que ha format part d'ella al llarg d'aquests 5 anys. En aquest apartat tractaré de donar les gràcies a totes aquelles persones que han disfrutat i patit amb mi, a parts iguals, aquesta tesi. Espere que hem pugueu perdonar si m´oblide d´alguna.

De les primeres etapes al laboratori en Burjassot, no puc oblidar-me de les meues companyes i companys del departament. Joaquín, Olga, Paco i Juanjo. La meua menció especial és, com no, per a Sheila i Pablo, aquesta tesi no haguera tingut el mateix ritme sense les rises i la bona predisposició per als experiments i les hores interminables.

Al meu primer estiu a Munich, vaig conèixer a la que seria en uns anys la meua co-directora de la tesi i a més de convertir-se en una molt bona amiga, és la dona que més admire en ciència. Amb ella vaig donar els primers pasos importants de la tesi i ha sigut la meua mentora en tots els àmbits de la vida. Gràcies, María.

De l´estància a Munich, els meus companys i companyes van ser la meua familia, i no és sorpresa, donat les hores que feiem al laboratori. Raquel, Jakob, Franzi, Giulia, Sarah. S, Peter i molts més amb els que vaig compartir habitació de cultius, seminaris, cafés i eixides a escalar o fer muntanya. Vull fer un apartat a banda per a mencionar a les persones que em van donar la força per a seguir en els moments més durs, Markus, Sarah i Thomas, gràcies per haver estat ahí. I com no, les poques hores que em quedaven per a estar a casa, Matthias no va ser sols el meu company de pis, va ser el meu amic i confident.

Ara fa dos anys que la vida em va portar a treballar al País Vasc. D´aquesta etapa he de mencionar als meus companys y companyes de l´Unitat de Cirugia Artroscópica per tot el suport que he rebut per poder finalitzar i en especial als “txikis” d´I+D. M´han acompanyat amb bon ánim i rises, moltes rises, aquesta etapa final. Maider, Jon, Saínza, Cris i Diego, gràcies per fer-ho tot tan fácil.

Hi han persones que han sigut una constant aquests 5 anys. Entre elles, les meues amigues. Elles saben el que han significat per a mi i no em cansaré mai de repetir-ho. A la meua familia, tots i cadascú d´ells; tios i ties, cosins i cosines, iaios i iaies, germanes majors i xicotetes. A Alex, que sempre ha estat. Gràcies.

D´ùltim agraïr a Mercedes, que ha sabut portar aquesta tesi a bon port amb l´experiència i un fum de correccions.

LIST OF ABREVIATIONS

RT room temperature

FN fibronectin

ECM extracellular matrix

α-SMA alpha smooth muscle actin

pFN plasma fibronectin

cFN cellular fibronectin

o/n overnight

TMLCs transformed mink lung reporter cells

TGF-β1 transforming growth factor beta1

DF dermal fibroblasts

NE neo-epidermis

FCS foetal calf serum

FA focal adhesion

IAC integrin adhesion complex

FAK focal adhesion kinase

ET epidermal tongue

K keratin

BS basement membrane

GF growth factor

TMD transmembrane domain

MIDAS metal ion-dependent adhesion site

NA nascent adhesion

SRM serum replacement medium

Rho Ras homologous family

C-terminal carboxil –terminal

N-terminal amino-terminal

LAP latency-associated pro-peptide

LTBP latent TGF-β binding protein

GT granulation tissue

EDA fibronectin extra-domain A

EDTA ethylendiaminotetraacetic acid

PC Panniculus carnosus

EDB fibronectin extra-domain B

Col I collagen type I

DMEM Dulbecco´s modified eagle´s medium

DNA deoxyribonucleic acid

FNcom commercial fibronectin

PBS phosphate buffer saline

PBS-T phosphate buffer saline tween-20

PCR polymerase chain reaction

PFA parafolmaldehide

BSA bovine serum albumin

V-region fibronectin variable region

K_{on} constant of association

H&E haematoxylin and eosin

kDa kilo Dalton

daw days after wounding

kPa kilo Pascal

AU arbitrary units

KI knock-in

ENFs *En1*-naïve fibroblasts

EPFs *En1*-past fibroblasts

INDEX

I SUMMARY

Upon skin barrier disruption, complex cellular and molecular events are activated to repair the damage and restore skin integrity. In adulthood, the outcome of this process can result in scarring and fibrosis, whereas complete tissue regeneration is observed in fetal wounds and wounds in lower vertebrates and invertebrates .Although there is abundant literature about the factors and mechanisms that determine the endpoint of either scarring/fibrosis or regeneration after tissue injury, the process is still poorly understood. After cutaneous injury, fibronectin (FN) is instantly released and deposited by cells, and represents a major ECM component in all stages of the wound healing process. FN leaks out from injured blood capillaries and provides, together with fibrinogen, the ECM of the forming granulation tissue (GT). In the following hours, this provisional matrix is remodeled and enriched by infiltrated hematopoietic cells, dermal and fascia fibroblasts that migrate into the dermal region of the wound. This newly formed fibrotic tissue provides structural support for migrating cells adhesion. It constitutes the foundation for either the regeneration of the wounded dermis or the formation of a permanent scar and is a key substrate for keratinocytes to re-epithelialize the wound gap in the epidermis. FN harbors the major cell binding motif defined by the arginine-glycine-aspartate (RGD) sequence located in the 10th type III module (FNIII10) and binds α5β1, αIIbβ3 (exclusive of platelets) and αv-class integrins. In the adjacent module (FNIII9), FN contains the so-called synergy motif that binds α5β1/αIIbβ3 integrins but not αv-class integrins and mediates the formation of catch bonds. The mutation of the FN synergy sequence in mice underscored its role in resisting or producing high forces, although up to a certain force threshold, αv-class integrins binding to FN compensate for the loss of the synergy site. In the present work, we investigated the role of FN synergy site during cutaneous wound healing in mice carrying a dysfunctional FN-synergy motif (*Fn1*$^{syn/syn}$). The course of fibrotic processes, such as adult skin wound healing, depends on several events that are modulated by mechanical signals and hence, on strong integrin-FN bonds: i) the population of basal keratinocytes that initiates migration from the wound margins towards the center of the wound express and activate α5β1 integrins, and form a sheet that advances by sensing the FN-substrate tension and generating force towards it ii) the GT is infiltrated by migrating dermal fibroblasts that secrete and assemble FN fibrils and fascia fibroblasts that pull their own ECM of FN and collagens iii) in the GT, a number of fibroblasts convert into myofibroblasts in a process regulated by mechanical forces and TGF-β1 signals and iv) further release of latent TGF-β1 from the ECM is induced by integrin-mediated force application to the ECM.

We demonstrate that *Fn1*$^{syn/syn}$ mice show a delayed wound closure at early times. This correlates with the presence of less granulation tissue in the initial stage of healing in *Fn1*$^{syn/syn}$

wounds, and reduced content of myofibroblasts and FN deposition. *In vitro* experiments using kidney and dermal fibroblasts derived from *Fn1*$^{+/+}$ and *Fn1*$^{syn/syn}$ mice, and plasma FN (pFN) purified from *Fn1*$^{+/+}$ and *Fn1*$^{syn/syn}$ mice as substrate, reveal that the FN synergy site is important to withstand mechanical tensions required for cell migration and TGF-β1 liberation from the ECMs. At early stages in the epidermis of *Fn1*$^{syn/syn}$ wounds we observe an increment in the α5β1 integrin expression at the epidermal tongue level compared to wounds from *Fn1*$^{+/+}$ mice. When studying keratinocytes behavior *in vitro* we observe apparently contradictory results during single-cell and collective migration. In single-cell migration, keratinocytes moving on FN^{syn} as substrates showed delayed wound closure due to lower speeds and decreased directionality. On the contrary, when keratinocytes are allowed to form cell-cell contacts and migrate in a collective way, the presence of FN^{syn} substrates accelerates the wound closure. This is also demonstrated to be directly linked to the myosin cytoskeleton contraction and the compensatory effects of cell-cell bonds reinforcement. Taken all these results together, we can conclude that the absence of the synergy site is important during the process of skin wound healing at early stages and that the implication is directly linked to processes where the FN-α5β1 bond needs to be reinforced due to high mechanical tension such as TGF-β1 liberation from the ECM and the migration process in cells involved in the healing process.

II INTRODUCTION

1. Skin biology and structure

Skin is the largest organ of the body. As it is in close contact with the environment its most relevant functions are related with protection against external physical, chemical and biological aggressions, prevention of water loss and thermoregulation of the body. The skin is constituted by three different layers: epidermis, dermis and hypodermis**.**

The **epidermis** is the outermost layer of the skin. It is a stratified, squamous epithelium constituted by keratinocytes that account for about 80 percent of the total cell content. Other cell types in the epidermis are: melanocytes, responsible for skin pigmentation and protection against UV radiation, Langerhans and Merkel cells with immunological and neuroendocrine functions, respectively. The epidermis is divided into four layers according to keratinocyte morphology and position. These layers are, from the bottom to the top of the epidermis: the basal, the spinous cell, the granular lipid-rich and the stratum corneum layer. The basal layer is where cells form a single sheet with intercellular junctions called desmosomes conferring stability to mechanical stress. The spinous cell layer is composed of around 8-10 layers of cells. The granular lipid-rich layer (3-5 cell layers) confers important water sealant functions. The stratum corneum is the last layer composed of flattened and densely packed dead cells (Gantwerker et al., 2012).

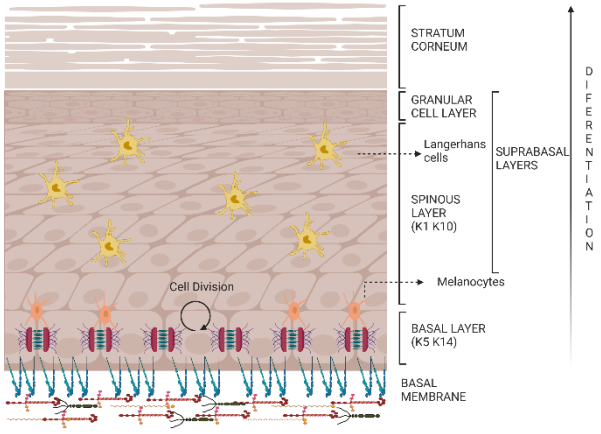

Figure1. Epidermal structure of intact skin including the basal layer in contact with the basal lamina; the suprabasal layer that includes the spinous layer and the granular layer; and finally the cornified (stratum corneum) layer. In addition to keratinocytes (brown) other resident cells with dendritic morphology such as Langerhans (yellow) and melanocytes (orange) are hosted in the skin epidermis.

Keratinocytes undergo a process called *keratinization* that implies the expression and assembly of the intermediate filament keratin within the cytoskeleton. Keratins contribute to the skin structural integrity and different keratin isoforms are expressed in keratinocytes depending on their state of differentiation. Basal cells with proliferative capacity express keratin-5 (K5) and K14, while postmitotic cells located in the spinous layer express K1 and K10. The epidermis is constantly being renewed. Cells in the basal layer divide and move up in the stratum providing

the renewal of the outer epidermis. Skin renewals take around 2-4 weeks and along the process keratinocytes undergo terminal differentiation together with keratin degradation. There is a continuous balance between proliferation, differentiation, and desquamation to maintain skin homeostasis. Keratinocytes undergoing terminal differentiation are replaced by stem cells coming from different skin locations such as the interfollicular epidermis or the sebaceous glands from hair follicles. Under some circumstances such as injury, the keratinocytes have the plasticity to exit from this cyclic process, changing its keratin expression. After skin injury, keratinocytes in the basal and suprabasal layer upregulate K6 and K14 respectively, acquiring migratory and proliferative abilities (Wojcik et al., 2000).

The epidermis is in close contact with the dermis through a porous basement membrane (BM) known as the dermal-epidermal junction that allows certain exchange between layers. Skin BM is mainly formed by collagen VII, laminin, perlecan, nidogen and fibronectin (FN). Cells in the basal layer connect to the BM through integrin receptors at their basal face, which is crucial for mechanical support, cell polarization to establish the direction of cell division, and cytoskeletal organization. Some rare genetic skin disorders as epidermolysis bullosa have their molecular basis in different BM protein mutations. For example, defective collagen VII generates a weak dermal-epidermal junction generating important skin lesions as blisters and skin deformities **(**Vanden et al., 2018**).**

The **dermis** is located immediately below the epidermis and it is mainly formed by fibroblasts surrounded by extracellular matrix (ECM) components. The dermis has been recently divided between two different layers depending on the developmental linage of their resident fibroblasts. The closest layer to the epidermis and so-called upper dermis is formed by fibroblasts surrounding hair follicles, which support hair growth and have sensorial functions. The lower dermis is formed by secretory fibroblasts that are responsible for ECM deposition (Driskell et al., 2013).

The **hypodermis**, also named subcutaneous layer, is located directly below the dermis and its function is to connect the upper part of the skin with the fibrous tissue composed of bones and muscles. The murine hypodermis is characterised by the presence of a thin layer of muscular tissue called the *Panniculus carnosus* (PC) that is much less abundant in human skin. This muscular layer confers to the murine skin contractile properties that increase the efficiency of wound closure (Fang and Mustoe, 2008). The PC separates as well the dermis from a thin layer below underneath called fascia, which contains abundant fibroblasts, collagen and other ECM proteins. The fascia is thicker in human skin than in mice and recently

has been described to be crucial during the healing of deep wounds (Abu-Hijleh et al., 2006**;** Correa-Gallegos et al., 2019).

2. The extracellular matrix: general aspects

The ECM is a highly specialized three-dimensional structure that surround and offers scaffold for cells. ECM is mainly formed by fibrilar proteins such as collagens, elastin or FN and non-fibrilar components such as laminins and glycosaminoglycans. The different ECM components bind to each other forming a complex network that gives structural support to cells attached through plasma membrane receptors. There are two types of ECM: interstitial matrices and basement membranes. Interstitial matrices form connective tissues in which FN and collagens are the most abundant components. Basement membranes separate epitheliums from the surrounding stroma and are composed of laminin, nidogen, FN and collagen IV as their most abundant components.

The composition of the ECM is developmental stage- and tissue-dependent. Every tissue has a unique ECM structure that is orchestrated in early developmental stages, maintained during the adult life, and remodelled in response to disease and injury (Lu et al., 2011). Mice with genetic mutations in ECM proteins such as FN, proteoglycans or collagens suffer from early embryonic lethality or severe tissue defects underlying the relevance of the ECM (Sasse et al., 2008**;** Rozario and DeSimone, 2011; Girós et al., 2011). The ECM is not a mere physical barrier for cells but it guides cellular processes such as migration, proliferation, differentiation and survival. The ECM is also able to store growth factors (GF), cytokines, and chemokines that are released to the interstitial space and signal cells in the close proximity. The relationship between cells-ECM is also influenced by mechanical properties that result from its composition, density, orientation, cross-linking state of the components and its stretching. Every tissue has a particular set of properties that are, in turn, regulated by cells in a process called mechanical homeostasis. Cells sense mechanical cues from their surroundings (stiffness, elasticity, viscosity) and respond adapting their shape or ECM mechanical properties, balancing between protein secretion and degradation. The process of mechanotransduction involves the tight work of three main elements: the ECM, the cells' membrane receptors and the cytoskeleton that is the cellular force generation machinery (Humphrey et al., 2014).

3. Integrins: linkers between ECM and cells

Changes in the ECM composition and physical properties are transmitted to cells via cell surface receptors such as integrins and syndecans. Integrins are the major family of cell-ECM receptors in metazoans. As transmembrane proteins, integrins have the ability to transmit signals in a bidirectional way and, in vertebrates, they can also take part in some cell-to-cell adhesions (Ross et al., 2013). They were first identified in 1987 and named integrins as they were able to "integrate" signals from the outside to the inside and vice versa. Bidirectional signalling is explained by its structure that connects the ECM with the cell cytoskeleton. Such important function has made them one of the most studied adhesion receptors in the last decades elucidating pivotal roles in development, immune responses, tissue repair and cancer progression (Bouvard et al., 2013; Hamidi and Ivaska, 2018).

3.1. Integrin structure

Integrins are type I transmembrane glycoproteins formed by two non-covalently associated α and β subunits. In mammals, there are 24 different integrin dimers that are the result of the combination of 8 α and 18 β subunits (Hynes, 2002). Some integrin heterodimers bind more than one ligand, and different heterodimers can bind the same ligand, being the affinity and intracellular signalling specific for each ligand-receptor interaction (Humphries et al., 2006).

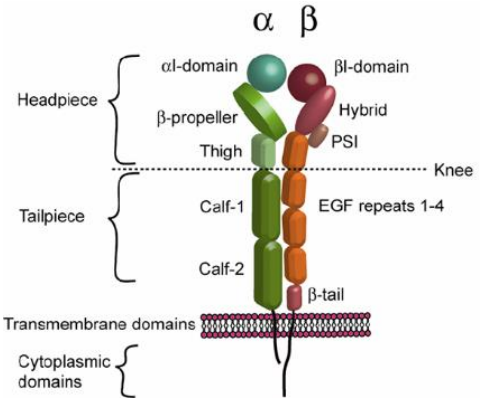

Figure 2. Integrin α and β subunits structure. The part of α and β subunits that directly participates in ligand binding is called the headpeace domain and is followed by a tailpiece in contact with the transmembrane domain embedded in the cell membrane. The cytoplasmic tail is located inside the cell and it is in charge of extracellular changes transmission by the union of scaffolding proteins **(**modified from Gahmberg et al., 2009)

Integrins are constituted by a large extracellular domain called the headpiece region. (Campbell and Humphries, 2011). They also contain an integrin transmembrane domain (TMD) that is embedded in the cell membrane. Integrins heterodimerize through their extracellular domain and reversibly associate through their TMDs. Structural changes in the headpiece upon

ligand binding are transmitted to the cytoplasmic tail across the TMDs in a process called outside-in signalling (Luo et al., 2007).

Unlike other transmembrane receptors, integrins have short cytoplasmic tails (around 20-50 amino acids) without catalytic activity (Fig. 2). These domains are sites of interaction for a bunch of scaffolding proteins which indirectly connect integrins with the actin cytoskeleton. The association of different proteins to integrin tails also induces changes in the TMDs conformation which are transmitted to the extracellular domain and so called inside-out activation (Kim et al., 2012).

3.2. Integrin activation

Integrin activation is the term used to describe the shift from a low-affinity ligand binding conformation into a new state in which the integrin is structurally more suitable for ligand binding. The activation state of integrins is commonly divided into three different conformational states; **bent-closed** and **extended-closed** that are low affinity conformations where ligand-binding site remains closed (Takagi et al., 2002). The active state is known as **extended-open** conformation and is characterized by the complete opening of the ligand-binding site (Fig. 3). The union of scaffolding proteins such as talin and kindlin (Moser et al., 2009; Calderwood et al., 2013) to the cytoplasmic β-tail induces transition from an inactive state into its extended-open conformation, in a process known inside-out activation. Talin and kindlin also have actin-binding domains that are indispensable for cell spreading and force generation (Theodosiou et al., 2016). There is other mode of integrin activation described: the outside-in activation. Recently, it has been hypothesized that the inside-out activation is not sufficient to overcome the thermodynamic barrier to stabilize the extended-open conformation needing the contribution of extracellular signals (Sun et al., 2019).

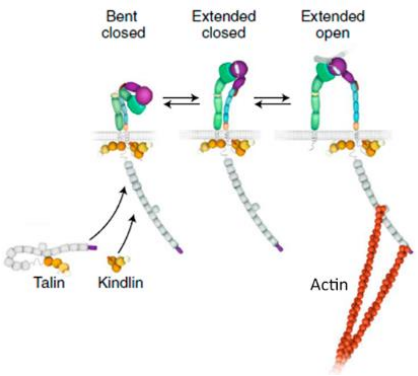

Figure 3. Model for integrin inside-out activation. In the bent-closed conformation the accessibility to the ligand binding site is restricted and known as a low-affinity state. In this model, the transition to an extended closed conformation is guided by the recruitment of scaffolding proteins, such as talin and kindlin, to the integrin cytoplasmic tail. The link to the actin cytoskeleton stabilizes the heterodimer in an extended open conformation in which the structural high affinity conformation allows ligand binding to the head domain. From Sun et al., 2019.

Integrin activation is the first attempt for cell attachment to the extracellular environment but cells in tissues are under constant stress being the reinforcement of adhesion sites essential to preserve tissue homeostasis or to overcome injury (Mezu-Ndubuis and Maheshwar, 2021).

3.3 The cell adhesome: from adhesion to force generation

The connexion between ECM networks and the intracellular cytoskeleton is mediated by a number of protein-protein interactions. This protein core is surrounding the integrin cytoplasmic tails and works as a mechanosensitive subcellular complex known as adhesome. The adhesome is a consensus of more than 200 scaffolding and signalling proteins (Horton et al., 2016). Mechanical forces exerted by cell surroundings through integrins induce scaffolding proteins conformational rearrangements allowing interactional changes between them or displaying cryptic phosphorylation sites which directly orchestrate mechanotransduction pathways (Shams et al., 2018). There are several adaptor proteins including focal adhesion kinase (FAK), paxillin and talin that are immediately recruited to the integrin tail in the process of nascent adhesion (NA) formation (Case and Waterman, 2015; Humphries et al., 2019). NAs maturation into focal adhesions (FAs) is dependent of FAK and paxillin actomyosin-binding through the recruitment of new actin-binding proteins into the integrin core such as vinculin (Zaidel-Bar et al., 2007; Choi et al., 2008). FAs maturation and clustering into larger fibrilar adhesions is essential for force generation and migration (Coyer et al., 2012; Wang and Wang, 2016). ECM-integrin patterns determine the organization of actin fibres in the same way that actomyosin contractility is essential for FA maturation and cells translocation (Geiger et al., 2009; Case and Waterman, 2015).

In the last decades it has been demonstrated the relevance of ECM biochemical and mechanical properties in determining cell motility, morphology and cell fate (Trappman et al., 2012; Elosegui-Artola and Oria, 2020; Plikus et al., 2021). Cells transduce mechanical loads from their surroundings into biochemical signalling pathways, inducing both transitory changes with cytoskeleton reorganizations and long lasting changes like gene expression (Cho et al., 2017; Kechagia et al., 2019). For instance, α5β1 and αvβ3 integrins upon ligand binding induce rapid kinase signalling events including FAK and Src phosphorylation that strength adhesion to the substrate and FAs reinforcement (Strohmeyer et al., 2017). In the same way, small GTPases from the Rho (Ras homologous) family, RhoA, Rac1 and CDC42, contribute to regulate a variety of cell responses as adhesion, spreading and migration (Bass et al., 2007; Lawson and Burridge, 2014). An important feature is that mechanical signals differ depending on the integrin heterodimer that is used to bind the substrate. Integrins α5β1 and αvβ3 both bind FN and

cooperate for rigidity sensing but have specific signalling functions. αvβ3 integrin has a more structural function inducing actin polymerization and stress fibres formation via RhoA/mDia activation, whereas myosin II-dependent contraction is coupled to FN-α5β1 binding and RhoA/Rock signalling activation (Schiller et al., 2013; Elosegui-Artola et al., 2014).

3.4. ECM-integrin forces in cell migration

Reciprocal relationship between physical properties of cell microenvironment and force exerted by cells is crucial during cell migration. To migrate, cells form integrin adhesion complexes that bridge the substrate and the actin cytoskeleton (Conway and Jacquemet, 2019). The migration hypothesis called "molecular clutch" was described for the first time by Mitchison and Kirschner (1988) and postulates that retrograde flow experienced by actin is transmitted to FAs generating the proper tension on the substrate to initiate cell movement. Scaffolding proteins connecting actin cytoskeleton with integrins, such as talin, vinculin and α-actinin, have been shown to experiment similar or lower retrograde flow indicating that forces are transmitted across molecules from FAs to the substrate as a "molecular clutch" (Thievessen et al., 2013; Sun et al., 2016). During single-cell migration, actin polymerization drives the formation of cell membrane protrusions such as lamellipodia or filopodia at the leading edge pushing the membrane forward. The actin network experiments itself a retrograde flow when pushing the cell membrane at the leading edge that is accompanied by a slower myosin-II contraction retrograde flow in the trailing edge (Fig. 4). When actin is engaged to the substrate through FAs, the retrograde flow decreases, and it turns into traction forces that will push the cell body forward. There is then an inverse relationship between actin speed and force exerted by the different components. ECM engagement with integrins can tolerate a certain force threshold, breaking the link when the force is exceeded which explains the different cell behaviours on substrates of different stiffness (Plotnikov et al., 2012; Elosegui-Artola et al., 2016). On soft substrates, FAs transit from low to high traction forces increments as the retrograde flow pulls the actin cytoskeleton. The deformable nature of soft substrates, with lower unbinding rates, allows FAs to reinforce adhesion to the substrate generating more linkages (Chan and Odde, 2008). On stiff substrates that oppose more resistance, links between the substrate and the actin network have stable traction forces and reach the breaking strength faster than on softer substrates. There is a certain rigidity that allows the maximum force generation with faster speeds and when it is surpassed the system stops following the molecular clutch prediction (Elosegui-Artola et al., 2018).

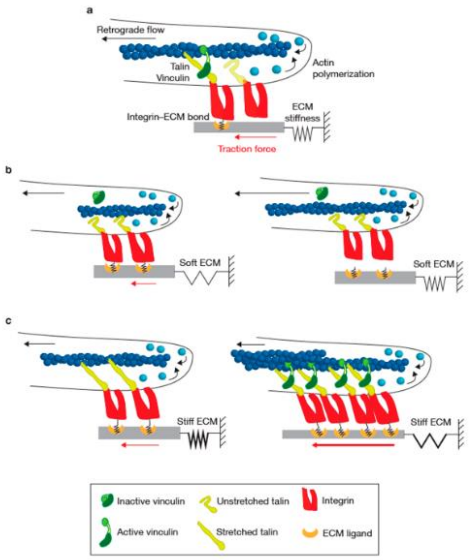

Figure 4. The molecular clutch hypothesis of cell mechanotransduction. a) Components of the molecular clutch; the action cytoskeleton, FA and the ECM. Actin polymerization is subjected to a retrograde flow that is transmitted to the integrin effectors and translate into traction forces on the ECM. Retrograde flow, ECM deformation and traction forces on a) soft and c) stiff substrates (Swaminathan and Waterman, 2016).

Collective cell migration has been described as the main way of migration in biological processes such as development, cancer progression and epidermal wound healing, among others. This way of movement is explained by the formation of cell-cell contacts that confer the system a new level of organization. Each cell taking part of the sheet is influenced by neighbouring cells exerting physically forces on each other that will influence the overall migration. In collective migration, leading cells at the front form protrusions at their free side membrane and influence cells movement on the trailing edge providing local guidance with chemical and mechanical cues (Trepat et al., 2009; Reffay et al., 2014,). FAs and adherent junctions are connected intracellularly through the actin cytoskeleton even sharing some signalling proteins and actin regulators such as FAK and vinculin (Yonemura et al., 2010) (Fig. 5). Changes in substrate rigidities are sensed by leader cells and hence guide the direction and speed migration of the cell sheet (Sunyer et al., 2016; Pandya et al., 2017). Some studies indicate that cells migrating in a collective way regulate mechanotransduction using a fine balance of tension between adherent junctions and adhesion sites (Liu et al., 2010). Under some migration conditions, antagonist regulation has been shown for adherent junctions and integrin-based adhesions. This is shown in studies where FAK activation by strong ECM-integrin engagement follows to the down-regulation of cadherin-based cell-cell unions (Yano et al., 2004). Conversely, on soft substrates showing weaker cell-substrate engagement, cell-cell contacts are shown to contribute to increase compaction and aggregation (Guo et al., 2006).

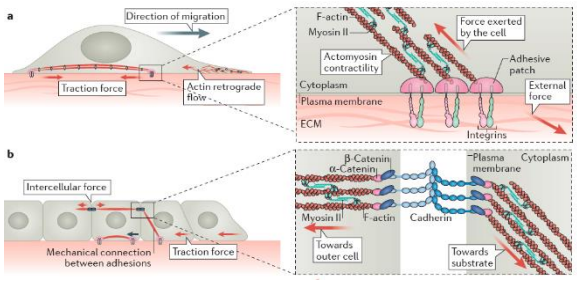

Figure 5. Single and collective cell movement. A) During single-cell migration traction forces are exerted to the ECM by actomyosin contractility through the FAs. B) Collective cell migration is characterized by cell-cell and cell-ECM contacts. Both junctions are connected through the actin cytoskeleton leaving the transmission of cell forces to the coordination of both of them (Ladoux and Mège, 2017).

4. Fibronectin: general aspects

FN is a large glycoprotein (250 kDa) ubiquitously expressed in the ECM of a wide variety of organs and tissues having critical functions in the early development of vertebrates. FN-null mice have a severe phenotype with embryonic lethality at embryonic day 8.5 (E8.5) presenting problems in neural tube closure, in the cardiovascular system and lack of somite formation (George et al., 1993). In addition to its relevance in morphogenesis, FN has been described as crucial during processes of ECM remodelling and tissue regeneration such as wound healing and cancer progression (Gaggioli et al., 2007; Lukjanenko et al., 2016).

FN appears in two different forms in the body: soluble and assembled into a fibrilar network. In the blood, FN is synthetized and secreted into the bloodstream by hepatocytes (called plasma FN; pFN) and is found in the globular soluble form. Integrins bind and unfold soluble FN triggering its polymerization into insoluble fibres by applying intracellular forces (Zhong et al., 1998; Schwarzbauer and Sechler, 1999; Mao and Schwarzbauer, 2005). Thus, pFN will be assembled into fibrils when integrins in blood cells, like platelets, become activated (Denis et al., 2007). In tissues, FN predominates into the fibrilar form (known as cellular FN; cFN) forming the interstitial matrices and binding other ECM proteins.

The FN molecule is encoded by a single gene and forms dimers of two nearly identical subunits joined by a pair of disulphide bonds at the carboxyl terminal (C-terminal) region. Each subunit is arranged in a modular structure consisting of three different types of the immunoglobulin-like (Ig) folding unit and named type I, II and III. FN has 12 type I modules distributed in three clusters along its structure, 2 type II modules and 17 type III modules, 15 are constitutively included and 2 are alternatively spliced (Fig. 6).

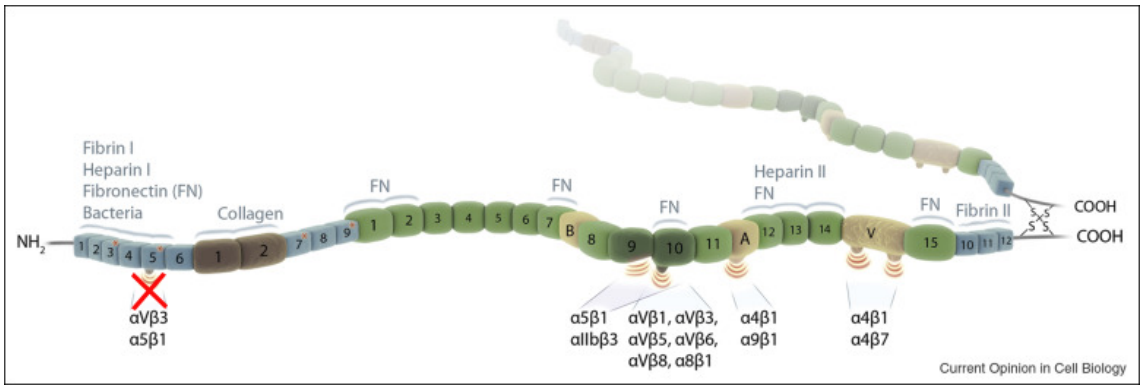

Figure 6. Modular representation of FN structure and its ligand binding sites. FN is a homodimeric protein with a disulphide C-terminal bond subunits. It has a modular structure composed of three different repeating units (type I in blue; type two in brown and type III in green colour). In type III modules, coloured in pale brown, are also represented the splice variants (EDA, EDB and V region). Written on top are the ligands that FN binds and down the integrin heterodimers that binds. Note that integrin binding sites at the N-terminal are updated due to recent findings (adapted from Leiss et al. 2008).

FN **type I modules** are around 40-45 amino-acid residues in length and appear at FN end parts (C- and N-terminal regions). The N-terminal domain (FNI_{1-5}) plays important roles in matrix assembly and has fibrin, heparin and self-assembly binding sites. There are two different fibrin binding sites in the FN molecule with important roles in haemostasis and wound healing as they are involved in platelet aggregation during the blood clot formation. FN also contains two heparin/heparan sulphate binding sites (Heparin I and II), located in opposite ends of the FN molecule. The Heparin II site has been described to have higher affinity for the heparan sulphate chains of the cell receptors syndecans. Syndecans are a family of four members that cooperate with integrins in cell adhesion processes such as cell spreading, intracellular integrin traffic and signalling (Morgan et al., 2007).

FN contains two **type II modules** located between the FNI_6 and FNI_7 modules. They are approximately 60 amino acids in length and contain a collagen binding site important in processes of EMC assembly (Sottile et al., 2007; Graham et al., 2019).

FN **type III modules** are approximately 90 amino acids long and form a seven-stranded β-sandwich that, contrary to type I and II modules, lacks intrachain disulphide bonds. This particularity gives enormous elasticity to this part of the molecule once is engaged by cell receptors. The variable number of FN type III modules results from differential mRNA splicing that generates until 20 different isoforms in humans or 12 in mice. Differential splicing results in the inclusion of two extra domains called A (EDA) and B (EDB) and located between $FNIII_{11}$/ $FNIII_{12}$ and $FNIII_7$/$FNIII_8$, respectively (White et al., 2008; Astrof and Hynes, 2009). Additionally,

there is a variable region (V or FNIIICS) between the $FNIII_{14}$ and $FNIII_{15}$ that leads to five different sequences, ranging from 0 to 120 amino acids in length (Muro et al., 2008; Hynes, 1990). Plasma FN lacks both extra domains and one monomer does not present the V-region (White et al., 2008). During embryogenesis, the expression of alternatively spliced regions is elevated and decreases after birth and with aging. However, during tissue repair and neo-angiogenesis, the "embryonic pattern" is temporarily restored with increased expression of FN-EDA and FN-EDB variants (Ffrench-Constant et al., 1989). It has been shown that EDA-FN and V-region bind cell receptors what predicts novel intracellular signalling in processes where they are found to be up-regulated as in wound healing processes (To and Midwood, 2011; Bhattacharyya et al., 2014).

FN contains five different self-attachment binding sites, located at $FNIII_{1\text{-}2}$ $FNIII_{7\text{-}8}$, $FNIII_{10}$, $FNIII_{15}$ and $FNIII_{12\text{-}14}$. These self-interaction sites are indispensable to form an insoluble 3D FN matrix in a cell-mediated process called fibrillogenesis. FN is secreted in a globular and folded form with some self-association binding sites exposed but with cryptic regions that will become accessible after FN conformational changes driven by its stretching in an integrin-driven process (Wierzbicka-Patynowski and Schwarzbauer, 2003).

4.1. FN integrin binding sites

FN binds a dozen of members of integrin family. The integrin binding sites in FN molecule are concentrated in type III modules. The V-region has been described to bind α4β1 and α4β7 integrins, both recognizing LDV and REDV sequences. In addition, α4/9β1 integrins recognize the EDGIHEL sequence present in FN-EDA splice variant (Liao et al., 2002, Shinde et al., 2015). α4/9β1 have essential functions mediating immune responses allowing hematopoietic cells adhesion to the endothelium and extravasation (Guan and Hynes, 1990, Garmy-Susiny et al.,2005).

4.1.1. The FN RGD motif

The major FN integrin binding region is an Asn-Gly-Asp (RGD) motif located in the $FNIII_{10}$ module, which was described for the first time to bind α5β1 integrins (Pierschbacher and Ruoslahti, 1984). In addition, the RGD sequence binds, α8β1, α9β1, the platelet-specific αIIbβ3 integrin and all members of the αv-class. The relevance of α5 and αv-class integrins becomes apparent in embryonic lethality of integrin mutant mice at E9.5 and E10-12, respectively. Mice double-null mutant for α5 and αv integrins present embryonic lethality at E7.5-8, similar to or even more severe than FN-null mice (Yang et al., 1999) indicating that αv-class integrins were

responsible for compensating α5-deficiency to some extent (Yang and Hynes, 1996) and that both α5β1 and αv-class integrins are crucial FN-binding integrins during development. The deletion of the RGD sequence in mice generates an early embryonic lethal phenotype similar to the observed in FN-null mice (Benito-Jardon et al., 2020) or in double α5/αv deficient mice (Yang et al., 1999). The mutation of the FN RGD motif into an RGE sequence impairs α5β1/αIIbβ3 binding, but the functions related with αv-class integrins remain intact (Takahashi et al., 2007; Girós et al., 2011).

FN fibril assembly is a cell-driven process that involves integrin-binding motifs and regions of self (FN-FN) interaction. When FN binds integrins via its RGD motif (Huveneers et al., 2008) integrin activation activates Rho kinases, enhances actin polymerization and stimulates cell contractility. Actomyosin contraction pulls FN monomers unfolding the dimers with cryptic binding sites now available to allow FN-FN and FN-ECM proteins interactions. Integrin α5β1 has been demonstrated as essential for this FN fibril formation process, although syndecans alone can drive FN matrix assembly that is, however, less crosslinked (Benito-Jardón et al., 2020).

4.1.2. The FN synergy site

Adjacent to the RGD motif ($FNIII_{10}$) there is an 8-amino acids sequence named the synergy site (FNIII9) that was described for the first time by Aota and Yamada in 1994. The mouse sequence (DRVPPSRN) is highly conserved in vertebrates with the exception of humans where a proline is substituted by a histidine amino acid (DRVPHSRN). Yamada and colleagues showed that the RGD motif did not gather full adhesive capacity in FN and hypothesized that flanking regions could enhance cell adhesion to FN (Nagai et al., 1991). Three years later, using FN fragments, it was described a minimal sequence (PHSRN in human) that enhanced FN adhesive capacity to α5β1 and αIIbβ3 integrins but not to other RGD-binding integrins such as αv-class components (Bowditch et al., 1994; Mardon and Grant., 1994; Danen et al., 1995). Mutagenesis analysis revealed the R1379 amino acid, from the PHSRN sequence, to be the key residue for the synergistic effect. However, a double mutant including the R1374 and R1379, from the extended synergy sequence (D**R**VPPS**R**N), had a dramatic effect in cell adhesion when the cell can only use α5β1 integrins (Aota et al. 1994; Redick et al., 2000). Site directed mutagenesis experiments in $FNIII_{8\text{-}10}$ fragments revealed that R1374 and R1379 were also essential to allow platelet attachment under shear stress through αIIbβ3 integrins (Chada et al., 2006).

The crystal structure of a $FNIII_{7-10}$ fragment was first published in 1996 by Leahy and colleagues showing that the FN RGD-containing loop and the synergy site sequence faced the same FN side being 30-40 Å apart and both accessible to a single integrin dimer (Leahy et al., 1996) (Fig. 7). The α5β1 integrin ectodomain stabilized in a complex with an anti-β1 antibody revealed that the synergy site binds the integrin through the α-subunit head domain whereas the RGD motif uses both α and β subunits reinforcing the idea of cooperation between the RGD motif and the synergy site for binding α5β1 and αIIbβ3 (Mould et al., 1997; Nagae et al 2012).

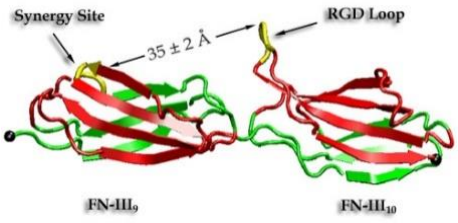

Figure 7. Cartoon conformational representation of $FNIII_9$ and $FNIII_{10}$ modules. Type III module secondary structure is color-coded with upper β-sheets in red, lower β-sheets in green and RGD and synergy motifs are in yellow. The cartoon represents a native conformation between the synergy site and the RGD motif in which the distance between them is around 35±2 Å. From **Krammer et al., 2002**

The knowledge of relevant residues for the synergy site function opened a new gate to investigate its function in cellular processes such as cell adhesion and FN fibrilogenesis. Some *in vitro* assays suggested that the synergy site could cooperate to the outside-in α5β1 integrin activation. Supporting this idea, it was described that some cell lines expressing α5β1 integrins that did not adhere to FN fragments with a mutated synergy site (PHSRN sequence was substituted by SPSDN), recovering full function with β1 integrin activators such as antibodies or manganese (Mn^{2+}) (Danen et al., 1995). However, electron microscopy and kinetic assays suggested that the synergy site function could help the encounter between ligand-receptor reducing the constant of association (K_{on}) (Takagi et al., 2003). Both hypotheses were later invalidated under physiological conditions when the *in vivo* FN synergy motif function was tested using genetically modified mice ($Fn1^{syn/syn}$) carrying a mutated synergy sequence (D**R**VPPS**R**N> D**A**VPPS**A**N) (Benito-Jardón et al., 2017) (Fig. 8). Contrary to the embryonic lethality expected from a complete absence of α5β1-FN adhesion, these mice were born following normal Mendelian rates, and tissue development was completely normal (Fässler and Meyer 1995; Yang et al., 1999). This result arose the question of whether the FN synergy site was critical for any cell function. Structural models showed that force-induced changes in spatial distance between the synergy site and the RGD motif could allow or not the synergy site to bind the α5 head domain. This implied that mechanical tension from the ECM could then regulate the adhesion force between ligand (FN-synergy site) and receptor (α5β1), being the synergy site a secondary attachment to increment bond strength (Krammer et al., 2002). This increment in bond strength upon force application has been called catch bond (Shi and

Boettiger, 2003; Kong et al., 2009). Different *in vitro* assays in our laboratory demonstrated that the synergy site reinforces the bond between RGD and α5β1/αIIbβ3 integrins upon force application and thus that the synergy site allows the catch bond formation between FN-α5β1/αIIbβ3 integrins (Benito-Jardón et al. 2017) (Fig. 9A). The relevance of catch bonds formation by the FN synergy motif was demonstrated during *in vivo* tail bleeding assays using *Fn1*$^{syn/syn}$ mice, in thrombus formation experiments and in platelet adhesion assays *in vitro*. *Fn1*$^{syn/syn}$ mice depicted longer times compared with *Fn1*$^{+/+}$ littermates demonstrating the importance of the synergy site to reinforce platelet αIIbβ3/α5β1 integrins adhesion to FN under blood shear flow (Fig. 9B) (Benito-Jardón et al., 2017). It still remains open, however, whether the FN synergy site-mediated reinforcement of α5β1 integrins adhesion is critical during other processes that imply high ECM-cell tensions, such as wound healing or cancer progression.

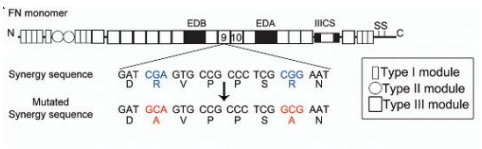

Figure 8. Cartoon of FN sequence with synergy site mutations. The synergy site deficient mouse strain (*Fn1*$^{syn/syn}$) was generated using gene targeting to introduce point mutations in the synergy site sequence. The two critical arginines along the synergy site sequence (FNIII9) were substituted by alanines (R1374A and R1379A) disrupting the *in vivo* function. From Benito-Jardón et al., 2017.

A FN synergy-inactivated and β3 integrin knockout mouse was generated (Fn1$^{syn/syn}$; Itgb3$^{-/-}$) to test whether the absence of a phenotype in *Fn1*$^{syn/syn}$ mice was a result of β3 class integrins compensation. Despite the presence of haemostatic defects in Itgb3$^{-/-}$ mice, around the 60% of the homozygous are born what differs from the embryonic lethality at E15.5 in double mutant mice. In addition, fibroblasts in culture either expressing α5β1 or αv-class integrins confirmed that a weak α5β1 adhesion and spreading onto pFN^{syn} was compensated by αv-integrins (Fig. 9A) (Benito-Jardón et al., 2017).

5. Skin wound healing

When the skin barrier is disrupted, a cascade of cellular and molecular events is activated to repair the damage and restore skin integrity. The most common response to injury in adult mammalian skin is scarring and fibrosis instead of the complete tissue regeneration (Erickson and Echeverri, 2018). Cutaneous wound healing process is divided into three overlapping but well-defined stages. Inflammation, proliferation and finally the last and longest phase that compresses the maturation/remodelling stage (Gurtner et al., 2008).

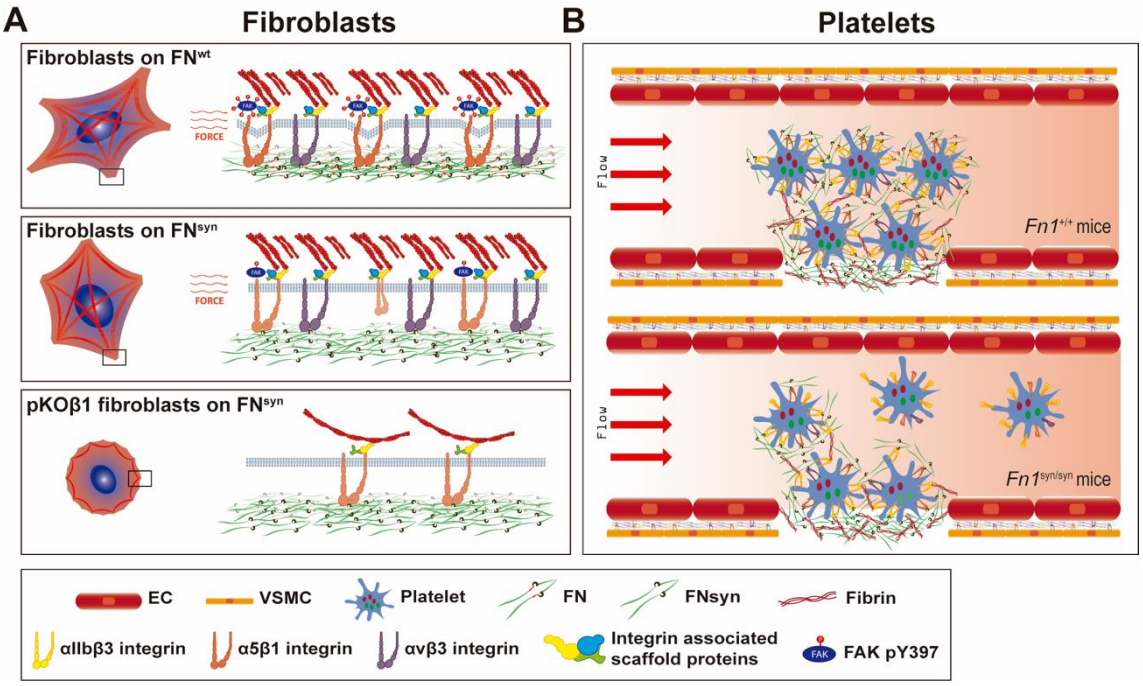

Figure 9. **The FN synergy site function.** (A) FN-KO fibroblasts seeded on pFN^{wt} (top) or pFN^{syn} (middle) reinforce their attachment upon force application when the synergy site is present (catch bond formation) but display less strength when seeded on pFNsyn. Fibroblasts expressing only α5β1 integrins seeded on pFNsyn have rounded shape (bottom) and are not able to assemble stress fibres. (B) FN with abolished synergy site have delayed platelet plug formation upon vessel injury as platelets cannot withstand blood flow pressure.

5.1. The haemostasis and inflammation phase

It takes from seconds to minutes to start after injury in mammalian animals (Eming et al., 2017). Platelets circulating in blood vessels have inactive integrins at their membrane under homeostatic conditions. Upon trauma, the activation of the coagulation cascade and the exposure to ECM proteins from damaged endothelium activate integrins allowing platelet adhesion and aggregation (LeBert and Huttenlocher, 2014; Rosique et al., 2015). Once activated, platelets release their FN content hosted in α granules that is incorporated to a pre-assembled fibrin matrix forming the so-called fibrin clot (Vadasz et al., 2015; Xu et al., 2016). Activated platelets bind pFN via α5β1 and αIIbβ3 integrins, both binding the FN-RGD motif with the contribution of the FN synergy site. Despite an obvious role in haemostasis, the deletion of pFN in mice did not abolish the plug formation nor increase bleeding times due to compensation by the fibrinogen (Sakai et al., 2001). Platelets and cells from damaged tissues at the wound site release a combination of pro-inflammatory molecules attracting immune cells as neutrophils, macrophages and mast cells that guide tissue immune response to prevent wound infection as well as to remove death cells and debris (El Ayadi et al., 2020). As long as inflammation progresses, immune cells recruited into the wound site secrete fibroblasts growth factor (FGF) and transforming growth factor (TGF-β1), as well as cytokines including

interleukin-1β (IL-1 β), tumour necrosis factor-alpha (TNF-α) and proteinases (Werner and Grose, 2003). TGF-β1 acts as a growth-inhibitory cytokine in normal skin homeostasis, but during wound healing it has important effects in initiating inflammation (Ashcroft et al., 1999) granulation tissue formation (Tomasek et al., 2002) and stimulation of keratinocyte migration (Reynolds et al., 2005). The resolution of the inflammatory phase is key for transitioning to the next phase. Prolonged or reduced inflammatory response has been linked to chronic wounds or aberrant scarring, leading to the formation of hypertrophic and keloid scars (Landén et al., 2016; Ogawa, 2017). It has been described that the excess of pro-inflammatory infiltrated cells can stimulate the production of ECM proteins like FN and hence delay or interfere in the healing process (Eming et al., 2010).

5.2. The proliferative phase

It begins one or two days after the injury and includes re-epithelialization and maturation of the granulation tissue**.** This phase is achieved by three main cell processes: proliferation, migration and contraction. The main cell types involved are keratinocytes, which regenerate the epidermal layer, and fibroblasts which form the granulation tissue (GT) in the dermis. Wound contraction has great contribution in wound closure. In humans it is achieved by activated fibroblasts (myofibroblasts) in the GT and in mouse models it is helped by a muscular tissue called *panniculus carnosus* located in the subcutaneous layer (Rippa et al., 2019).

Re-epithelialization of the epidermis starts from hours to days after injury in mouse and human wounds (Gurtner et al., 2008). Keratinocytes at the wound margins form what is called the epidermal tongue (ET) which migrates and spreads towards the centre of the wound to restore the epidermal barrier. Keratinocytes forming the ET migrate in a collective manner as a coherent sheet forming cell-cell adhesions based on both tight and adherent junctions. Intravital microscopy have recently demonstrated the existence of two different epidermal zones during re-epithelialization: (1) a proliferative rear hub formed by cells in the new epidermis and inside hair follicles that help to restore the epidermis; and (2) a second zone formed by a non-proliferative leading edge of keratinocytes that will guide ET migration towards the centre of the wound. It has been shown that both basal and immediately suprabasal keratinocytes contribute to the migration of the epidermal tongue (Nunan et al., 2015). Upon damage, keratinocytes are activated and suffer changes in keratin gene expression triggered by pro-inflammatory signals and the loss of attachment to the BM at the wound site. At the same time, a new matrix will guide the keratinocytes migratory response (Clarck et al., 1982; Barker and Engler, 2017). Cells in the epidermis reorganize their

cytoskeleton in order to make it more suitable for a migratory phenotype helped by the rapidly induced expression of keratin K6, K16 and K17 (Paladini et al., 1996; Freedberg et al., 2001). K14 expressed by basal keratinocytes in physiological conditions is up-regulated upon injury over the different stratus with increased expression in basal keratinocytes.The new gene expression profile in keratinocytes is also characterized by the up-regulation of integrin receptors such as α5β1 (Cavani et al., 1993; Aragona et al., 2017), αvβ6 (Larjava et al 1993) and αvβ5 (Clark et al., 1990) in keratinocytes located at the leading edge of the tongue that recognize the proteins forming the provisional matrix like FN, vitronectin and tenascin C.

The formation of the granulation tissue (GT) in the dermis is a pre-requisite for the migration of keratinocytes in the epidermis. The GT is defined by infiltrated macrophages, fibroblasts and blood vessels surrounded by a dense ECM deposited by local cells. The origin of fibroblasts´ population in the GT has been controversial. Some studies suggested that this population could derive from blood-circulating hematopoietic cells with mesenchymal characteristics (fibrocytes) that are infiltrated during the vessels break (Suga et al., 2014; Rinkevich et al., 2015). Others suggested that they could also derive from resident mesenchymal progenitor cells such as adipocytes (Galdelkarim et al., 2018) or could be reminiscent fibroblasts at the wound site (Hinz et al., 2007, 2012). Using lineage tracing, Driskell et al 2013 demonstrated that fibroblasts in skin connective tissue arise from two distinct lineages in development and repair what leads to either regeneration or scar formation. One linage is forming the upper dermis and consequently in charge of regulating hair follicle growth. This type was described to not express the Engrailed-1 (*En1*) transcription factor and hence called *En1*-naïve fibroblasts (ENFs). On the other hand, reticular fibroblasts at the lower dermis are described to synthesise the bulk of the fibrilar ECM and hence related with the fibrotic response. This linage is called *En1*-past fibroblasts (EPFs) as they do express the transcription factor. The transition from scar to regeneration has been described to depend on the presence of these two linage independently from the environment (Jiang et al., 2018). In wounded adult skin, the initial wave of dermal repair is mediated by the lower lineage, and upper dermal fibroblasts are recruited only during re-epithelialization. Recently, Correa-Gallegos et al., 2019 changed the paradigm and demonstrated that in deep injuries the 80% of dermal cells at the wound come from the fascia. In this publication collagen matrix was proved to be moved upwards like a pliable gel steered by fascia myofibroblasts. It is remarkable that fibroblasts sources for skin wound healing differ depending on the original wound size.

As long as fibroblasts cover the wound, there is an overall increment in mechanical tension as fibroblasts start to align with the early deposited FN and collagen matrix. The mechanical

tension that cells experiment as a consequence of increased rigidity has been described as the key controller for fibroblast differentiation into myofibroblasts (Klingberg et al., 2014, Hinz et al., 2001b; Hinz B, 2010). Myofibroblasts were first described by Gabbiani et al. in 1971 as differentiated cells that promote wound closure by contraction. These cells express the actin isoform alpha smooth muscle actin (α-SMA) that is associated to the actomyosin stress fibres conferring contractile capacities. This actin isoform is constitutively expressed in endothelial cells but is upregulated in fibroblasts during fibrotic responses (Hinz et al., 2001a, Barkauskas and Noble, 2014; Duffield, 2014; Prabhu and Frangogiannis, 2016; Kisseleva, 2017). The ECM stiffness ranges from 0.01-10 kPa in the fibrin-FN clot, to ~18 kPa in early GT and reaching levels of ~50 kPa in mature GT (Wells, 2013; Achterberg et al., 2014). Myofibroblasts appearance in the GT is hence linked to the increment in the overall wound stiffness and tension. Mechanical tension together with TGF-β1 signalling and the positive feedback created by FN deposition regulate fibroblast activation at the wound site (more detailed in Section 6).

5.3. The remodelling phase

It is the last and longest part of the healing process and can last from months up to years. It involves the remodelling of the epidermis, dermis and ECM. In this stage, regulatory mechanisms ensure that all cellular processes that had been activated start to slow down or silence and tissue develops the structure that will last in future. Invertebrates and lower vertebrates have the capacity to totally regenerate tissues and even complete parts of the body with the same structural and functional properties (Maden, 2018). This ability is conserved in early mammalian embryos (in rodents until around E16.5-18.5) but is progressively lost after birth or before the third trimester of gestation in humans, where regeneration is replaced by scarring and fibrosis (El Ayadi et al., 2020). In the epidermis, keratinocytes reach a proliferative peak when wound margins find each other at the wound centre. This is observed by an increment in the epidermal thickness in early closed skin wounds and it is progressively switched off reaching normal epidermal thickness at later times. In the GT, proliferation also decreases and ECM composition deposited by myofibroblasts changes. Collagen III is progressively replaced by collagen I that determines the final shape of the wounded skin (LeBert et al., 2015). Abundant FN deposited in the GT during the proliferation phase starts to disappear by the coordinated work of different metalloproteinases. Pathological healing observed in keloids and hypertrophic scars is characterized by a prolonged inflammatory phase that leads into an aberrant deposition of EMC proteins, such as collagen and FN. Once the wound is closed and cytokines signalling cesses myofibroblasts undergo apoptosis (Desmoulière et al., 1995). Some strategies to prevent aberrant scar formation have

been focused in accelerating myofibroblasts apoptosis in different tissues (Wells and Leung, 2020).

6. FN in skin wound healing

The role of the FN in wound healing has been studied for years. It is now clear its important implications in forming the platelet clot and shaping the GT ECM. Some indirect FN implications arose from animal models studying the wound healing process in FN-binding integrin knockouts. Impairment in healing is observed in mice with conditional depletion of β1 integrins in dermal fibroblasts, which leads to reduced α-SMA expression and GT formation due to diminished TGF-β1 release from ECM (Liu et al., 2010). FN stores TGF-β1 and hence it plays an important role in its activation. TGF-β1 is secreted by cells in an inactive form which is non-covalently bond to a latency-associated pro-peptide (LAP) that is covalently bond to the latent TGF-β binding protein (LTBP) forming all together the Large latent complex (LLC). LTBP binds cFN fibrils in the $FNIII_{12-14}$ region (Horiguchi and Rifkin, 2012). LAP has an RGD motif in its structure that binds αv-class integrins on one side and to the ECM through LTBP on the other side generating a perfect pulling axis (Fig. 10). *In vivo* experiments where either αv-LAP bond or LTBP binding to the ECM were blocked, produced similar defects to the TGF-β1 knockout mice phenotype, demonstrating its importance in TGF-β1 liberation into the ECM and hence in its activation (Yoshinaga et al., 2008; Henderson and Sheppard, 2013; Murray et al., 2017). TGF-β1 has to be released from LAP to be functional and bind cellular receptors. Upon wounding, GT myofibroblasts perform strong contractile forces on FN-containing ECMs via integrins allowing TGF-β1 release and thus activating fibroblasts creating a positive feedback (Wipff et al., 2007; Giacomini et al., 2012; Klinberg et al., 2014). This behaviour explains the gradual appearance of myofibroblasts along the healing process.

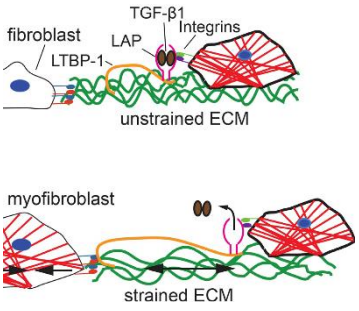

Figure 10. Mechanical activation of TGF-β1. TGF-β1 is secreted covalently bond to LAP and stored in the FN-containing ECM bond to LTBP-1. An RGD binding site in LAP structure allows αv-integrins attachment and hence cell binding. The contraction of myofibroblasts is transmitted to LAP inducing a conformational change that liberates TGF-β1. The overall increment in ECM fibrils alignment allows LAP to sense a cell-induced tension and hence to increase TGF-β1 activation inducing myofibroblasts conversion (Klinberg et al., 2014)

In early-deposited ECM, fibres have a high degree of freedom applying no resistance to pulling forces. Together with cell remodelling activity, collagen and FN start to align and provide great mechanical resistance that is linked with increase TGF-β1 activation and hence to myofibroblasts conversion (Achterberg et al., 2014).

TGF-β1 activates canonical Smad2/3 signalling pathway that induces expression of α-SMA in fibroblastic cells (Evans et al., 2003) (Fig. 11). Targeted genes that have been directly linked to TGF-β1/SMAD signalling pathway exert chemotactic and pro-mitotic activities essential during the inflammatory response and the GT formation. At later stages, TGF-β1 promotes FN synthesis and collagen deposition by fibroblasts (Heldin et al., 2009). TGF-β1 has a second increment wave during the proliferation phase that has been reported to contribute to the process of fibroblasts differentiation into myofibroblasts and hence in wound contraction (Desmoulière, 1993, Martinez et al., 2010).

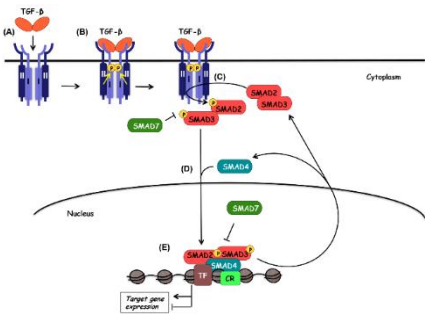

Figure 11. TGF-β/SMAD intracellular signalling pathway. A) TGF-β1 initially binds the heterodimeric complex of type I and II receptors. B) The growth factor binding starts a phosphorylation cascade that is initiated at the receptor level and it is transmitted to C) SMAD2 and SMAD3. D) Upon activation the complex binds the SMAD4 mediator and form a trimeric complex that translocates into the nucleus where it associates with E) DNA binding transcription factors in order to regulate the transcription of target genes (Tzavlaki and Moustakas, 2020).

III OBJECTIVES

Previous results from our laboratory demonstrated the relevance of the FN synergy site in reinforcing the engagement between α5β1/αIIbβ3-FN and the compensatory effects of αvβ3 class when the synergy site is non-functional. Mice lacking the FN synergy site require longer times to form a platelet plug in injured vessels, demonstrating the relevance of the synergy site in maintenance of platelet adhesion under high blood flow (Benito-Jardón et al., 2017). The principal objective of this PhD is to investigate the possible roles of the synergy site a biological process where cells are subjected to high tension such as the healing of cutaneous wounds. To that end, we studied:

A. The *in vivo* relevance of the FN synergy site in a mouse wound healing model using *Fn1*$^{syn/syn}$ mice and their wild type *Fn1*$^{+/+}$ littermates. For that purpose we analysed:

- The macroscopic wound closure in *Fn1*$^{+/+}$ and *Fn1*$^{syn/syn}$ mice during a period of 25 days after healing.
- The formation of the new epidermis in wounds collected from *Fn1*$^{+/+}$ and *Fn1*$^{syn/syn}$ mice at different time points.
- The GT formation studying cell proliferation, migration and myofibroblasts conversion in wounds from *Fn1*$^{+/+}$ and *Fn1*$^{syn/syn}$ mice at different time points.
- The neo-vascularization in the GT of wounds from *Fn1*$^{+/+}$ and *Fn1*$^{syn/syn}$ mice.

B. The *in vitro* relevance of the FN synergy site using cell types involved in the healing process and purified plasma FN (pFN) from *Fn1*$^{+/+}$ (pFN^{wt}) and *Fn1*$^{syn/syn}$ (pFN^{syn}) mice. We then analysed:

- Single-cell migration of wild-type keratinocytes migrating on plastic dishes or compliant substrates of different stiffness with pFN^{wt} or pFN^{syn} as substrate.
- Collective migration of wild-type keratinocytes on pFN^{wt} or pFN^{syn} as substrate in plastic dishes.
- Fibroblast migration in scratch assays with *Fn1*$^{+/+}$ and *Fn1*$^{syn/syn}$-derived immortalized fibroblasts.
- Conversion of dermal fibroblast to myofibroblasts using compliant substrates of different stiffness coated with pFN^{wt} or pFN^{syn}.
- Release of TGF-β1 from *Fn1*$^{+/+}$ and *Fn1*$^{syn/syn}$-ECMs assembled by dermal fibroblasts.

IV MATERIALS AND METHODS

1. Mouse strain

Fn1$^{syn/syn}$ mice were previously generated in our laboratory using gene targeting technique (Benito-Jardón et al., 2017). The synergy site function was disrupted by the substitution of the two arginines by alanines (R1374A and R1379A) in the sequence of the synergy site (DRVPPSRN). Briefly, constructed targeting vector (Fig. 12) was transferred by electroporation to embryonic stem cells (ESC) and neomycin resistant clones were selected and screened by Southern blot. Clones with the mutation were injected into mouse blastocysts with C57BL/6 background and chimeras with the neo^{+} allele carrying the synergy mutations were crossed with a deleter-Cre mouse strain to remove neo cassette flanked by two loxP sites.

Fn1$^{syn/syn}$ mice are viable and fertile. The strain was maintained in heterozygosis (*Fn1*$^{+/syn}$) to generate littermates with *Fn1*$^{+/+}$ and *Fn1*$^{syn/syn}$ genotypes for wound healing experiments and skin dermal fibroblasts (DF) isolation and for pFN purification from blood plasma (Section 6.2).

Mice used in our studies were housed in special pathogen free facilities and transferred to a conventional area for wound procedure and to follow the healing process. All mouse work was done according to the normative of Valencian Community Government (permission number: 2016/VSC/PEA/00070).

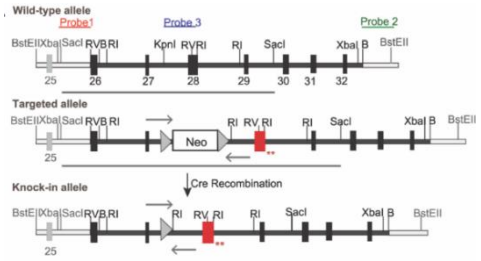

Figure 12. FN gene and targeting vector cartoon to generate transgenic mouse strain with inactivated synergy site function. The targeting vector consisted of a fragment containing exons 26 and 27, a neomycin cassette flanked by two loxP sites, a fragment with exon 28 which encoded the synergy site sequence carrying point mutations and a fragment with the exons 29 to 32. Grey arrows indicate forward and reverse allele for mouse genotyping. Picture modified from (Benito-Jardón et al., 2017).

2. Genotyping

Mice genotyping was done after DNA extraction from ear biopsies. Tissue samples were incubated with 500 µl of DNA extraction lysis buffer (1 M Tris-Base, 0.5 M EDTA, 20% SDS, 5 M NaCl) shacking overnight (o/n) at 55°C. Samples were centrifuged at 14000 rpm for 5 min and supernatant transferred to a new tube. For DNA precipitation, an equal volume of isopropanol was added and centrifuged for 5 min at 14000 rpm. Supernatant was discarded, DNA washed with 500 µl of cold 70% ethanol and centrifuged for 5 min at 14000 rpm. After centrifugation,

supernatant was discarded and tubes were left open on the bench for 10 min to allow ethanol evaporation. DNA was dissolved in 50 µl autoclaved water for 1 h at 55°C, shaking.

Polymerase chain reaction (PCR) was used for genotyping using the previous extracted DNA as template. PCR components were mixed as indicated in Table 1 and added to the DNA from each mouse.

DNA fragments were amplified in a thermocycler following the PCR protocol in Table 2. After amplification, DNA samples were separated in 2% agarose electrophoresis prepared in TAE (prepared from 50X, 50 mM EDTA, 2 M Tris-base, 1 M acid acetic glacial) buffer. Expected bands for wild type and mutant alleles are 300 bp and 400 bp (Fig. 13), respectively.

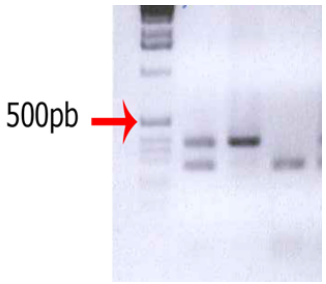

Figure 13. DNA bands after *Fn1*$^{+/+}$ and *Fn1*$^{syn/syn}$ samples amplification by PCR. Size differences are caused by the presence of loxP sequence in the mutant allele after recombination with Cre-deleter mice strain.

Table 1. PCR components used to prepare master mix for genotyping *Fn1*$^{+/+}$, *Fn1*$^{+/-}$ and *Fn1*$^{syn/syn}$ mice.

COMPONENT	**FINAL CONCENTRATION**
Reaction Buffer (15mM $MgCl_2$) (Uvat Bio)	1X
Forward Primer 5´-CCCGTTTTCACTCTCGTCAT-3´ Reverse Primer 5´-TCACAAGGAAACCAGGGAAC-3´	10 pmol
dNTPs (EurX)	0.25 mM
Taq Polymerase (Uvat Bio)	1X (0.05 units/µL)
Autoclaved MiliQ water	Up to 50 µl
gDNA	1-2 µl

3. Cell lines

The **keratinocyte** cell line used in our migration assays was kindly provided by Reinhard Fässler (Department of Molecular Medicine at Max Planck Institute of biochemistry, Munich). Primary

keratinocytes were isolated from wild type mice and immortalized spontaneously (Rognoni et al., 2014). Keratinocytes were grown in keratinocyte-growth medium (KGM, see details below, Culture Media and Buffers) on plastic dishes coated with 30 µg/ml collagen I (Purecol® 3 mg/ml, Advanced Biomatrix) and maintained in low Ca^{2+} concentration (0.45 µM $CaCl_2$) to avoid differentiation.

Fn1$^{+/+}$ and *Fn1*$^{syn/syn}$ **fibroblasts** used for scratch assays (Section 8.4) were isolated from embryonic mouse kidney and immortalized using SV40 large T antigen (Benito-Jardón et al., 2017). Once immortalized, cells were maintained in 10% FCS DMEM with 1% (v:v) penicillin-streptomycin.

Transformed mink lung epithelial cells (MLECs) kindly provided by Daniel Rifkin´s Laboratoy (Abe et al., 1994) were maintained in 10% FCS DMEM with 1% penicillin-streptomycin. These cells are transfected with a permanent expression vector containing the plasminogen activator inhibitor-1 (PAI-1) promotor truncated and fused with the gene reporter of luciferase. PAI-1 promoter has been described to be upregulated by the presence of TGF-β (Abe et al., 1994; Thalacker and Nilsen-Hamilton, 1994). MLECs were then used to measure active TGF-β in conditioned media using a luminescence reaction (Section 7.2).

Table 2. PCR protocol for mice synergy mutation genotyping.

STEP	Number cycles	TIME	TEMPERATURE (°C)
1. Initial Denaturation		5 min	95
2. Denaturation	30´	30 sec	95
3. Annealing		30 sec	58
4. Extension		45 sec	72
5. Final Extension		10 min	72
6. Holding stage		~	4

3.1. Dermal Fibroblasts isolation from mouse skin

Dermal fibroblasts (DF) were isolated from *Fn1*$^{+/+}$ and *Fn1*$^{syn/syn}$ mice. Mice were sacrificed using Isofluorane (Abbott) inhalation. Hair from the back was removed using a clipper and then skin wiped with 70% ethanol. Skin from the back was separated from muscle and fat tissue using scissors and forceps and deposited into autoclaved PBS (Phosphate Buffered saline tablets, Sigma-Aldrich). Samples were transferred under the hood and skin was then cut into small pieces of around 1 cm^2 of size. Skin pieces were deposited into 6-multiwell dishes to let them stick to the plastic for 5 minutes. Once attached, 10% FCS DMEM with 1% penicillin-

streptomycin was added to keep the explants feed but avoiding the complete coverage to avoid detachment from plastic wells. Medium was changed every two days unless it reached yellowish colour. DFs came out from skin between 3 and 10 days after skin isolation. When sufficient cells migrated out from the tissue, skin explants were removed and cells detached using trypsin. Cells were spin down and grown in plastic dishes to let them reach confluence. DF were used for myofibroblasts conversion on compliant substrates and TGF-β1 activation assays (Section 7.1 and 7.2).

4. Wound healing assays

Full thickness 6-mm diameter wounds (4 per animal) were made on the back of *Fn1*$^{+/+}$ and *Fn1*$^{syn/syn}$ 10-week-old females (6 mm Biopsy Punch, Stiefel Laboratories, Germany). Backs were shaved two days before wounding to synchronize hair follicles stage. Mice were injected with 0.3 mg/ml Buprecare (0.1 mg/kg body weight) as analgesic, 30 min before and 4% Isofluorane as anaesthesia during surgery. Analgesia was again administrated 4 h after surgery and hydrogel solution mixed with analgesic administrated for the following days. After surgery, mice were maintained in separated cages to avoid wound infections. Wounds were photographed immediately after wounding (t0) and at indicated time points after wounding. The initial photographed area was taken as 100% opening and referred to calculate the % of macroscopic wound closure.

5. Tissue processing and histological analysis

At 4, 7, 9, 15 and 25 days after wounding (daw), mice were killed and dorsal wounds were dissected and fixed for up to 48 h in 70% ethanol. Wounds were bisected through the centre following the direction of the hair and each half of the same wound was embedded in paraffin subsequently to a dehydration process (Table 3). Finally, samples were cut with a microtome to obtain sections of 4 μm thickness.

Table 3. Dehydration program and paraffin embedding.

PRODUCT	TIME (h)
70% Ethanol	1
96% Ethanol I	3
96% Ethanol II	1.5
100% Ethanol I	2
100% Ethanol II	6

Xylene I	1.5
Xylene II	2.5
Paraffin I	2.5
Paraffin II	2

For histological analysis, paraffin was removed using the following protocol. Samples were immersed in two consecutives xylenes of 10 min each. Then, samples were hydrated with decreasing ethanol concentrations (100 I, 100 II, 90, 80, 70, 50%), 5 minutes each. Finally, samples were washed with dH_2O and kept in PBS (prepared from 10X; PBS 1.37 M NaCl, 27 mM KCl, 100 mM Na_2HPO_4, 2 mM KH_2PO_4) before staining.

5.1. Haematoxylin and eosin staining

Sections were immersed for 5 min in Mayer´s solution (Sigma-Aldrich) for nucleus staining and washed out with running tap water for 5 min to eliminate the excess of solution. A 0.5% eosin solution (Sigma-Aldrich) in ethanol for 2 min was used for cytoplasm staining. Excess of dye was removed with tap water and then samples transferred to increasing concentrations of alcohols for 1 min (95, 100 I and 100% II) and cleared with xylene twice before mounted with water-free solution Entellan (Merck).

5.2. Masson´s trichrome staining

To quantify collagen deposition, wound samples were stained with Masson´s Trichrome Kit (Sigma Aldrich), consisting in: Weigert´s iron Haematoxylin, Biebrich´s Scarlet-Fucsin, Phosphotungstic-Phosphomolybdic acid and in Aniline Blue. The staining results in dark-blue nuclei, red cytoplasm and muscle fibres and light-blue collagen fibres. Nucleus were stained with Weigert´s iron Haematoxylin solution for 5 min and washed out in running tap water to remove excess of solution. Cytoplasm and muscle fibres were stained using a Biebrich´s Scarlet-Fucsin solution for 5 min and then rinsed with deionized water. To sharpen blue collagen staining, slides were first placed in a mixture (1:1) of two acids (Phosphotungstic-Phosphomolybdic acid solution) for 5 min and finally collagen stained with Aniline Blue solution for other 5 min. To obtain better blue staining slides were rinsed in 1% acetic acid for 2 min. The solution was discarded and samples washed with tap water before dehydration with ethanol (95, 100 I and 100% II). Before mounting, slides were briefly clear twice in xylene. Slides were mounted with water-free solution Entellan (Merck).

5.3. Immunostaining

5.3.1. Tissue Immunostaining

For tissue immunofluorescence (IF), sections were permeabilized after paraffin removal with 0.1% Triton-X-100 (Sigma-Aldrich) for 20 min and then blocked with 3% BSA (bovine serum albumin) in PBS for up to 30 min at RT to avoid unspecific binding. Samples were incubated o/n with primary antibody (Table 4) diluted in blocking solution (3% BSA and 0.01% Triton-X-100 in PBS) at 4°C inside a humid chamber. To eliminate unbound antibody slides were rinsed 3 times with PBS before incubation with secondary antibody for 1 h 30 min at RT in blocking solution. Excess of secondary antibody was washed out with PBS and nuclei stained with Hoechst (Thermo Fisher, 1:10000 in PBS) for 10 min washing out the excess with three consecutive PBS washes (Table 4). Slides were prepared for microscopy analysis with Gelvatol mounting media.

Antigen retrieval after paraffin removal was necessary for cytoplasmic and nuclear proteins (indicated in Table 4 as AR). Briefly, after paraffin removal slides were immerse in citrate buffer (10 mM citric acid, pH 6 and 0.01% Tween 20) and heated using the microwave at maximum power for 10 min to unmask epitopes. Slides were cooled down for about 15 min at RT and then washed with PBS. After antigen retrieval the above protocol was followed for blocking the sections and antibody incubation.

5.3.2. Cell immunostaining

For cells immunostaining, cells were cultured on glass coverslips, and fixed with 2 or 4% paraformaldehyde (PFA) in PBS for 10 min at RT. After fixation, excess of PFA was removed rinsing coverslips with 3 washes of PBS, 5 min each. Cells were permeabilized with 0.1% Triton-X-100 in PBS for 10 min at RT. Next, coverslips were blocked with 3% BSA in PBS for up to 30 min at RT to avoid unspecific binding and then incubated with primary antibody diluted in blocking solution o/n at 4°C in a humid environment. Unbound antibody was washed out from coverslips with 3 washes of PBS and then incubated with secondary antibody diluted in blocking solution for 1 h and 30 min at RT. Secondary antibody was eliminated with PBS washes and then coverslips incubated with DAPI (Thermo Fisher , 1:10000 in PBS) solution for 5 min at RT to stain the nuclei. Excess of DAPI was washed out with 3 washes of PBS shacking, and mounted with Gelvatol mounting media. Images were taken with a Confocal Laser Scanning Microscope Zeiss 780LSM and analysed with ImageJ.

Table 4. List of antibodies and staining with correspondent dilution used for different techniques.

Antibody	Distributor	Technique/Working Dilution
Rabbit anti-mouse Fibronectin	Millipore (AB2033)	WB 1: 10.000 IF 1: 1.000
Rabbit anti-mouse krt-6	Covance (PRB-169P)	IF 1: 500 (AR)
Rabbit anti-mouse krt-14	Covance (PRB-160P)	IF 1: 500 (AR)
Mouse anti-α-SMA-Cy3 Conjugated	Sigma-Aldrich (C6198)	IF 1: 500
Chicken anti-mouse Paxillin	BD Transduction Laboratories TM	IF 1: 300
Rabbit anti-mouse p-His H3	Upstate (16-189)	IF 1: 300 (AR)
Rabbit anti p-Smad2/3 (Ser465,Ser467)	Thermo Fisher (MA5-15122)	IF 1:300 (AR)
Rabbit anti-Ki67	Abcam (ab238020)	IF 1:200 (AR)
Rabbit anti- α5 integrin	Abcam (ab150361)	IF 1:200
Rhodamine Phalloidin	Thermo Fisher (R415)	IF 1:500
Phalloidin Alexa Fluor™ 488	Thermo Fisher (A12379)	IF 1:500
PE rat anti-α5 integrin	Pharmingen (557447)	FC 1:200
PE hamster anti β3 integrin	BD Bioscience (12-0611)	FC 1:200
Anti-rabbit Alexa Fluor™ 488 (secondary)	Thermo Fisher (A32731)	IF 1:200
Anti-rabbit Alexa Fluor™ 647 (secondary)	Invitrogen (A32728)	IF 1:200

6. FN purification from mouse blood plasma

6.1 Plasma isolation from blood

To purify FN from plasma, blood was extracted from *Fn1*$^{+/+}$ and *Fn1*$^{syn/syn}$ mice as follows (permission ref 2016/VSC/PEA/00215). Mice were anesthetized with Isofluorane and blood was taken from the tear duct using non-heparinized capillary previously treated with 0.5 M EDTA to avoid blood coagulation. Plasma was then separated from the cellular part by centrifugating at 4°C for 20 min at 3000 rpm. After centrifugation, the plasma in the

supernatant was collected into a new tube. After a second centrifugation was necessary and supernatant was again collected and stored at -80°C until FN purification.

6.2 Fibronectin purification from plasma (pFN)

The collagen/gelatine binding site along the FN structure is used for FN purification using an affinity chromatography column made of Gelatine-Sepharose bed column (GE Healthcare Life Science). The Gelatine-Sepharose was first packed and equilibrated with TBS (0.15 M NaCl in 10 mM Tris-HCl, pH 7.4). Gelatin-Sepharose and plasma were incubated together (1: 3 ratio) o/n at 4°C in a rotator at 3 rpm to allow FN binding in a long incubation. After incubation, the bed column was placed in a plastic column and FN-free plasma was eluted and stored at 4°C until the end of the purification (Fig. 14A post-column incubation fractions). Several washes of 0.5M NaCl 10 mM Tris-HCl pH 7.4 and TBS buffer were used to avoid the presence of unspecific or FN bound proteins in the purified FN (Fig. 14A 0.5M NaCl and TBS fractions). Next, Sepharose was incubated with 4M urea in TBS for 1 h at RT rotating and poured into the column. Urea eluates containing pFN were collected in 1 ml fractions for up to 20 fractions (Fig. 14A pFN fractions). Occasionally, to avoid missing fractions with protein, A_{280} was measured to detect the presence of protein in the fractions until an absorbance of zero is reached. The presence and purity of pFN in the fractions was tested by Comassie staining (0.1% Brilliant Blue R (Sigma), 50% methanol, 10% acetic acid) in 8 % SDS-PAGE gels. Selected pFN fractions were mixed and dialyzed for 16 h against TBS using dialysis tubes (SERVA) and changing TBS buffer each 8 h. After dialysis, the purity and concentration of FN was confirmed by Comassie and Western blot, respectively. For Comassie staining, BSA with different concentrations was used for unwanted proteins testing. On the other hand, commercial FN with known concentration was used in a western blot to confirm the absence of protein degradation and for FN concentration calculation using ImageJ program (detailed below Section 11.6). Protein was aliquoted and stored at -80°C until required.

Gelatin-Sepharose was regenerated with 8M urea and repeated TBS washes and finally stored at 4°C in 0.05% sodium Azide in TBS.

7. Foetal calf serum preparation

7.1 FCS fibronectin-depleted

To avoid calf wild type FN contamination in our experiments, serum was depleted from FN using the same affinity columns as for FN purification. In this case, 100 ml of fetal calf serum (FCS) were incubated with 7 ml Gelatine-Sepharose o/n at 4°C rotating at 3 rpm. Serum FN-

depleted was collected through the column under sterile conditions and an aliquot was kept to confirm the absence of FN by Western blot. The column was then regenerated with 8M urea in TBS (prepared from 10X of 1.5 M NaCl, 100 mM Tris-base, pH 7.4) and washed with TBS before storage.

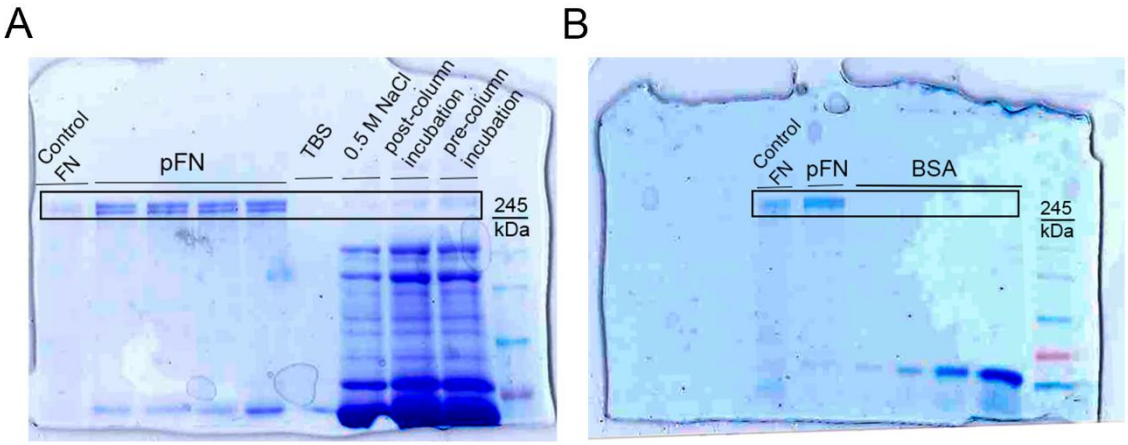

Figure 14. pFN purification from *Fn1*$^{+/+}$ and *Fn1*$^{syn/syn}$ mice. A) Coomassie blue staining of plasma aliquots before and after overnight incubation with gelatine bed column. Column eluates after 0.5M NaCl and TBS washes with. pFN eluate using 4M Urea. Commercial pFN is used as a control in a concentration of 50 µg/ml. B) Coomassie blue staining of purified pFN after dialysis. Commercial pFN control (50 µg/ml) and BSA in a concentration of 20, 10, 5 and 2.5 µg/ml.

7.2 FCS chelation

As calcium induces keratinocytes differentiation, the FCS used for preparing KGM was previously chelated using the resin Chelex 100 (Bio-Rad). To this end, Chelex beads were suspended in PBS to a final concentration of 40 g/ml adjusted to pH 7.4. Beads were then washed with 1L of miliQ water by filtration through a filter paper using a Bucher funnel (VWR) and then mixed with FCS (20 g Chelex/50 ml FCS) o/n at 4°, stirring. Chelated FCS was collected by filtration and Ca^{2+} levels measured using the *Calcium Assay kit* (Bioassay Systems), finally FCS was filtrated to avoid contaminations and stored at -20°. Resin was regenerated with 1M HCl first and next with 1N NaOH for 30 min stirring, washed 4 times with miliQ water by filtration in between the HCl and NaOH washes. Once regenerated, resin was dissolved in miliQ water, autoclaved and stored at 4°C.

8. Dermal fibroblasts (DF) assays

8.1 DF conversion into myofibroblasts in compliant surfaces

For DF conversion assays, commercial polyacrylamide (PA) gels were used (Matrigen softwell, 35 mm dish, 20 mm glass bottom, soft view, easy-coating hydrogels of 4 and 50 kPa, Cell

Guidance Systems) in order to obtain similar wound healing rigidities. After DF isolation from mouse skin, cells were maintained in 10% FCS DMEM with 1% penicillin-streptomycin. Cells medium was removed and two PBS washes were done before adding 10% FN-depleted FCS medium for 24 hours. Cells were then trypsinized and centrifuged before seeding onto PA gels. Gels were previously coated with 10 µg/ml pFN^{wt} or pFN^{syn} for 90 min at RT and then blocked with 3% BSA for 30 min. Cells were allowed to attach for 24 h to compliant substrates and then stained for F-actin and α-SMA (Section 5.3.2). Percentage of myofibroblasts was calculated as the number of $\alpha\text{-SMA}^{+}$ cells related to the total number of nucleus per picture. For each biological replicate DFs were extracted from different $Fn1^{+/+}$ and $Fn1^{syn/syn}$ mice. Statistical significance was calculated from the three different replicates per rigidity and analysing around 15 pictures per replicate.

8.2 TGF-β1 bioassay

This bioassay is based on the capacity of TGF-β to up-regulate genes under the PAI-1 promotor (Abe et al., 1994). MLECs were used to quantify active TGF-β released by $Fn1^{+/+}$ and $Fn1^{syn/syn}$ DFs into the culture media. Wild type or mutant DFs were seeded onto 96-well plates (5×10^3 cells/well) previously coated with 10 µg/ml pFN^{wt} or pFN^{syn}. Cells were allowed to attach and form a mature ECM for 3 days in 1% FN-depleted FCS medium. After 3 days, conditioned media from DFs were collected and added to 96-well plate containing MLECs (2.5×10^4 cells/well). MLECs were previously grown in 0.1% BSA serum-free medium for 4 h. MLECs were incubated for further 14 h in DFs conditioned medium. Total levels of TGF-β1 were assessed by heating half of collected DFs conditioned media for 5 min at 80°C (Abe et al., 1994). The other half was added directly to MLECs to measure active TGF-β1. To calculate the percentage of cells-activated TGF-β1, the amount of active TGF-β1 was related to the amount of total TGF-β1 obtained from the same heat-activated medium. After the incubation, cells were lysed and the luciferase activity was calculated by the production of light (Luciferase Assay System Kit, Promega) measured with a luminometer. Statistical significance was calculated with average data from three biological replicates coming from 2-3 technical replicates per condition.

9. Migration assays

9.1 Single-cell migration assays

For single cell migration experiments *Culture-Insert 2-well Self-Insertion* (Ibidi) were used to create a gap similar to the wound. 24-well plates were previously coated with pFN^{wt} or pFN^{syn} (10 µg/ml solution) for 90 min at 37°C and excess of protein was washed out with PBS washes.

Free-coating spaces were blocked with 3% BSA in PBS for 30 min at RT to avoid not specific binding. Blocking solution was removed with two PBS washes and, plastic wells were dried for 10 min under the hood before Ibidi-device insertion.

Cells were grown o/n in KGM with 10% FN-depleted FCS. For migration assays, cells were trypsinized using powder trypsin 0.4 g/100 ml in PBS (Gibco), centrifuged in serum-free medium for 5 min at 890 rpm and suspended in 1 ml of FN-depleted medium. 7.5 x 10^4 cells were seeded inside each culture-insert and allowed to adhere for 5 h. Culture-Inserts were removed and cells allowed to migrate and fill the gap. Migration was recorded with Zeiss Axiovert microscope and VisiView (Visitron System) software, taking one picture every 5 min. For statistical analysis three different replicates were performed (more detailed in Section 11.3).

9.2 Random single cell migration on PDMS gels

For migration assays, PDMS gels of different stiffness were used (Ibidi µ-Dish 35 mm, high ESS) using 1.5, 15 and 28 kPa gels for keratinocytes seeding. Plasma treatment was used to activate PDMS gels hydrophobic surface for 10 min before coating with pFN^{wt} or pFN^{syn} (10 µg/ml) for 1 hour at RT. Three consecutive PBS washes were performed to wash out the excess of coating. Cells were then counted and 4 x 10^4 were seeded in each 35 mm dish (low concentration) to allow random cell migration using KGM with 8% FN-depleted serum. Migration was recorded with a Zeiss Axiovert microscope and VisiView (Visitron System) software, taking one picture every 15 min. For statistical analysis three different replicates were performed per stiffness (more detailed in Section 11.3).

9.3 Collective migration assays

For collective migration experiments Culture-Insert 2-well Self-Insertion (Ibidi) were used following the same protocol as Section 8.1. After centrifugation, cells were resuspended with KGM 8%-FCS FN-depleted with 1.5 mM $CaCl_2$ to allow cell-cell adhesions. 4 x 10^4 cells were seeded per culture-insert well and cell-cell interaction were let to form in an o/n incubation. Culture insert was removed and cells allowed to migrate covering the gap. Migration was recorded with GE Healthcare IN CELL ANALYZER 2000, taking pictures every 10 min.

Proliferation inhibitor (Cytosine β-D-Arabinofuranoside, 40 µM; Sigma Aldrich) or cytoskeleton contraction inhibitor (Blebbistatin, 2 µM; Sigma Aldrich) were added to FN-depleted medium before starting the experiment and kept during the migration process.

9.4 Scratch assay

For scratch assays, glass coverslips were coated with laminin (10 µg/ml) 1 h at 37°C. Excess of laminin was removed with 3 washes of PBS and then free-coating spaces were blocked with 3% BSA in PBS for 30 min at RT. *Fn1*$^{+/+}$ and *Fn1*$^{syn/syn}$ fibroblasts growing on DMEM 10%-FCS with 1% penicillin-streptomycin were trypsinized and seeded with 9% serum replacement medium (SRM) (6.5% AIM-V, 5% RPMI and 1% Non-Essential Amino acid Solution) 1% FN-Depleted FCS and 90% DMEM. Cells were trypsinized, centrifuged and seeded (3.5 x 10^5 cells/coverslip) on previously prepared laminin-coated coverslips in SRM medium. After 5 hours incubation, the αv-blocker Cilengitide (10 µM) was added to the cells for 2 h and washed it before inducing the scratch. In parallel, untreated cells were kept in SRM without Cilengitide as control. Cells were then let to form a monolayer and scratch was performed after 24 h of cell seeding.

Migration was recorded with GE Healthcare IN CELL ANALYZER 2000, taking one picture every 15 min.

10. Surface integrin profile analysis by flow cytometry

Cells were detached with trypsin, centrifuged with 10% FCS DMEM medium to inactivate trypsin and resuspended in 3% BSA in PBS to count them. Around 5 x 10^5 cells were placed in a tube, centrifuged and resuspended in 200 µl of FACS Buffer (3% BSA in TBS). Cells were distributed in round bottom 96-welll dishes. The 96-well dish was centrifuged and cells subsequently resuspended in FACS buffer with primary antibody solution (dilution 1: 200 in FACS Buffer). Incubation with primary antibody (Table 2) was allowed for 1h on ice. To wash excess of primary antibody cells were centrifuged twice and washed with FACS buffer. In case the primary antibodies were non-labelled, cells were resuspended in secondary antibody dilution (1:200 in FACS buffer) and incubated 30 min on ice. Unbound antibodies were washed out by two consecutives centrifugations and FACs buffer washes. Finally, cells were resuspended in 300 µl FACS buffer and analysed with a FACS Canto (BD Bioscience) flow cytometer. Integrin profile was done using 3 technical replicates, plus non-stained cells and isotype control for each antibody.

11. Protein analysis by western blot

11.1 Protein extraction

Proteins were extracted from cells in culture or tissue sample lysates. For cell protein extraction, 150 µl cold-RIPA buffer (500 mM Tris-Base (pH 7.4), 1 % NP-40, 0.5 % sodium deoxycholate, 1 mM EDTA, 0.1 % SDS) was added to each well of 12-well plate. Multiwell was

placed on ice for 15 min. Cell lysates were collected into a tube using a pipette tip or a scraperand centrifuged at 10.000 x g for 10 min at 4° C and supernatant collected for protein quantification.

11.2 Protein concentration measurement

Protein concentration was quantified using BCA Protein Assay Kit (Thermo Scientific). BSA dilutions in RIPA-buffer were used to prepare standards with known protein concentration (2, 1.5, 1, 0.5, 0.25 mg/ml). Working reagents were mixed following manufacture instructions in a 96-well plate and then BSA standards and the protein samples were added to each well in two replicated. Protein concentrations were quantified measuring A_{562} in a spectrophotometer.

11.3 Immunoblot

Cell lysates were resuspended in 5X Laemmli buffer (60 mM Tris-base pH 6.8, 2% SDS, 5% Glycine, 0.01% Bromophenol blue and 2 % β-mercaptoethanol), heated at 95°C for 5 min and used immediately or stored at -20°C. For immunoblot, 50 µg of protein were separated in 12% or 8% SDS-PAGE gels under reducing conditions in blotting buffer (250 Mm Glycine, 25 mM Tris-Base, 20% methanol). Proteins were transferred to a PVDF membrane (Amersham, GE Healthcare), at 100 V for 90 min at 4°C. Membranes were blocked with 3% skim milk (Sigma) in TBS-T (TBS 1X, 0.1% Tween 20) for 1h at RT or with 3% BSA in TBS-T for phosphorylated proteins. Membranes were incubated with primary antibodies diluted in blocking solution o/n at 4°C. Unbounded antibodies were washed out shacking in TBS-T. Membranes were incubated with secondary antibodies labelled with horseradish peroxidase (HRP) for 90 min at RT and washed with TBS-T before incubating with Immobilon Western HRP Substrate (Millipore). Proteins were detected using an Imaging Systems (Biorad) developer using auto-exposure option for best signal.

12. Image analysis with ImageJ

12.1 GT and epidermal thickness analysis

For the GT area and epidermal thickness quantification H&E images were used. GT was measured, when visible, in the two different parts of each wound and then the mean value was calculated to minimized wound preparation differences. GT was considerate to be the area underneath the epidermis and in between the two sides of adipose tissue. For epidermal thickness quantification, in open wounds, the measurement was made on the two sides of the wounded epidermis and in both wound parts. The thickness was measured in the furthest part

of the epidermal tongue from the edge of the wound. In closed wounds, when the two parts of the epidermal tongue were fused, three different measurements along the epidermis were made and then mean value was calculated for both wound sides.

12.2 Fluorescence Images Analysis

To measure the area covered by α-SMA and FN in the GT of wounds the following process was followed. Stained wounds were photographed using a Widefield Leica fluorescence microscope from one edge of the wound to the other and then merged using Photomerge tool in Photoshop to generate a view of the whole wound. Images from complete wounds were opened with ImageJ, converted to 8-bit and GT area delimited with freehand selector tool. GT was considered as the dermic part under the migrating keratinocytes including the centre of the wound but excluding adipose tissue from the selection. First GT area was delimited for each wound: *edit< clear outside < analyse < measure*. To measure the fluorescence in the total GT area, images were converted to binary by *image < adjust < threshold* followed by *analysis < analyse particles*, selecting particle size from 0-infinity. The total area obtained in a new window was considered as the wound area covered by the stained protein. Threshold was not adjusted as all pictures were taken previously with the same settings.

12.3 Cell Migration Analysis

For the analysis of keratinocyte migrations the Manual Tracking plug-in was used to record cell paths. Time-lapse images were taken every 5 or 10 min for single-cell or collective migration, respectively and every 15 min for scratch assays migration. Frames from 4-6 different areas of the open-gap created by the insert or scratch were photographed per condition. From each biological replicate, between 6 and 10 different cells were tracked from each recorded area. Information was then loaded to the Chemotaxis tool of ImageJ. This plug-in was used to calculate the average speed, directionality and distance of all cells tracked in each area.

12.4 Nuclear markers analysis

To quantify positive cells for nuclear markers we used ImageJ program. First, the area of interest (dermis, epidermis etc) was delimited and measured using the freehand selector tool. Next, we follow the next steps: *image < adjust < threshold* followed by *analysis < analyse particles*, selecting particle size from 0-infinity.

12.5 Masson´s trichrome staining analysis

Collagen deposition was analysed in wounds stained with Masson´s trichrome staining. To measure the area covered by collagen fibres images were opened with imageJ, converted to RGB (Image< type< RGB colour) and processed using Colour Deconvolution tool in "Plugins" menu, selecting Masson´s Trichrome option in the new window. This plugin deconvolves images into red, blue and green component; being the bluish-colour window the collagen component. The area of the blue collagen fibres was measured following the same steps as with fluorescence images. Briefly, first the GT area was delimited and crop from the rest of the wound, threshold was adjusted the same for all images and collagen area was calculated using analyse particles tool in analyse menu.

12.6 Protein quantification.

For pFN protein quantification, the new purified pFN was loaded in a SDS-PAGE together with three other known concentrations of commercial FN (5, 10 and 20 µg/ml). Western Blot image was uploaded in ImageJ program. Image was converted to a grey-scale using the method *Image>Type>8-bit.* Next, Rectangular Selections from the toolbar were used to draw a rectangle around the first lane. Next, the rectangle was set on place selecting *Analyse>Gels>Select First Lane.* The process was repeated for all bands as followed *Analyse>Gels>Select Next Lane.* The profile for each band was then calculated selecting Analyse>Gels> Plot Lanes. Using the Straight Line from the toolbar, a line was drawn across the base of each peak to enclose it and then using the Wand tool to select the inside peak which represents the relative density of each band. Once all peaks were enclosed and highlighted, the area of each one was calculated as *Analyse < Gels < Label Peaks*. The pFN concentration was then calculated relative to the area of each peak and the already known concentrations.

12.7 Focal Adhesions Quantification

To quantify the size and number of FA, keratinocytes were seeded on collagen I (30 µg/ml Purecol® 3 mg/ml, Advanced Biomatrix), pFN^{wt} or pFN^{syn} and stained for paxillin and F-actin following steps in Section 5.3.2. Between 10 and 12 pictures for each condition were taken using a confocal microscope. Cell area and number or size of FA were measured for around 2-3 cells for each picture. The area was measured using phalloidin-channel with the drawing toll to cover the whole cell area. The size and number of focal adhesions were measured using the paxillin channel and following the next steps, selecting cell area with *Polygon Tool > Edit > Clear Outside < Image < Adjust < Threshold < Size particles 0.05-infinty < Measure*.

12.8. FN fibrils analysis

After scratch assay, cells migrating on glass coverslips for 20 h were fixed and stained following steps in section 5.3.2. FN staining was used to observe and analyse the new fibrils assembled by fibroblasts to migrate and cover the scratch gap. FN quantification was performed using Skeleton plug from ImageJ programme. To measure the FN fibrils, the immunostained FN area was measured and normalized to the total area and cell number in each image. To quantify the number of branches, images were set to binary and same threshold was applied to all of them, follow by despeckle function to remove background and next with skeleton pluging. The amount of FN fibres and braches was normalized to the image area. 4 images were analysed per condition and distinct areas were analysed from the scratch gap.

13. Statistical analysis

All the experiments, unless indicated were done using 3-4 independent biological replicates and independently processed. Results represented as mean ± standard error of the mean (SEM). Statistical analysis was performed by Student´s t-test for independent or paired parametric data and Mann Whitney U test was used for independent non-parametric data. A p-value less than 0.05 was considered statistically significant.

Culture media and Buffers

Keratinocyte-Growth Medium (KGM);

PRODUCT	**END-CONCENTRATION**
MEM	500 ml
Insulin (Sigma)	5 µg/ml
EGF (Sigma)	10 ng/ml
Transferin (Sigma)	10 µg/ml
Phosphoethanolamine (Sigma)	10 µM
Ethanolamine (Sigma)	10 µM
Hydrocortisone (Calbiochem)	0.36 µg/ml
Glutamine (Invitrogen)	1X
Pen/Strept (Invitrogen)	1X
Chelated FCS	8%
$CaCl_2$	45 µM

Fibroblasts Medium: DMEM with 10% FCS and 1% penicillin-streptomycin

SRM: 6.5% AIM-V, 5% RPMI and 1% Non-Essential Amino acid Solution

PBS: 10X 1.37 M NaCl, 27 mM KCl, 100 mM Na_2HPO_4, 2 mM KH_2PO_4.

TBS 10X: 1.5 M NaCl, 100 mM Tris-base, pH 7.4

TBS 10X (FN purification) : 0.15 M, 10 mM Tris-Base, pH 7.4

TBS-T: TBS 1X, 0.1% Tween 20

Purification washing buffer: 0.5M NaCl 10 mM Tris-HCl pH 7.4

TAE buffer: 50X 50 mM EDTA, 2 M Tris-base, 1 M acid acetic glacial

FACS buffer: 3% BSA in TBS

Laemmli buffer (LB): 60 mM Tris-base pH 6.8, 2% SDS, 5% Glycine, 0.01% Bromophenol blue and 2 % β-mercaptoethanol.

RIPA buffer: 500 mM Tris-Base (pH 7.4), 1 % NP-40, 0.5 % sodium deoxycholate, 1 mM EDTA, 0.1 % SDS. Before using buffer was supplemented with proteinase inhibitors (Complete proteinase inhibitor cocktail tablet, Roche)

DNA lysis buffer: 1 M Tris-Base, 0.5 M EDTA, 20% SDS, 5 M NaCl. 10 ng/ml Proteinase K was added to the solution before using it.

Commasie staining solution: 0.1% Brilliant Blue R (Sigma), 50% methanol, 10% acetic acid

Commasie destaining solution: 40% methanol, 10% acetic acid

Citrate buffer: 10 mM citric acid, pH 6 and 0.01% Tween 20

Blotting buffer: 250 Mm Glycine, 25 mM Tris-Base, 20% methanol

Blocking solution: 3% BSA and 0.01% Triton-X-100 in PBS

V RESULTS

I *In vivo* skin full-thickness wound repair in FN synergy site deficient mice

1. Macroscopic dermal wound closure in *Fn1*$^{syn/syn}$ mice

To study the consequences of the FN synergy site inactivation (*Fn1*$^{syn/syn}$), we used a mouse model of skin wound healing. To this end, full-thickness 6-mm diameter excisional wounds (day 0) were generated in the back skin of wild type (*Fn1*$^{+/+}$) and mutant (*Fn1*$^{syn/syn}$) mice littermate and the wound closure and tissue regeneration were analysed. Macroscopic wound closure was followed in both genotypes at 0, 4, 7, 9 and 15 days after wounding (daw) (Fig. 15A). To this end, the wounded area was measured and the wound closure was calculated relative to its size at day 0 (Fig. 15B). As shown, at 4 daw the mean wound size is reduced to about 66% and 59% of its initial area in, with a significant increase of wounded area in *Fn1*$^{syn/syn}$ mice compared to *Fn1*$^{+/+}$ mice. This difference is not significant in the following days and at 9 daw almost all wounds are macroscopically closed and a mild, but not significant, delay in wound closure is observed in *Fn1*$^{syn/syn}$ mice. These results point that apparently the absence of the FN synergy site would be affecting the first healing stages.

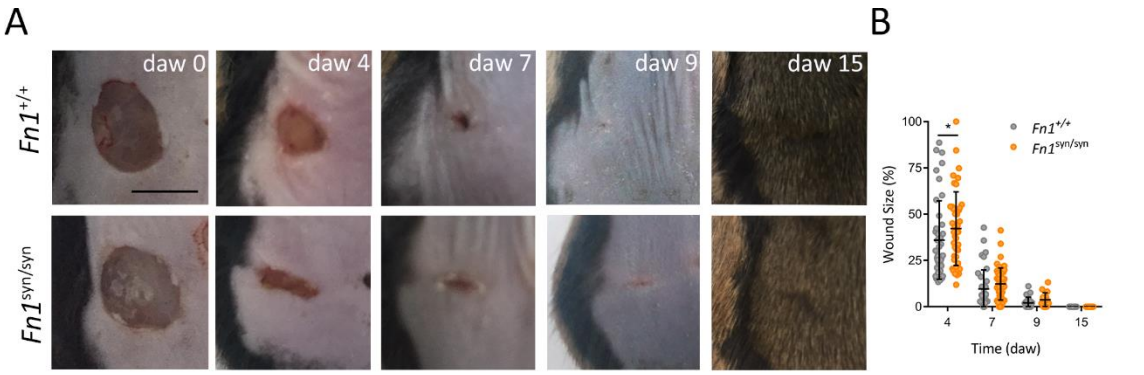

Figure 15. **Macroscopic aspect and analysis of wounded areas in the back skin of *Fn1*$^{+/+}$ and *Fn1*$^{syn/syn}$ mice.** (A) Representative images from *Fn1*$^{+/+}$ and *Fn1*$^{syn/syn}$ mice back wounds at 0, 4, 7, 9 and 15 days after wounding (daw). (B) Analysis of wounds size calculated as the wound area at each time point referred to its area at day 0. n= the number of wounds analysed in *Fn1*$^{+/+}$, *Fn1*$^{syn/syn}$ respectively, at the mentioned time point. n=57, 62 (0 daw); n=40, 41 (4 daw); n= 38, 47 (7 daw); n=21, 18 (9 daw); n=12, 12 (15 daw). Lines in the scatter plot represent the mean values and error bars represent the SEM value. Scale bar 0.5 cm.

2. Re-epithelialization analysis in wounds from *Fn1*$^{+/+}$and *Fn1*$^{syn/syn}$ mice

Re-epithelialization is the term used to describe the replacement of an injured epidermis by a new one after trauma. In full-thickness wounds, re-epithelialization occurs by the replacement

of lost cells by migrating keratinocytes that cover the wound gap together with the contribution of proliferative epidermal cells (Headon et al., 2017). Recent studies have identified two different epidermal zones that contribute differently to re-epithelialization (Aragona et al., 2017). At the wound edge, keratinocytes are characterized by rapid cell migration and the absence of cell division. The more distal part is characterized by high cell proliferation and very little migratory activity (Fig. 16) (Park et al., 2017).

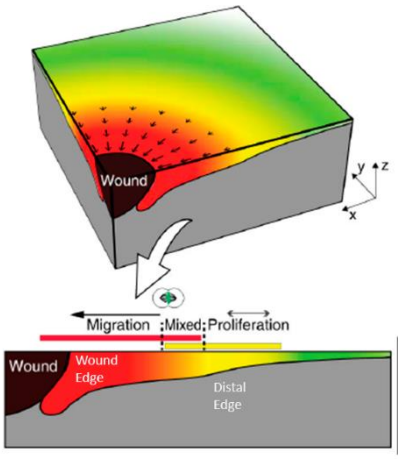

Figure 16. Contribution to epidermal re-epithelialization after skin injury. Keratinocytes located in more distal wound parts are characterized by high proliferation rates and low migration rates. By contrast, as keratinocytes get closer to the wound edges are rapidly adapted to initiate migration upon injury (modified picture from Aragona et al.2017)

2.1. Histological epidermal analysis of wounds from *Fn1*$^{+/+}$ and *Fn1*$^{syn/syn}$ mice

To analyse the skin morphology during the healing process, wounds from *Fn1*$^{+/+}$ and *Fn1*$^{syn/syn}$ mice were dissected at different time points, fixed and paraffin embedded. Sections of the central part of the wound were haematoxylin and eosin (H&E) stained at different healing stages (Fig. 17A). For restoring the epidermal layer, a tongue of keratinocytes initiates a process of migration on a provisional ECM composed primarily by fibrin and FN.

In order to study how the FN synergy site contributes to epidermal barrier restoration, different parameters were measured in wounds from *Fn1*$^{+/+}$ and *Fn1*$^{syn/syn}$ mice at different time points. Epidermal thickness was measured at all-time points in both genotypes (Fig. 17B). At 4 daw the epidermal thickness was measured for the epidermal tongue as wound closure was still not achieved. No significant differences are observed in epidermal thickness during early stages, although at 9 and 15 daw the epidermis from *Fn1*$^{syn/syn}$ wounds is significantly thinner compared to *Fn1*$^{+/+}$ wounds, it reaches again similar values at 25 daw (Fig. 17B). The wound length was then measured at all time points from *Fn1*$^{+/+}$ and *Fn1*$^{syn/syn}$ wounds as shown in Fig 17C, and no significant differences are observed. Using the wound length value for each wound, the percentage of wound re-epithelialization and epidermal tongue migration were then calculated at 4 and 7 daw (Fig. 17E and 17F) (Sanchis et al., 2012). No differences are

observed in any of them. All these results together point that the advance of the keratinocyte tongue during the wound healing is not affected by the inactivation of the FN synergy site.

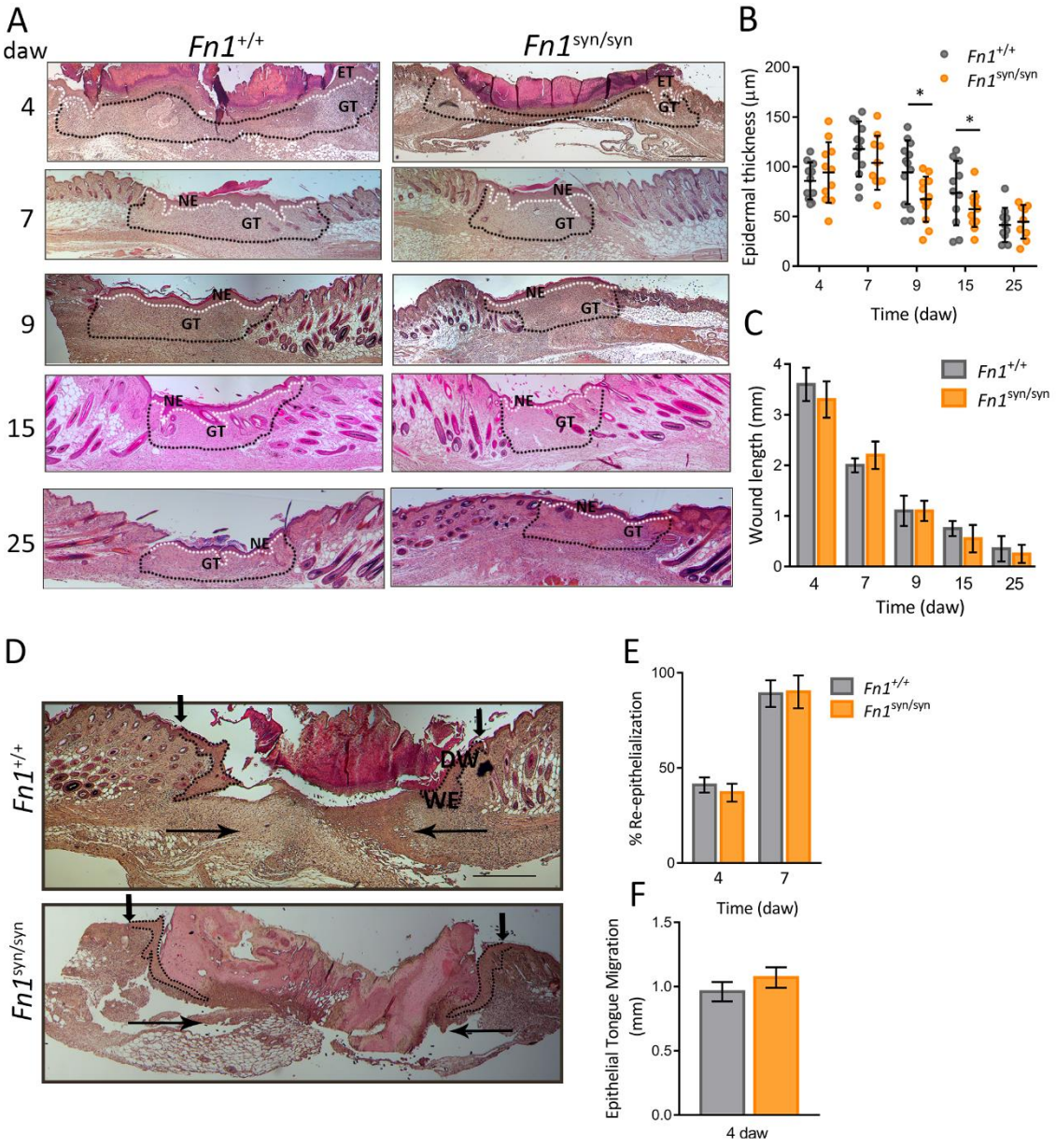

Figure 17. Analysis of *in vivo* cutaneous wound healing in mice expressing fibronectin with the synergy site inactivated. (A) Representative H&E images from wounds at the different time points in *Fn1*$^{+/+}$ and *Fn1*$^{syn/syn}$ mice. The granulation tissue is indicated with black dotted lines. (B) Sectional epidermal thickness quantification using H&E staining at each time point in *Fn1*$^{+/+}$ and *Fn1*$^{syn/syn}$ wounds. (C) Quantification of the cross-sectional wound length measured in H&E images as the distance between wound edges at the different time points [n= 12, 12(4) n= 14, 14(7) n=11, 11(9) n=10, 12(15) n=10, 10(25)]. D) Representative images from epidermal wound closure at 4 daw in *Fn1*$^{+/+}$ and *Fn1*$^{syn/syn}$ wounds. (E) Percentage of re-epithelialization in *Fn1*$^{+/+}$ and Fn1$^{syn/syn}$ wounds measured as covered distance by ET (thin arrows in D) *100/distance between original wound edges [n=11, 11(4) n= 14, 14(7)]. (F) Quantification of the distance (mm) covered by the ET from the original wound edge at 4 daw in *Fn1*$^{+/+}$ and Fn1$^{syn/syn}$ wounds [n=11, 11(4)]. If possible, the distance was calculated as the mean of both wound sides. Values are

shown as mean ± SEM. Statistical significances were calculated using Student t-test with p-value * p<0.05. ET; epidermal tongue, NE; neo-epidermis, GT; Granulation tissue, WE; wound edge, DW; distal wound. Scale bar 200 µm.

2.2. Analysis of keratinocyte activation in wounds from *Fn1*$^{+/+}$ and *Fn1*$^{syn/syn}$ mice

Upon wounding, keratinocytes withdraw from terminal differentiation and undergo changes in proliferation and gene expression referred as "keratinocyte activation". This activation triggers cytoskeletal rearrangements such as expression of new keratin patterns that allow keratinocytes to develop a migratory phenotype. In order to evaluate the FN synergy site function in keratinocyte activation during wound re-epithelialization, keratin-14 (K14) was analysed as basal keratinocyte marker and keratin-6 (K6) expression for suprabasal keratinocytes (Fig. 18A).

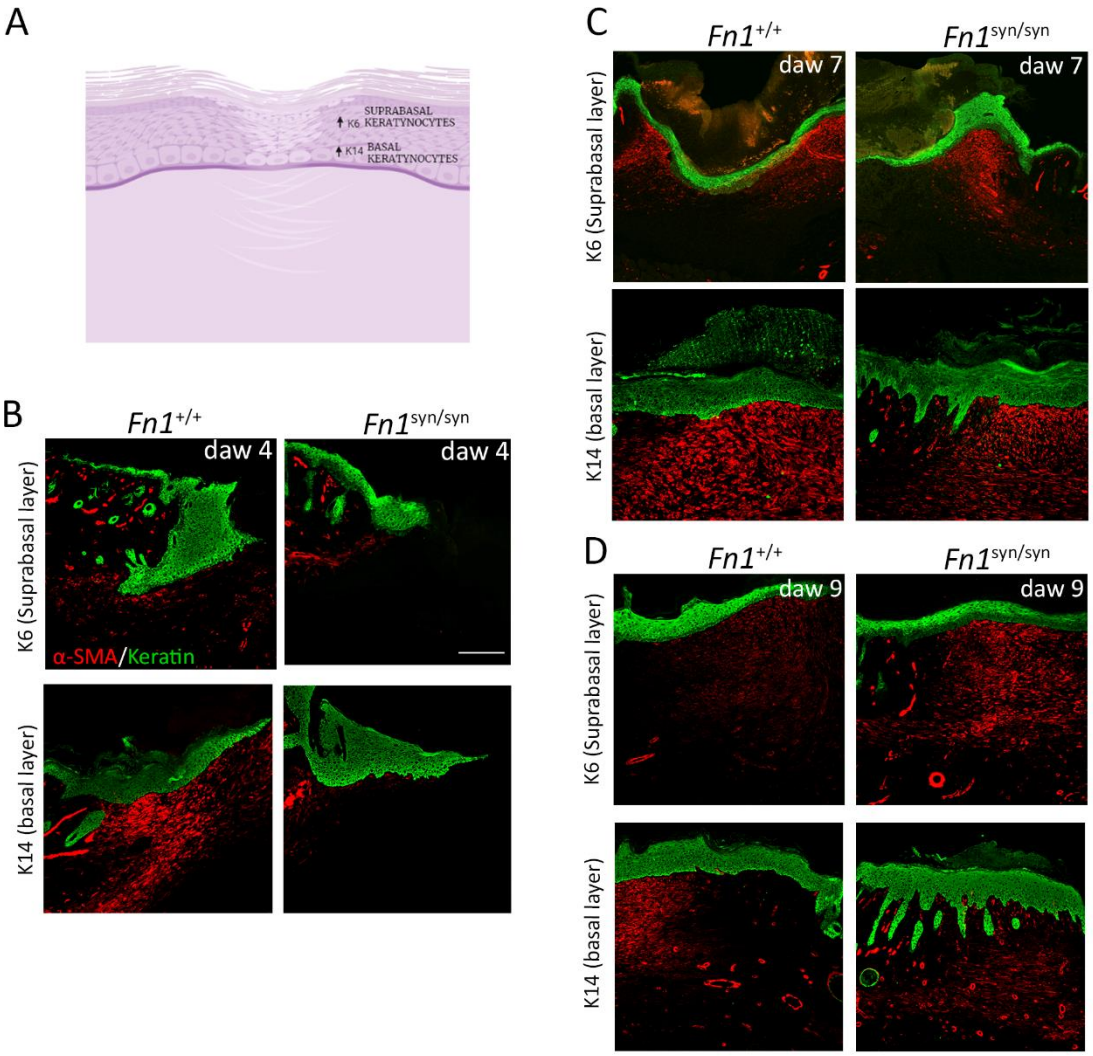

Figure 18. Keratinocyte activation in wounds from *Fn1*$^{+/+}$ and *Fn1*$^{syn/syn}$ mice. A) Illustration of up-regulated keratins in basal and suprabasal layer during the wound healing process. Representative images from Keratin-6,

keratin-14 (green) and α-SMA (red) staining in *Fn1*$^{+/+}$ and *Fn1*$^{syn/syn}$ wounds at 4 (B), 7 (C) and 9 daw (D). Scale bar 200 μm.

At 4 daw K6 expression is observed throughout the whole keratinocyte tongue being more prominent in suprabasal regions (Fig. 18B). At 7 and 9 daw fluorescence is restricted to the suprabasal region with no obvious differences between wild-type and mutant genotypes (Fig 4C and D). K14 expression is observed along the whole keratinocytes tongue at 4 daw and more clearly expressed in basal keratinocytes (Fig. 18B). As the healing process progresses the fluorescence becomes more specific in the basal layer at 7 and 9 daw (Fig. 18C and 18D). The apparent absence of differences between *Fn1*$^{+/+}$ and *Fn1*$^{syn/syn}$ wounds in K6 and K14 expression show that the synergy site function is not essential in keratinocyte activation during the first stages of wound healing.

2.3. α5β1 expression in the epidermal tongue of *Fn1*$^{+/+}$ and *Fn1*$^{syn/syn}$ wounds

Keratinocyte migration is an early healing event motivated by the loss of original cell-cell and cell-ECM adhesions and the formation of new ones. Up-regulation of integrins and the remodelling of a FN-fibrin provisional matrix allows keratinocytes to migrate from wound sides to the centre of the wound and thus to close the epidermal gap (Werner and Grose, 2003). Activated keratinocytes are characterized by rapid changes in their integrin profile to adapt migration into the new-formed provisional ECM. Keratinocytes up-regulate α5β1, αvβ1, αvβ5 and αvβ6 integrins during this process (Aragona et al., 2017, Watt et al., 2002). We focus on α5β1 integrins expression because its bond to the FN-RGD motif is reinforced by the FN synergy site. In normal unwounded skin, α5 integrin is strongly expressed by suprabasal keratinocytes (Fig. 19A, unwounded skin). At 4 daw, we immunolocalized α5 integrin expression in the neo-formed epidermal layer in basal keratinocytes of the migratory front (Fig. 19A indicated by red dots line) both in wild-type and mutant mice.

The percentage of α5-positive keratinocytes for was then calculated referred to the total number of basal keratinocytes in the epidermal tongue (Fig. 19B). In *Fn1*$^{syn/syn}$ wounds more than the 80% of basal keratinocytes are positive for α5-subunit compared to the 40% in *Fn1*$^{+/+}$ wounds. The present results suggest that increased α5β1 integrin expression levels could be compensating the absence of the synergy site in *Fn1*$^{syn/syn}$ wounds.

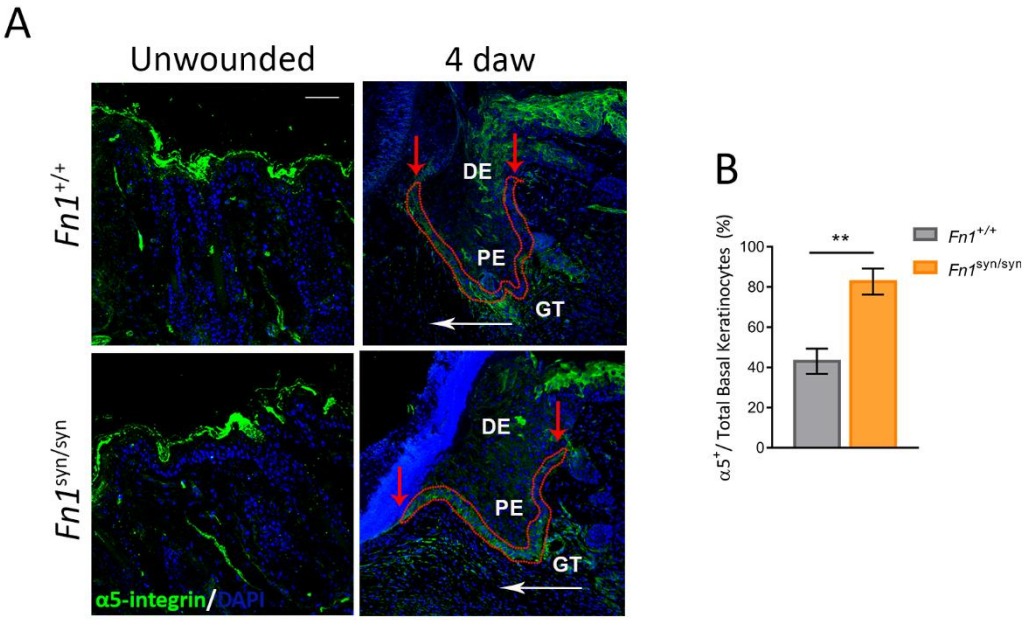

Figure 19. Integrin α5-subunit expression in wounds from Fn1$^{+/+}$ and Fn1$^{syn/syn}$ mice. A) Representative immunofluorescence from wounds at 4 daw stained for α5-subunit integrin (green), α-SMA-positive cells (red) and nuclei staining with DAPI (blue) and α5 expression in unwounded skin B) Percentage of α5 integrin-positive basal migratory keratinocytes related to the total number of basal keratinocytes in the epidermal tongue (total keratinocytes from the two red arrows) (n=8,6). Values are shown as mean ± SEM. Statistical significances were calculated using Student t-test with p-value ** p<0.01. Scale bar 200 µm. GT; granulated tissue, PE; proximal epidermis, DE; distal epidermis.

2.4. Proliferation analysis in the epidermis of *Fn1*$^{+/+}$ and *Fn1*$^{syn/syn}$ wounds

The leading edge of migrating keratinocytes is followed by a proliferative hub of basal cells. To study this population, we used phospho-histone H3 (pH3) expression as a marker of dividing cells along the healing process in Fn1+/+ and Fn1syn/syn wounds.

At 4 daw we observed that the number of pH3-positive cells in mutant wounds (164 ± 22 cells/mm^2) is comparable to wild-type values (192.4 ± 15.2 cells/mm^2). Distribution of pH3-positive is observed at the more distal part of the epidermal tongue and the interfollicular epidermis (Fig. 20A, white arrows). Proliferation increases at 7 daw in the already closed epidermis in both genotypes reaching comparable values in wild-type (395.1 ± 43.1 cells/mm^2) and mutant (382.1 ± 53.4 cells/mm^2) wounds (Fig. 20B). Proliferation rate slightly decreases at 9 daw in *Fn1*$^{+/+}$ wounds (357 ± 41.8 cells/mm^2) whereas in *Fn1*$^{syn/syn}$ the proportion of dividing cells is significantly reduced (215.7 ± 48.7 cells/mm^2) compared to wild type. These results are consistent with the reduced epidermal thickness observed at 9 and 15 daw in *Fn1*$^{syn/syn}$ wounds (Results Section 2.1).

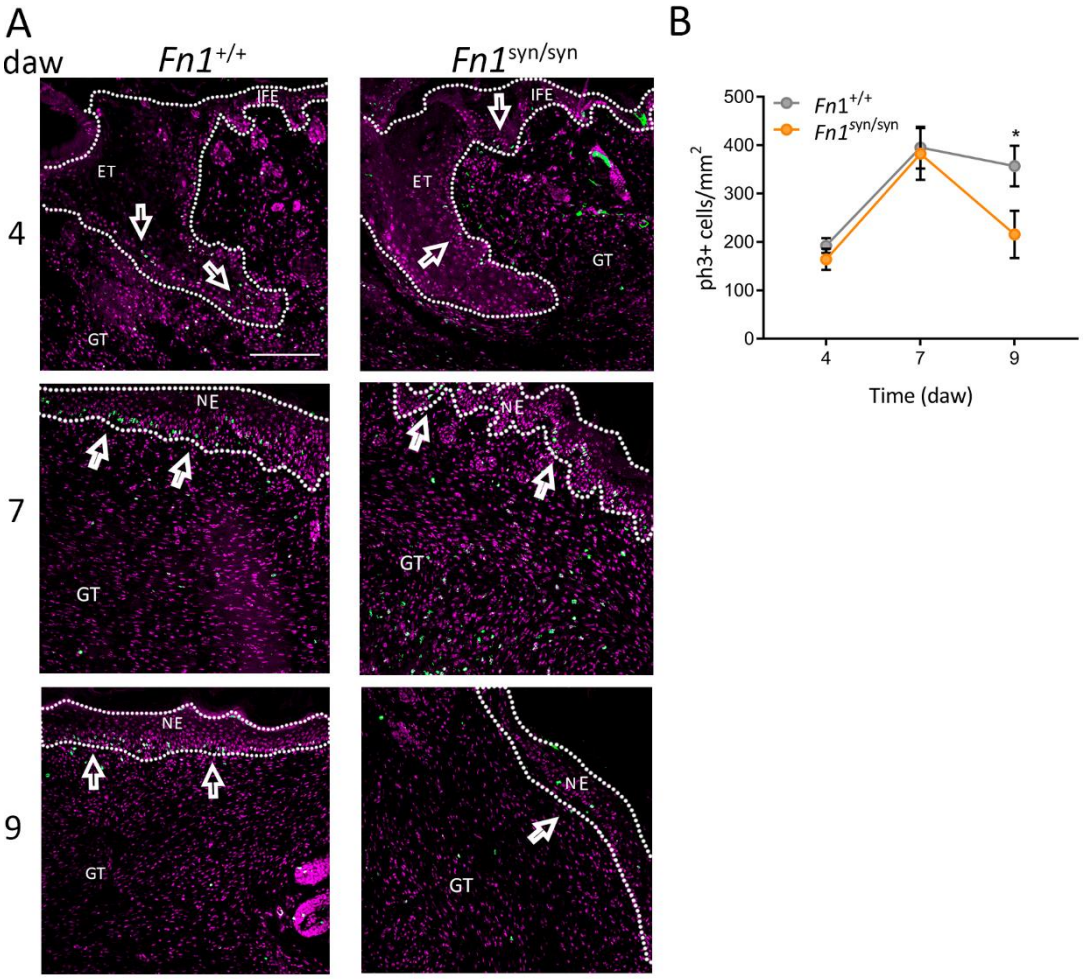

Figure 20. Epidermal proliferation along the healing process in wounds from *Fn1*$^{+/+}$ and *Fn1*$^{syn/syn}$ mice. A) Representative immunofluorescences of pH3-positive cells (green) and nuclei staining with DAPI (purple) at indicated time points. (B) Quantification of pH3-positive cells density in the epidermis of *Fn1*$^{+/+}$ and *Fn1*$^{syn/syn}$ wounds at 4, 7 and 9 daw [n=11, 11(4) n=10, 10(7) n=7, 7(9)]. Values are shown as mean ± SEM. Statistical significances were calculated using the Student t-test with p-value * p<0.05. ET; epidermal tongue, NE; neo-epidermis, GT; granulation tissue, IFE; interfolicullar epidermis. Scale bar 200 µm.

3. Dermal regeneration in *Fn1*$^{+/+}$ and *Fn1*$^{syn/syn}$ wounds

Granulation tissue (GT) is formed in the dermis of wounds during the proliferative phase and has a main role in the healing process. An early formed FN/fibrin matrix secreted and assembled by platelets is used by infiltrated cells, to migrate towards the wound bed. TGF-β1 secreted by recruited platelets together with the increment in ECM tension releases active TGF-β1 that signals dermal fibroblasts conversion into myofibroblasts. Myofibroblasts are high-contractile cells and key responsible for the synthesis of FN and collage I/III during the proliferative healing phase. This ECM guides cells towards proper healing and to recover the initial skin structure.

We studied the relevance of the FN synergy site in GT formation and composition during skin wound healing in *Fn1*$^{syn/syn}$ mice and compared to *Fn1*$^{+/+}$ mice at different time points.

3.1. GT formation in *Fn1*$^{+/+}$ and *Fn1*$^{syn/syn}$ wounds

First, we analysed the GT formation by measuring the dermic area underneath the epidermis using Masson´s trichrome-stained sections (Fig. 21A, GT indicated by black dotted lines). In *Fn1*$^{+/+}$ wounds, GT covers a sectional area of 1.4 ± 0.09 mm^2 at 4 daw, decreasing rapidly in size during the following days and reaching 0.8 ± 0.08 mm^2 at 7 daw. At later stages the GT size is greatly reduced remaining a sectional area of 0.3 ± 0.05 mm^2 at 25 daw. In *Fn1*$^{syn/syn}$ wounds, we observe smaller GT areas at 4 daw, comprising about half of the sectional area (0.8 ± 0.1 mm^2) in comparison with GT in *Fn1*$^{+/+}$ wounds (Fig. 21B). However, GT areas reach similar values to wild type wounds in the following days.

Myofibroblasts are the major cell type forming the GT and are key responsible for the ECM deposition and wound contraction (Driskell et al., 2013; Hinz, 2016). Its contractile activity is a result of the high expression of α-smooth muscle actin (α-SMA). α-SMA expression was then used as a marker of myofibroblasts to study its appearance during the healing process. In intact skin, α-SMA is only expressed by smooth muscle cells surrounding blood vessels. Upon wounding, the first α-SMA-positive cells in the GT area are visible in the lateral margins of the wound (4 daw) predominating in the zones beneath the neo-epidermis (Fig. 21A). During the following days (7-9 daws) and concomitant to the closure of the epidermal layer, lateral waves of α-SMA-expressing cells extend to the upper central part of the wounds and occupy the whole GT area. Importantly, in 9 daw *Fn1*$^{+/+}$ wounds there is a progressive decrease in the GT density of myofibroblasts and at 15 daw the α-SMA-positive cells are again restricted to new blood vessels. In *Fn1*$^{syn/syn}$ wounds the distribution of myofibroblasts is similar to the one described in wounds expressing FN^{wt}, although during the first stages of healing (4 daw) the size of the area occupied by α-SMA-positive cells is significantly reduced when compared to *Fn1*$^{+/+}$ wounds (Fig. 21C).

As myofibroblasts are the main cell type responsible for the new ECM deposition, the area occupied by collagen in *Fn1*$^{+/+}$ and *Fn1*$^{syn/syn}$ wounds was measured using Masson´s Trichrome staining and analysed using ImageJ Colour Deconvolution plugin (Materials and Methods Section 11.5). The area covered by collagen fibres was reduced to half, measuring 0.52 ± 0.07 mm^2 in *Fn1*$^{syn/syn}$ compared to 1.2 ± 0.1 mm^2 in 4 daw *Fn1*$^{+/+}$ wounds (Fig. 21D).

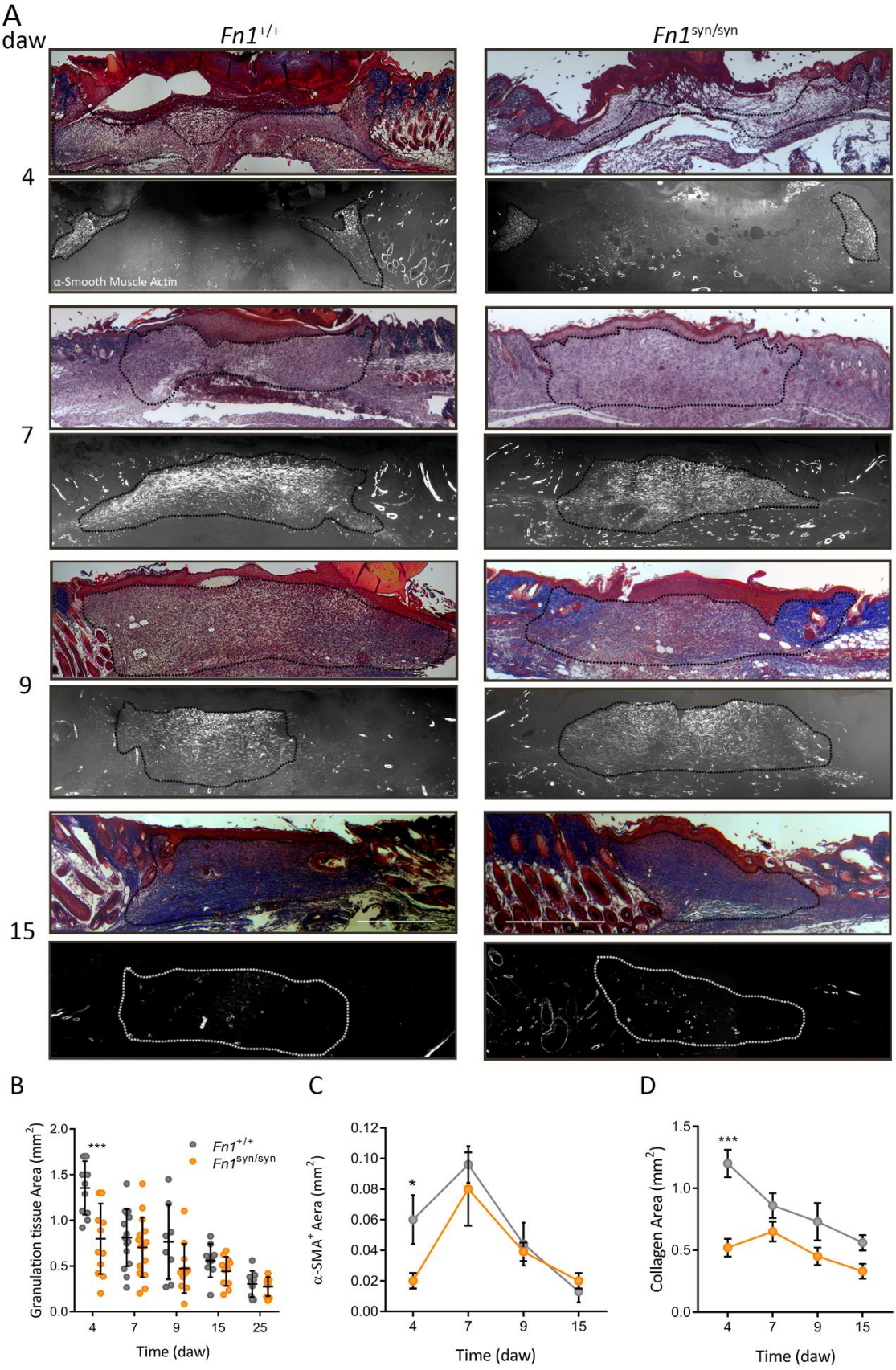

Figure 21. GT analysis along the healing process in *Fn1*$^{+/+}$ and *Fn1*$^{syn/syn}$ wounds. A) Representative pictures of Masson´s Trichrome collagen staining at 4, 7, 9 and 15 daw together with correspondent α-SMA immunostaining composition of full size wounds. B) Sectional GT area quantification using histological images at each time point in

Fn1$^{+/+}$ and *Fn1*$^{syn/syn}$ wounds [n= 12, 12(4 daw) n= 14, 12 (7) n=11, 11(9) n=10, 12(15) n=10, 10(25)] (described in Materials and Methods). C) Quantification of α-SMA-positive area in wounds from *Fn1*$^{+/+}$ and *Fn1*$^{syn/syn}$ mice at different time points. D) Quantification of the collagen area along the healing process in *Fn1*$^{+/+}$ and *Fn1*$^{syn/syn}$ wounds using Masson´s Trichrome staining. Values are shown as mean ± SEM. Statistical significances were calculated using the Student t-test with p-value * $p<0.05$ *** $p< 0.001$. Scale bar 500 µm.

As the healing process moves forward, the collagen area decreases with time in both genotypes at similar rates.

All these results together point an important role of the FN synergy site in the process of GT formation during the skin wound healing. The absence of the synergy site delays the GT formation in dermal wounds probably due to a problem in myofibroblasts conversion. In accordance, the amount of collagen deposited in *Fn1*$^{syn/syn}$ is compromised by the delay in myofibroblasts appearance.

3.2. FN distribution in the GT from *Fn1*$^{+/+}$ and *Fn1*$^{syn/syn}$ wounds

In healthy skin, FN is mainly present at the BM in the dermal-epidermal junction, surrounding hair follicles and BM of blood vessels (Richard and Clark, 1990). Upon wounding, FN appears at 4 daw located in the lateral margins of the GT with very few expression at the centre of the wound (Fig. 22A and 22B, 4 daw). As the healing process progresses the FN area covers the entire wound bed reaching the highest expression at 7 daw (Fig. 22A and 22B, 7 daw). FN expression starts to decrease at 9 daw but remains still elevated at 15 daw (Fig. 22A and 22B, 9 and 15 daw). The area of GT covered by FN was measured in mutant and wild-type wounds at different time points along the healing process (Fig. 22C). At 4 daw, the mean sectional area covered by FN in *Fn1*$^{+/+}$ is 0.10 ± 0.01 mm^2 while the content is significantly reduced to 0.045 ± 0.0081 mm^2 in *Fn1*$^{syn/syn}$ wounds. Along the following days, the FN deposition increases significantly in the *Fn1*$^{syn/syn}$ wounds reaching similar levels to *Fn1*$^{+/+}$ wounds (Fig. 22B, 7 daw). In *Fn1*$^{syn/syn}$ wounds there is a rapid decrease in FN expression at 9 daw that is not appreciated in *Fn1*$^{+/+}$ wounds until 15 daw. At 15 daw FN expression reach 0.013 ± 0.007 mm^2 and 0.018 ± 0.005 mm^2 in *Fn1*$^{+/+}$ and *Fn1*$^{syn/syn}$ wounds, respectively (Fig. 22A and 22B, 15 daw). As summary, at 4 daw we observe a concomitant reduction in characteristic ECM proteins in GT such as FN and collagen, together with a reduction in the amount of myofibroblasts, suggesting that the fibrotic process associated to the healing is reduced or delayed in *Fn1*$^{syn/syn}$ wounds.

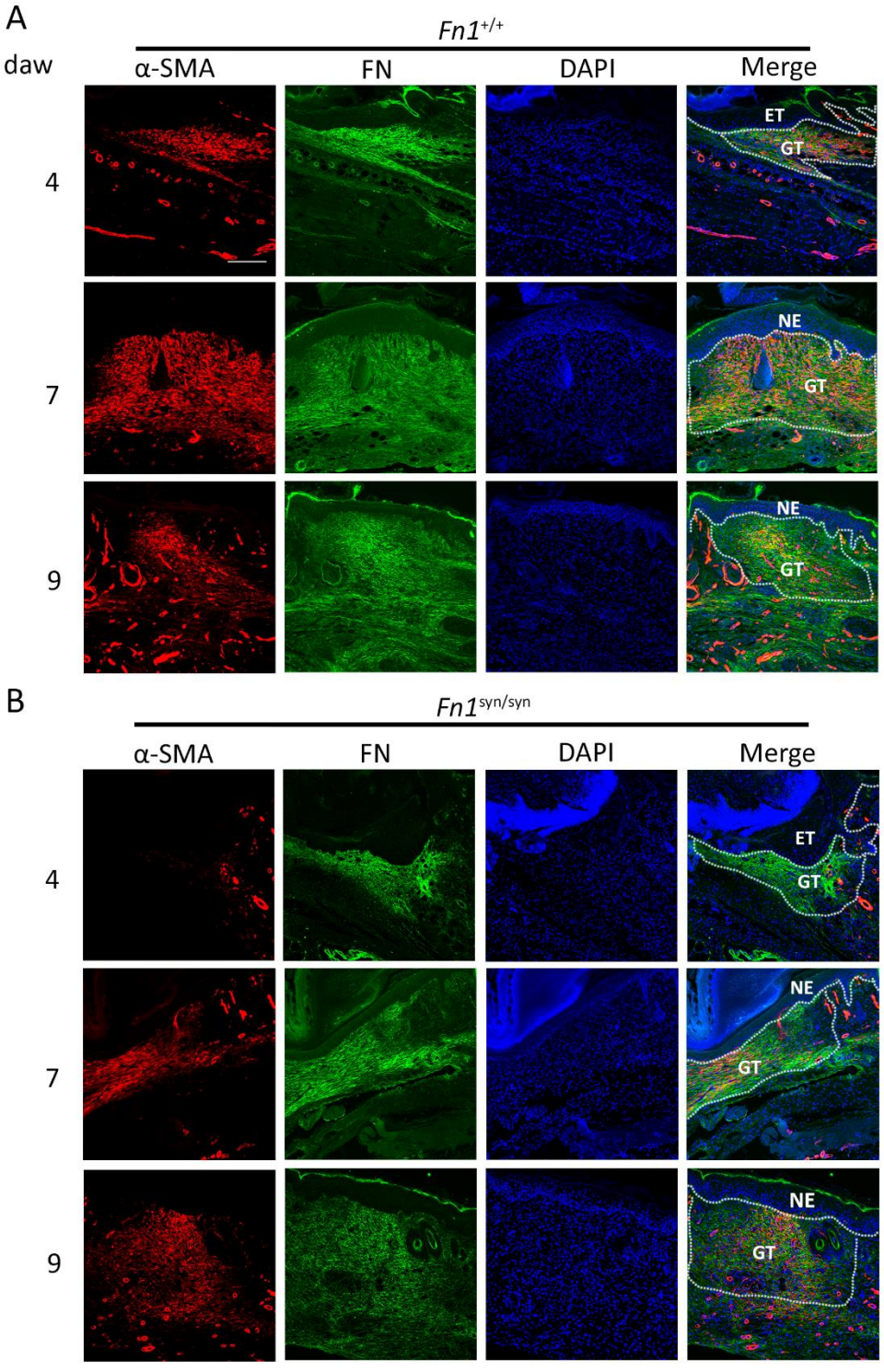
A
Fn1+/+
daw
α-SMA
FN
DAPI
Merge
4
7
9
ET
GT
NE
B
Fn1syn/syn
C
FN Area (mm2)
0.20
0.15
0.10
0.05
0.00
*
4
7
9
15
Time (daw)

Figure 22. **FN distribution in wounds from *Fn1*$^{+/+}$ and *Fn1*$^{syn/syn}$ mice.** A) Representative images from FN (green) distribution, α-SMA (red) and nuclei staining (blue) from *Fn1*$^{+/+}$ and B) *Fn1*$^{syn/syn}$ wounds at 4, 7, 9 and 15 daw. C) Quantification of total FN area in wounds from *Fn1*$^{+/+}$ and *Fn1*$^{syn/syn}$ mice at 4, 7, 9 and 15 daw. Values are shown as mean ± SEM. Statistical significances were calculated using the Student t-test with p-value * p<0.05. [n= 12, 12(4) n= 14, 12 (7) n=11, 11(9)]. ET; epithelial tongue NE; neo-epidermis, GT; granulation tissue. Scale bar 200 μm.

3.3. Cell proliferation analysis in the GT of *Fn1*$^{+/+}$ and *Fn1*$^{syn/syn}$ wounds

Together with myofibroblasts conversion, migration and proliferation are the two main processes involved in the GT formation during the healing process (Rognoni et al., 2018). To test whether the size of GT area in *Fn1*$^{syn/syn}$ wounds is compromised by defective cell proliferation, wounds were analysed at different healing stages.

To this end, two proliferation markers were analysed: histone H3 phosphorylation (pH3) immunostaining (Fig. 23A) for cells in mitosis and Ki67 a marker for proliferative cells at different cycle stages. At 4 daw, pH3-positive cells were significantly less visible in the GT of *Fn1*$^{syn/syn}$ wounds (67.21 ± 9 cells/mm^2) compared to wounds from *Fn1*$^{+/+}$ mice (92.15± 8.5 cells/mm^2). However, the proportion of dividing pH3-positive cells in *Fn1*$^{syn/syn}$ wounds (99.1 ± 22.9 cells/mm^2) increased significantly at 7 daw, reaching values similar to wild-type wounds (94.6 ± 21 cells/mm^2). The number of dividing cells decreased at 9 daw in both genotypes with slower rates in *Fn1*$^{syn/syn}$ wounds (55.5 ± 8.8 cells/mm^2) compared to wild-type (32.45 ± 4.3 cells/mm^2) (Fig. 23B).

To corroborate a defect in cell division, Ki67 expression was analysed in proliferating cells in wounds at 4 daw. The number of Ki67-positive cells was referred to the number of nuclei in the same GT area (Fig. 23C). Consistently with pH3-positive cells data, the proportion of Ki67$^+$ cells at 4 daw is significantly reduced in *Fn1*$^{syn/syn}$ wounds compared to *Fn1*$^{+/+}$ wounds (Fig. 23D). Proliferation in the GT at 4 daw is according to the present study possibly truncated by the absence of the synergy site.

3.4. New vessels formation in the GT of *Fn1*$^{+/+}$ and *Fn1*$^{syn/syn}$ wounds

Upon skin injury, blood vessels in the wounded zone become damaged and new vessels formation is necessary to restore skin integrity and finish the healing process. Integrins have been directly linked to the neovascularization processes in tumour progression as blocking antibodies for α5 and β1 subunits are described as anti-angiogenesis strategies (Ramakrishnan et al 2006, Bosnjak et al., 2015). To analyse the implication of the FN synergy site in neovascularization during the healing process, new vessels were stained with α-SMA and quantified in Fn1$^{+/+}$ and Fn1$^{syn/syn}$ wounds at later healing stages.

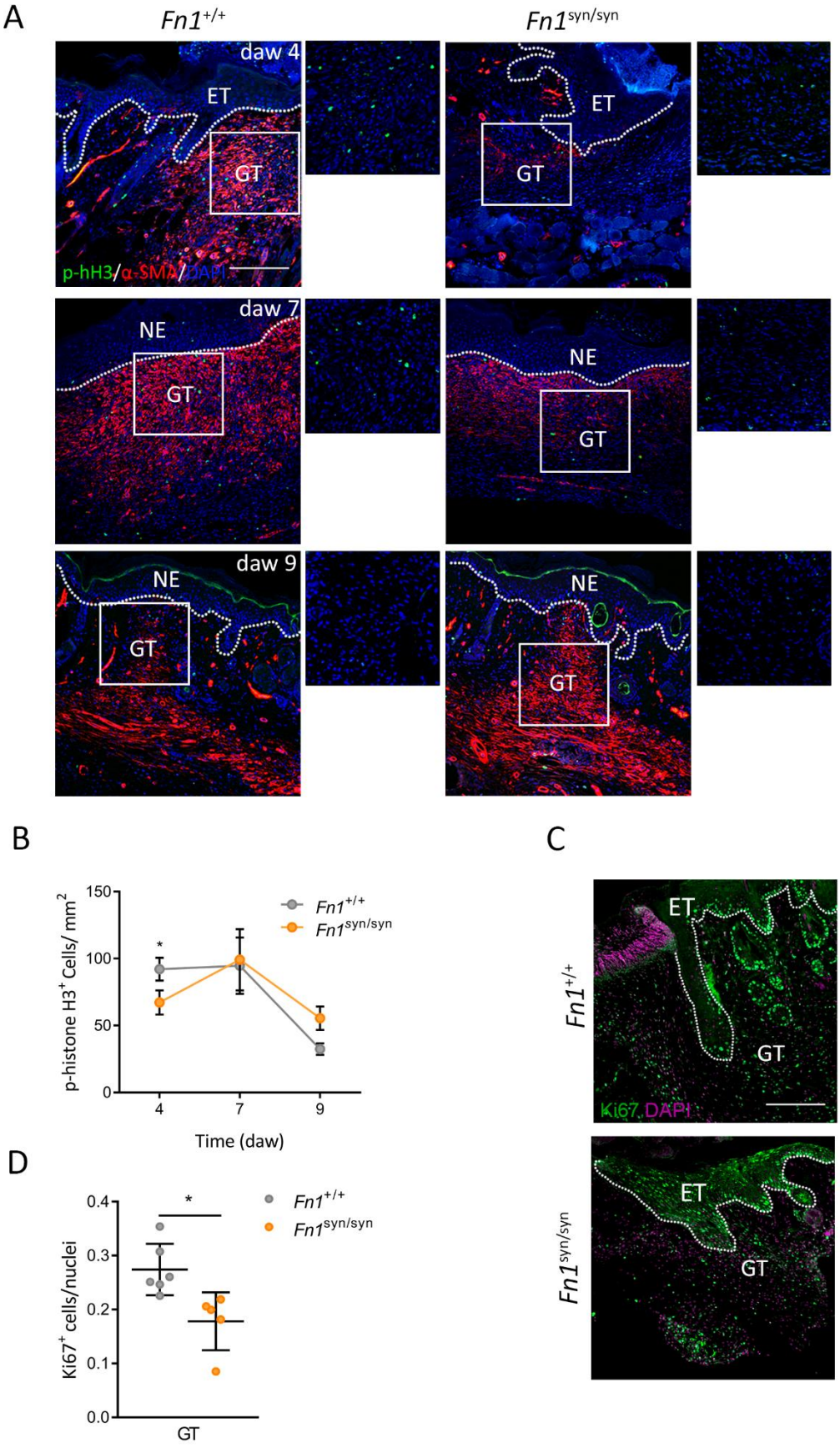

Figure 23. Changes in proliferation along the healing process in the GT from Fn1$^{+/+}$ and Fn1$^{syn/syn}$ wounds. (A) Representative immunofluorescence of p-histoneH3-positive cells (green), α-SMA-positive cells (red) and DAPI

(blue) at indicated time points. (B) Quantification of p-histoneH3-positive cells per area in the GT at 4, 7 and 9 daw [n=11, 11(4) n=10, 10(7) n=7, 7(9)]. (C) Representative immunofluorescence of proliferation marker Ki67 (green) and DAPI (purple) at 4 daw in GT from $Fn1^{+/+}$ and $Fn1^{syn/syn}$ wounds (D) Quantification of Ki67-positive cells related to the number of nuclei per area in the GT [n=6, 5(4)]. Values are shown as mean ± SEM. Statistical significances were calculated using the Student t-test with p-value * p<0.05. NE; neo-epidermis, ET; epidermal tongue, GT; granulation tissue Scale bar 200 μm.

As shown in Figures 7 and 8, abundant new vessels are visible in the GT at 9 daw. Vessel density was then quantified in the GT area of wounds at 9 and 15 daw (Fig. 24A). Despite the absence of the FN synergy site the density of vessels formed at 9 and 15 daw in *Fn1*$^{syn/syn}$ GT was similar to those in *Fn1*$^{+/+}$ wounds (Fig. 24B). These results indicate that adhesion to FN by α5β1 integrin is not limiting the neovascularization when the synergy site is absent.

3.5. p-Smad2 activation in the GT from *Fn1*$^{+/+}$ and *Fn1*$^{syn/syn}$ wounds

During the process of wound healing, fibroblasts conversion into myofibroblasts is driven by an increment in the overall ECM mechanical tension that triggers the liberation of growth factors such as TGF-β1 to the surroundings (Hinz et al., 2001b). TGF-β1, produced by platelets, macrophages and fibroblasts at the wound site, has been demonstrated to induce collagen and FN synthesis, as well as the expression of α-SMA protein. TGF-β1 contributes to myofibroblasts differentiation through the activation of SMAD signalling pathway (Penke and Peters-Golden, 2019).

Considering the reduced levels of myofibroblasts observed in *Fn1*$^{syn/syn}$ wounds at 4 daw, we analysed the TGF-β1-induced signalling in wounds were the FN synergy site was absent. To that purpose, SMAD pathway activation was analysed in the GT of wounds from wild-type and mutant mice by quantifying phosphorylated-Smad2 positive cells (Fig. 25A). At 4 daw there is significantly less p-Smad2 positive cells in the GT from *Fn1*$^{syn/syn}$ wounds (0.34 ± 0.048 cells/nuclei) compared to *Fn1*$^{+/+}$ wounds (0.49 ± 0.029 cells/nuclei). The number of p-Smad2 positive cells in the GT at 7 daw in *Fn1*$^{syn/syn}$ wounds (0.46 ± 0.05 cells/nuclei) increases reaching similar values to wild-type wounds (0.52 ± 0.03 cells/nuclei) (Fig. 25B). These results suggest that the absence of the FN synergy site could be impairing α5β1 integrin-mediated actomyosin contraction and hence the TGF-β1 release from the ECM.

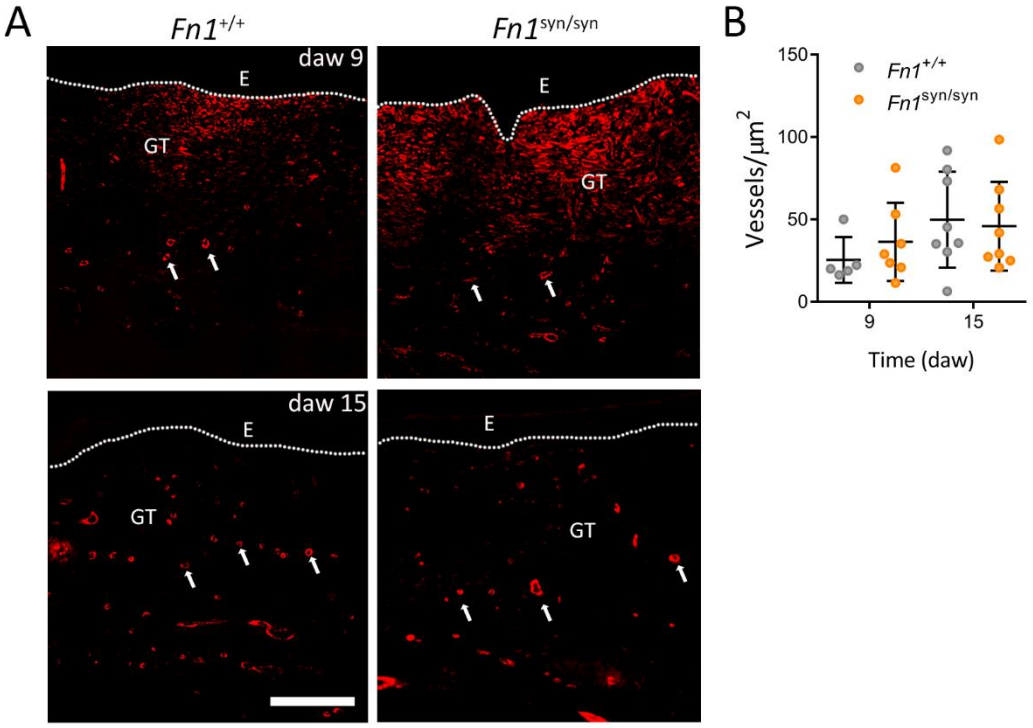

Figure 24. New vessels formation in wounds from *Fn1*$^{+/+}$ and *Fn1*$^{syn/syn}$ mice. (A) Representative immunofluorescences of α-SMA (red) to stain blood vessels at 9 and 15 daw. B) Quantification of the number of vessels per area in the GT of wounds [n=5, 7(9) n=8, 8(15)]. Values are shown as mean ± SEM. Statistical significances were calculated using the Student t-test. Scale bar 200 µm.

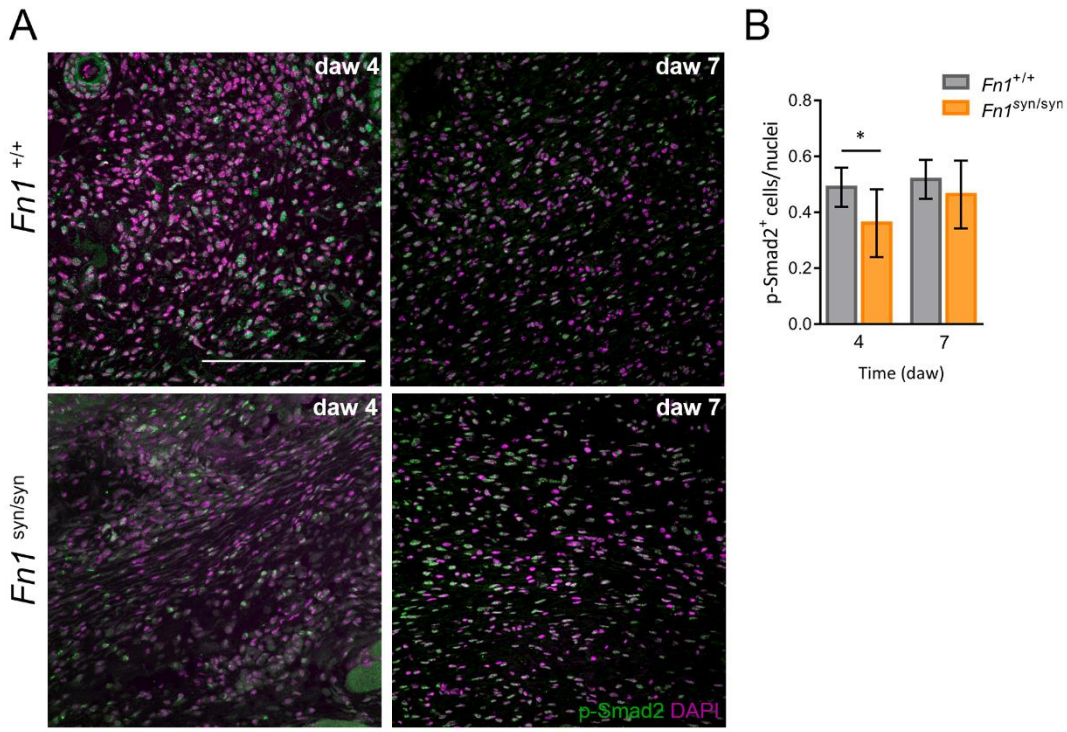

Figure 25. TGF-β1 signalling activation in wounds from *Fn1*$^{+/+}$ and *Fn1*$^{syn/syn}$ mice. (A) Representative immunofluorescences of wounds GT stained with p-Smad2 antibody (green) and DAPI (purple) for nuclei staining at

4 and 7 daw. B) Quantification of p-Smad-2-positive cells per nuclei in the GT at 4 and 7 daw. 10-12 pictures were analysed per wound from different GT areas [n=7, 8(4) n=8, 8(7)]. Values are shown as mean ± SEM. Statistical significances were calculated using the Student t-test with p-value *p<0.05. Scale bar 200 µm.

3.6. p-Smad2 analysis in the epidermal tongue from *Fn1*$^{+/+}$ and *Fn1*$^{syn/syn}$ wounds

TGF-β1 signalling has been also linked to the process of re-epithelialization promoting keratinocyte migration during the wound closure through Smad2 and Smad3 signalling pathway (Ashcroft et al., 1999; Hosokawa et al., 2005; Reynolds et al., 2005) and promoting integrins up-regulation (Gailit et al., 1994). We then evaluated p-Smad2 at early stages in the epidermal tongue by staining for this protein.

At 4 daw higher cytoplasmic p-Smad2 positive cells are observed in wounds from mutant mice compared to those expressing FN^{wt} (Fig. 26A) in the epidermal tongue, reaching 3-fold increment in fluorescence intensity (Fig. 26B). Despite differences at the cytoplasm level, nuclear p-Smad2 staining do not differ between both genotypes (Fig. 26B). The present results indicate that despite the observed increment in cytoplasmic SMAD phosphorylation in mutant wounds, nuclear signalling is diminished related to the total cell amount compare to wild-type.

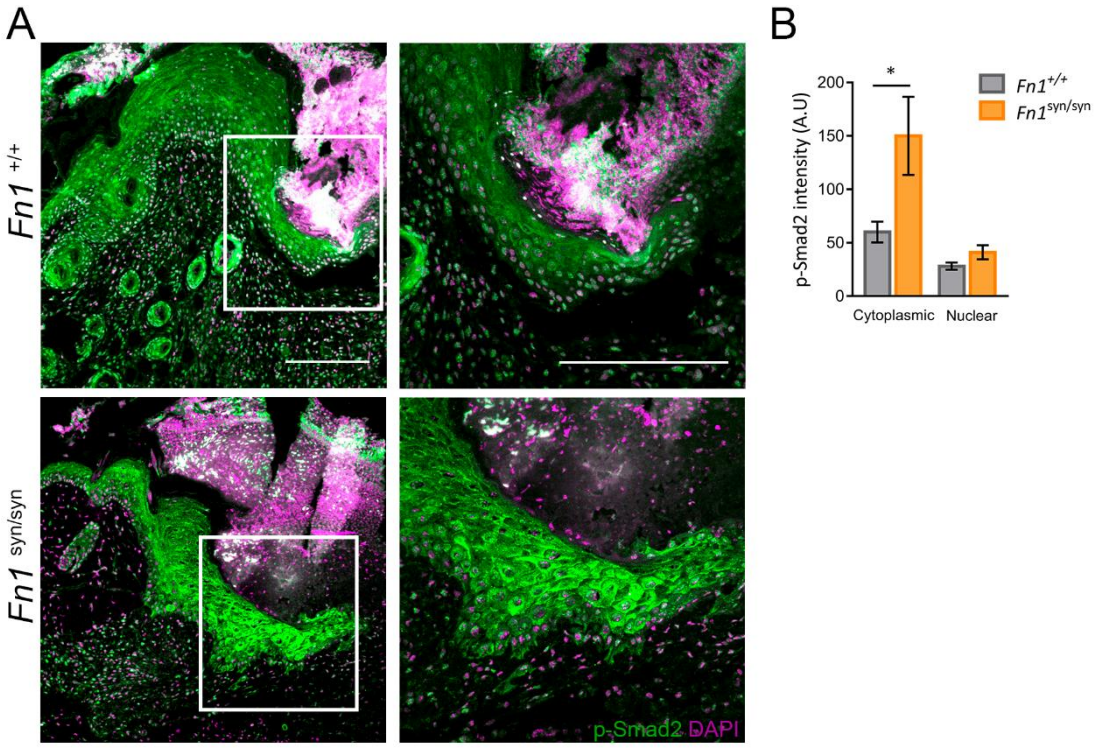

Figure 26. Detection of p-Smad2 levels in the epidermis of *Fn1*$^{+/+}$ and *Fn1*$^{syn/syn}$ wounds. (A) Representative immunofluorescence of p-Smad2-positive cells (green) and DAPI (purple) at 4 daw in the epithelial tongue. (B) Quantification of p-Smad2 fluorescence intensity in the cytoplasmic and nuclear area of the epidermal tongue [n=6,

8(4)]. Values are shown as mean ± SEM. Statistical significances were calculated using the Student t-test with p-value * $p<0.05$. Scale bar 200 µm.

II The relevance of the FN synergy site in keratinocytes migration

1. Purification of plasma FN from mouse blood

In our *in vitro* assays, we used pFN purified from blood collected from *Fn1*$^{+/+}$ (pFN^{wt}) and *Fn1*$^{syn/syn}$ (pFN^{syn}) mice. The pFN was purified by affinity chromatography using a column of gelatine. We analysed the purified protein by Coomassie blue staining to discard the presence of other proteins (see Materials and Methods 6.2). FN concentration was then measured by Western blot using known amounts of commercial FN (Fig 27A).

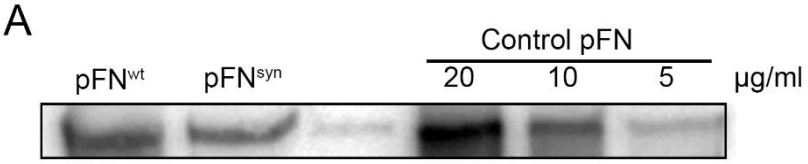

Figure 27. Quantification of purified pFN after affinity chromatography. A) Western blot of purified pFN after dialysis. Commercial pFN was used as a control for protein quantification (20, 10 and 5 µg/ml).

2. Keratinocyte cell line characterization

In our *in vitro* migration assays, we used a spontaneously immortalised keratinocyte line (Rognoni et al., 2014) kindly provided by Reinhard Fässler (Max Plank Institute for Biochemistry). It has been described that keratinocytes do not express β3-class integrins, neither *in vivo* nor in cell culture (Adams and Watt, 1991; Duperret et al., 2015). To confirm this, we analysed by Flow Cytometry the integrin profile in our keratinocyte line (Materials and Methods section 9). As some integrin heterodimers were previously analysed in Rognoni et al., (2014), we focused in α5 and β3 integrin expression levels. As shown in Figure 28A, the keratinocyte cell line contains α5 integrins but lacks β3 integrin expression.

Although keratinocytes have been described to not synthesize FN, we discarded its potential secretion of FN, as it could mask our results with wild-type cellular FN (cFN). We analysed the presence of FN in the keratinocyte conditioned medium after 3 and 20 h of cell culture. As it is shown in Figure 28B, FN was not present in the keratinocyte conditioned medium. As control, we used fibroblasts conditioned medium which it is well known to contain soluble cFN.

Next, the focal adhesions of keratinocytes to pFN^{wt} and pFN^{syn} were analysed. Keratinocytes were seeded on glass coverslips previously coated with collagen I, pFN^{wt} or pFN^{syn,} and grown in DMEM with 1% FN-depleted serum for 5 h. Cells were then stained for paxillin and actin to analyse focal adhesions (FA) formation and cytoskeleton assembly, respectively (Fig 28C). Keratinocyes were stained for FN but as shown in Figure 28C no staining is observed in keratinocytes supporting results from conditioned medium. No differences are observed in the number or area of FA in keratinocytes seeded on pFN^{wt} or pFN^{syn} after 5 h (Fig. 28D and 28E).

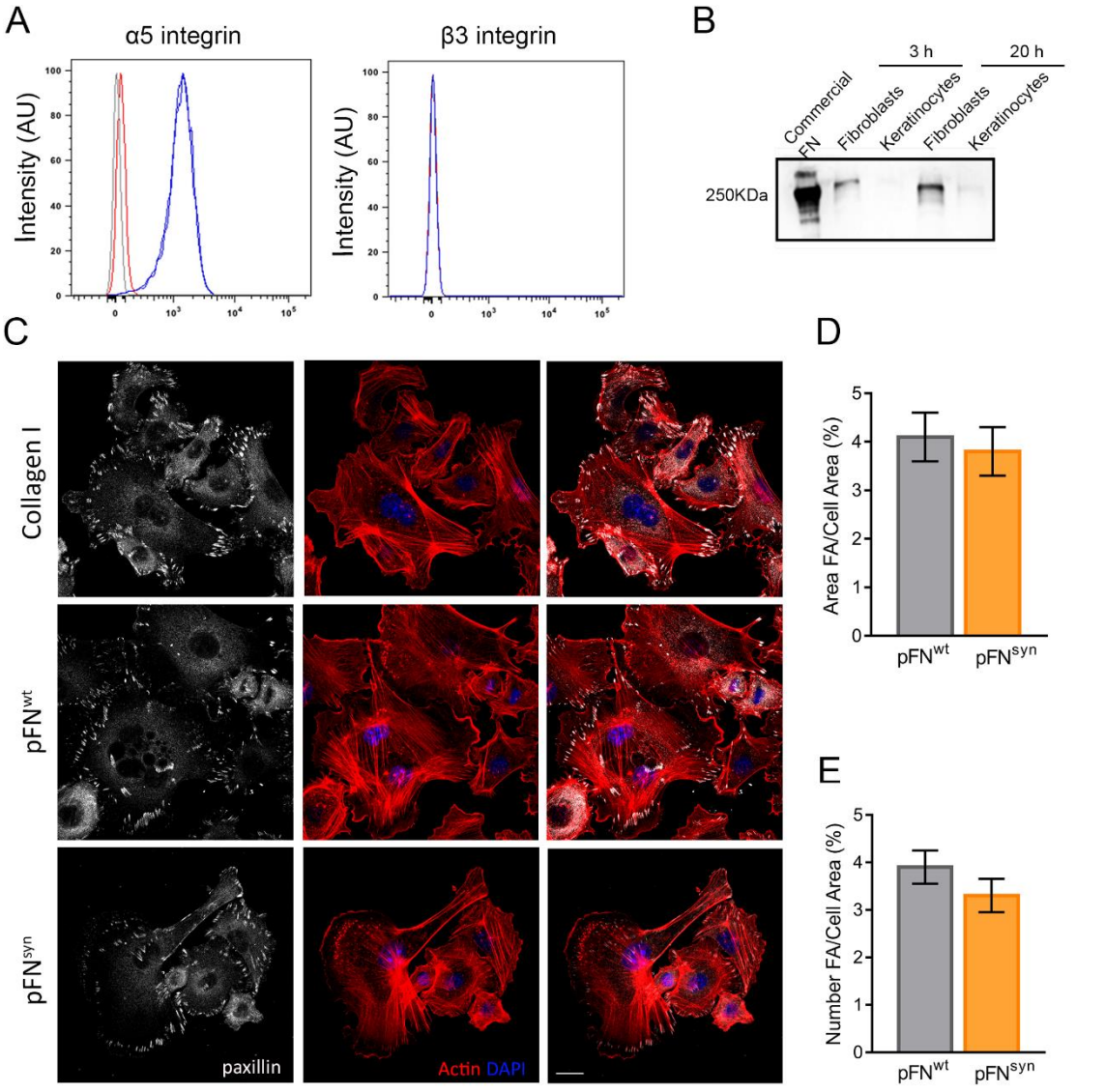

Figure 28. Keratinocytes characterization *in vitro*. A) Representative histograms of integrin levels (blue) of keratinocytes analysed by Flow Cytometry. Red line indicates isotype control for α5 or β3 integrin subunit and grey line represents unstained sample. B) Western Blot analysis of conditioned media by keratinocytes or fibroblasts after 3 and 20 h in culture C) Representative images of keratinocytes grown in FN-depleted KGM and seeded on collagen I, pFN^{wt} or pFN^{syn} .F-actin (red), paxillin (white), DAPI (blue) and FN (green). Quantification of the percentage covered by D) FA and E) number of FA per cell area. Between 10 and 12 pictures were analysed per condition with 4 or 6 cells per picture. Scale bar 10 μm.

3. Keratinocyte migration analysis using pFN^{wt} and pFN^{syn} as substrate

Single cell migration involves the establishment of a front-to-rear polarity axis guided by actin polymerization in response to chemical or physical cues (Petrie et al., 2009). Cells form FA that link the actin cytoskeleton to the surroundings through integrins engagement. Anchoring to an immobile object allow cells to generate traction forces to move forward. The most accepted migration hypothesis is called “the molecular clutch” and it has been also proposed to explain cells mechanotransduction (Elosegui-Artola et al., 2018, Swaminathan and Waterman, 2016). Myosin II contraction leads to an actin retrograde flow that has been demonstrated to be inversely correlated with migration rates.

Wound healing of the skin implies processes of single cell migration. Even so, after a wound injury keratinocytes migrate as a compact sheet establishing cell-cell contacts that allow connections with the actin cytoskeleton and crosstalk between focal adhesions and adherent junctions (Mui et al., 2016). The front-to-rear polarity in single cell migration is replaced by a leading population that pulls the follower cells by sensing mechanical and chemical cues. Force propagates from the front to the back of the monolayer, presenting stronger FA at the leading edge (Trepat et al., 2009, Tambe et al., 2011). To study *in vitro* the role of the FN synergy site during skin healing we analysed both, keratinocyte single-cell migration and collective migration.

3.1. Keratinocyte single-cell migration analysis on plastic surfaces coated with pFN^{wt} or pFN^{syn}

To prevent substrate damage by wound scratch assay we used self-insert devices simulating a wound gap to study single cell migration. After removing the inserts, the free-cells gap coated with pFN^{wt} and pFN^{syn} is covered by migrating keratinocytes which use the pFN as substrate. To analyse the course of cell migration, we took pictures every 5 minutes during 15 hours using a time lapse microscope. The percentage of gap closure was calculated at different time points measuring the most advanced line and made it relative to the initial gap area at time 0 (Fig. 29A).

Keratinocytes migrating on pFN^{syn}-coated substrates have a significant delay filling the gap compared to those migrating on pFN^{wt} (Fig. 29B). Cell mean speed and directionality were analysed by tracking single cells in different frames over 7 h of migration (Fig. 29C). Accordingly, keratinocytes using pFN^{syn} as substrate have a significant reduced mean speed (0.61 ± 0.18 µm/min) compared to keratinocytes migrating on pFN^{wt} (0.86 ± 0.29 µm/min) (Fig.

29D). We observed the same tendency when we analysed cells directionality. Cells migrating on pFN^{wt} substrates move in a relatively straight line (0.44 ± 0.017 AU) compared to those moving on pFN^{syn} substrates where migration is rather random (0.54 ± 0.006 AU) (Fig. 29E). All these results together indicate that the FN synergy site can determine cell speed and directionality during single-cell migration and, more important, a relevant role of integrin α5β1-FN adhesion strength to move the cell forward.

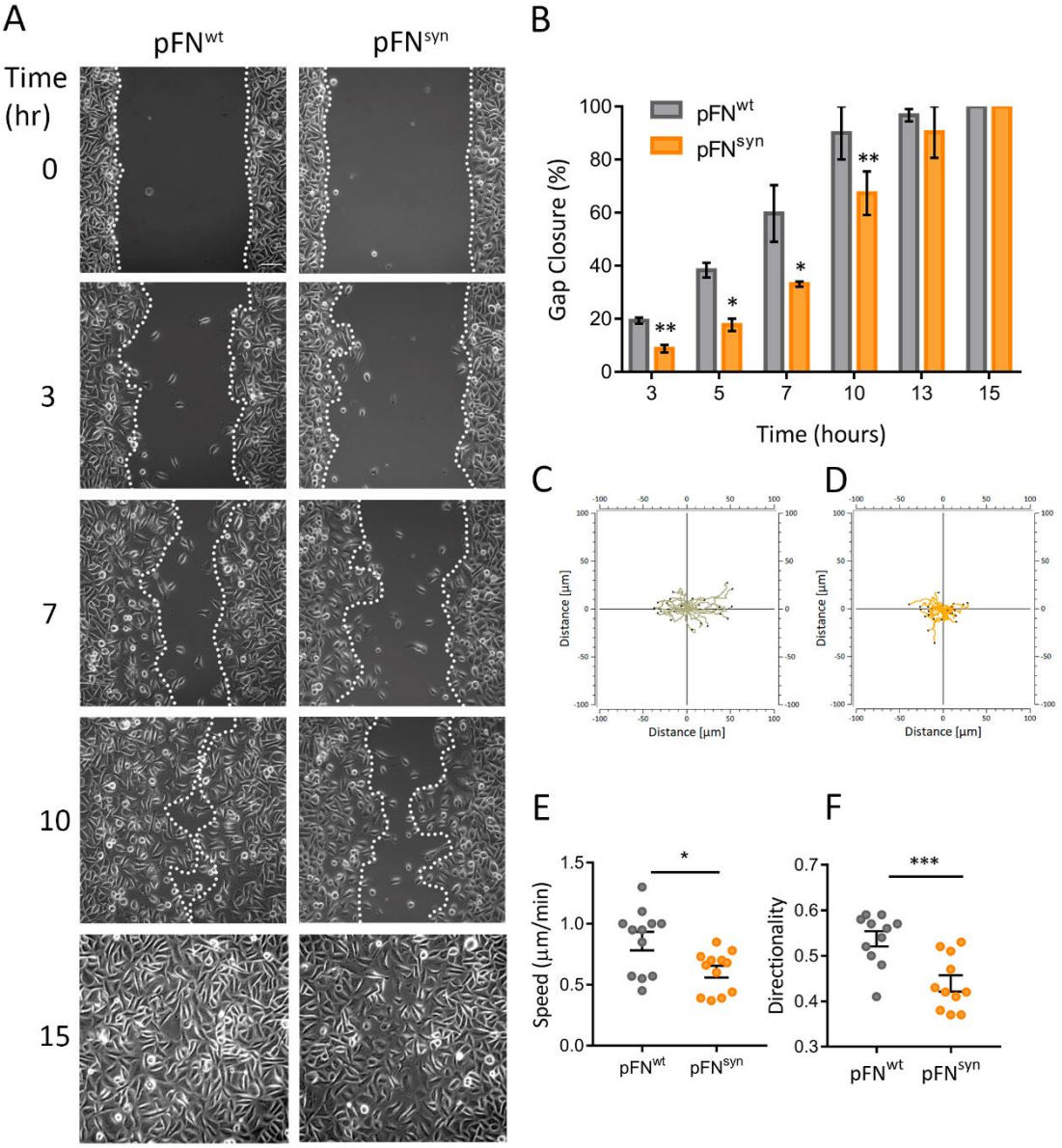

Figure 29. Keratinocyte single-cell migration on plastic dishes coated with purified pFN^{wt} or pFN^{syn}. A) Representative images of keratinocyte during single-cell migration at 0, 3, 7, 10 and 15 hours after removing self-insert device. B) Percentage of gap closure calculated as the free-cell area at each time point relative to the initial area for keratinocytes migrating on pFN^{wt} or pFN^{syn} at shown time points. Cell track of representative cells migrating on C) pFN^{wt} or D) pFN^{syn} substrates. Graphs representing the D) mean speed and E) cell directionality of three different biological replicates. Four different areas were recorded per experiment and each dot represents around

8-10 cells per area for each different replicate. Statistically significance was determined using the Student t-test p-value * p<0.05 and ***p<0.001. Scale bar 0.5 cm.

3.2. Single-cell migration on pFN^{wt} and pFN^{syn} -coated substrates of different rigidity

Substrate rigidity has been widely described as a main player in guiding the migration process (Elosegui-Artola et al., 2014). We therefore investigated how substrate stiffness affects the migration of keratinocytes moving as single cells by using PDMS compliant substrates coated with pFN^{wt} or pFN^{syn}. Cells were let to migrate up to 8 hours and pictures were taken every 15 minutes using a time lapse microscope.

On soft substrates (1.5 kPa) keratinocytes seeded on pFN^{wt} move significantly faster (0.4 ± 0.09 µm/min) than those migrating over pFN^{syn}-coated substrates (0.3 ± 0.07 µm/min). When increasing the rigidity to 15 kPa, cells accordingly move faster in both conditions but with a steeper increment in pFN^{wt}-substrates. Cells moving in compliant surfaces of 15 kPa show also slower speed on pFN^{syn} of 0.33 ± 0.06 µm/min compared to 0.46 ± 0.1 µm/min on pFN^{wt}. When testing stiffer substrates using 28 kPa PDM gels, differences are still present between the two conditions with mean speed of keratinocytes moving on pFN^{syn} of 0.35 ± 0.021 µm/min compared to speed of 0.5 ± 0.03 µm/min on pFN^{wt} (Fig. 30A). Previous studies where single cell migration showed higher myosin-II activity on stiff substrates also showed a concomitant increased in cell speed (Engler et al., 2006; Clarck et al., 2007). Taking this into account, our data show that FN synergy site is essential to withstand loading forces during single-cell keratinocyte migration that could be affecting myosin-II activity, and its role is more evident when cells are on soft substrates.

A

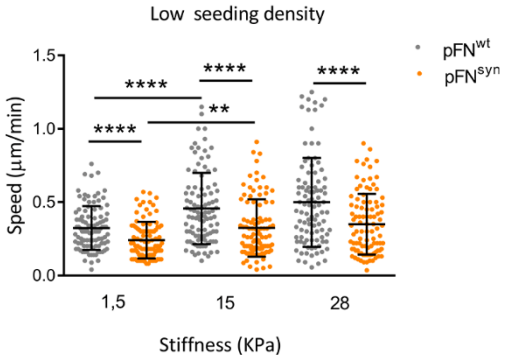

Figure 30. Migration analysis on PDMS compliant surfaces coated with pFN^{wt} or pFN^{syn}. A) Analysis of mean cell speed of keratinocytes seeded at low density on PDMS gels with rigidities of 1.5, 15 and 28 kPa. For 1.5 and 15 kPa three different biological replicates were analysed and around 30 to 50 cells were tracked from each experiment.

For 28 kPa two biological replicates were analysed. Statistically significance was determined using a Student t-test p-value ** p<0.01 ****p <0.0001.

3.3. Keratinocyte collective migration analysis on plastic surfaces coated with pFN^{wt} or pFN^{syn}

Keratinocytes form cell-cell adhesions *in vivo* and in *vitro* in the presence of high Ca^{2+} concentrations (Zhang et al., 2017). To study how the absence of the synergy site affects the collective migration, we cultured keratinocytes in medium containing 1.5 mM of Ca^{2+} to allow the formation of cell-cell contacts. We used the same self-insertion devices and procedure described in Results section 3.1 for the present experiments.

To analyse collective cell migration, the leading edge (blue colour) and inner mass (orange colour) progress over a time period of 7 h after barrier removal was analysed (Fig. 31A). Pictures were taken every 10 min with a time-lapse microscope. The overall distance covered by the wound edge on pFN^{syn}-coated substrates increases faster after 1 to 4h barrier removal compared to cells migrating on pFN^{wt}-coated substrates (Fig. 31B). Greater covered distance is also observed at the inner mass after 2 h moving on pFN^{syn} substrates compared to those cells moving on pFN^{wt}. However, the differences between cells on pFN^{syn} and pFN^{wt} persist for longer in the inner mass compared to the leading edge (Fig. 31C). Wound closure at the leading edge is reflected in the measured mean speed within the first 4 h of migration (Fig.31D). As observed in Figure 30D, wound closure is faster on pFN^{syn} compared to pFN^{wt} substrates.

To discard the contribution of cell proliferation, we added Cytosine β-D-Arabinofuranoside, to the culture medium which inhibits cell division (Fig. 31E). The mean speed at the leading edge on pFN^{wt} (0.55 ± 0.02 μm/min) and pFN^{syn} (0.67 ± 0.06 μm/min) in the presence of the proliferation inhibitor is comparable to the mean velocities on pFN^{wt} (0.53 ± 0.06 μm/min) and pFN^{syn} (0. 67 ± 0.09 μm/min) without proliferation inhibition, indicating that cell division does not significantly influence cell sheet movement in our migration model.

Collective migration is the result of integrin-dependent forces towards the substrate and cadherin-based intercellular forces that maintain cell-cell contacts. To test the involvement of actomyosin-dependent cell contractility in our collective migration experiments, we added blebbistatin to the culture medium, a myosin-II activity inhibitor, in moderate levels (2 μM) to avoid the completely detach of cells. Under these conditions, cell sheets migrating on pFN^{wt} treated with blebbistatin increase their velocity (Fig. 31F). On the contrary, cell sheets of keratinocytes on pFN^{syn} and treated with blebbistatin significantly reduced their velocity

reaching similar values to cells on pFN^{wt} without blebbistatin (Fig. 31G). These results indicate first, that partially reduced actomyosin contraction, such as on pFN^{syn} or low levels of blebbistatin migrating on pFN^{wt}, confers a migratory advantage, and second, this advantage is lost when the two factors (migration on pFN^{syn} and blebbistatin treatment) act together.

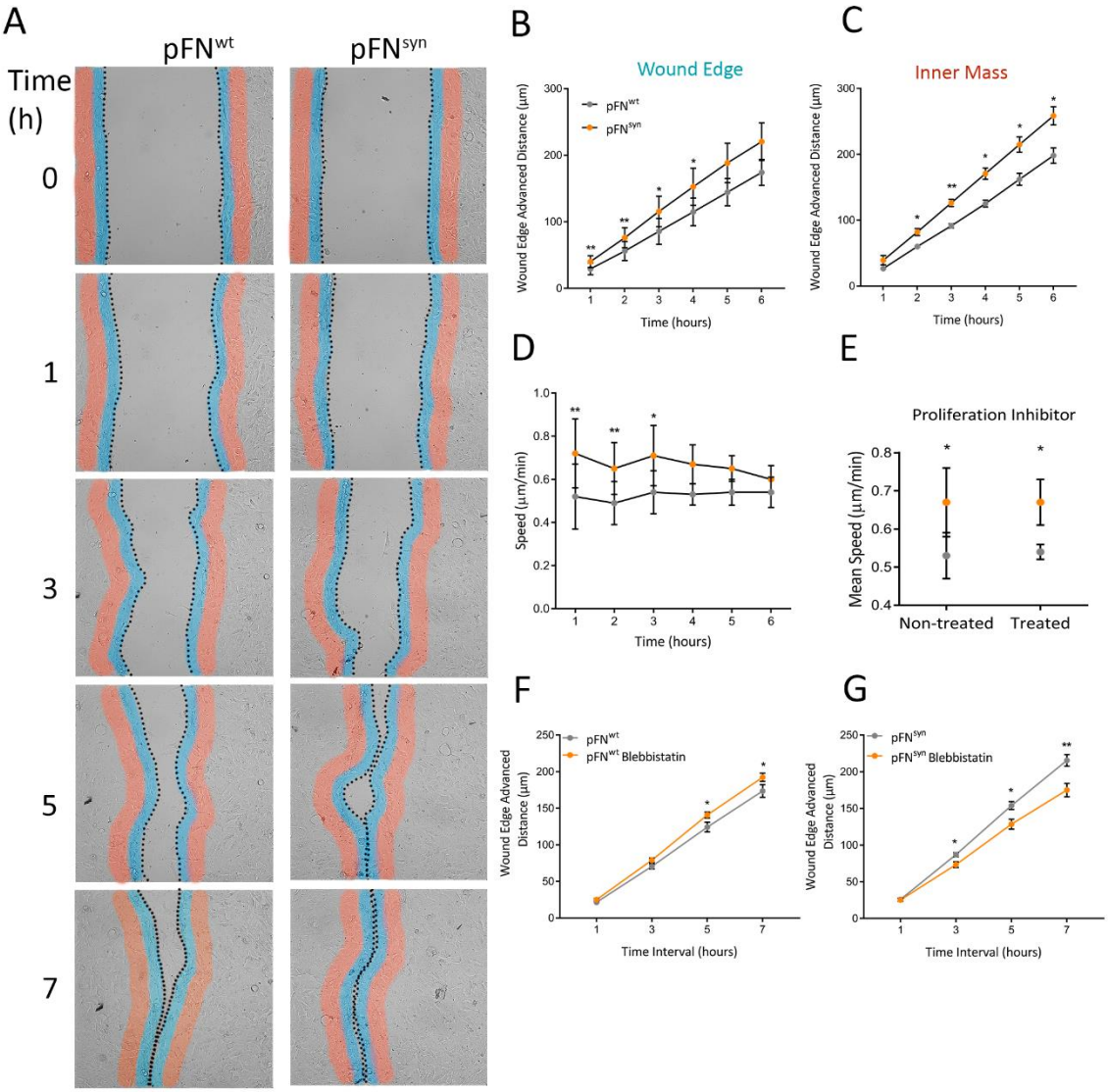

Figure 31. Keratinocyte collective migration on plastic coated with purified pFN^{wt} or pFN^{syn}. A) Representative images of keratinocyte collective migration at 0, 1, 3, 5 and 7 hours after removing the self-insertion device. Cells marked in blue colour correspond to the leading front and cells at the inner mass are highlighted in red colour B) Distance advanced by keratinocyte at the leading front or C) the inner mass migrating on pFN^{wt} or pFN^{syn} along different time points. D) Mean speed of collective sheet over the distance advanced on pFN^{wt} and pFN^{syn} substrates at the leading edge. E) Mean speed of cells treated or non-treated with Cytosine β-D-Arabinofuranoside to inhibit cell proliferation. Distance advanced by the cell front after 7 h migrating on F) pFN^{wt} and G) pFN^{syn} –coated plastic substrates with or without a treatment with blebbistatin (2µM) to inhibit cytoskeleton contraction. Results are the mean ± SEM from three independent experiments. Statistically significance was determined using the Student t-test p-value * $p<0.05$ and ** $p<0.01$

III The relevance of the FN synergy site in fibroblasts migration and differentiation *in vitro*

After skin injury, the dermal tissue is destroyed and has to be replaced by the surrounding cells. Fibroblasts are the main cell type in charge of synthesising the ECM proteins that fill the wounded area mainly formed by FN and collagen III/I. It has been described that fibroblasts change their pattern of integrins expression in order to adapt to the new ECM composition and adopt a migratory phenotype (Koivisto et al., 2014, Schnittert et al., 2018). Integrins that are up-regulated are mainly FN-binding heterodimers such as α5β1 and αv-class integrins which bind the RGD motif. In addition, fibroblasts undergo conversion to myofibroblasts stimulated by increased ECM stiffness and the presence of active TGF-β1. One of the most important hallmarks of myofibroblasts conversion is the expression of the high contractile actin α-SMA.

1. Analysis of *Fn1*$^{+/+}$ and *Fn1*$^{syn/syn}$ fibroblasts migration by scratch assay

To directly analyse the function of the FN synergy site in the process of matrix remodelling and fibroblast migration, immortalized *Fn1*$^{+/+}$ and *Fn1*$^{syn/syn}$ fibroblasts (Benito-Jardón et al., 20017) from wild-type and mutant mice were seeded on laminin-coated glasses and let to secrete and assemble their own ECM. In addition, we cultured fibroblasts in presence of Cilengitide, a αv-class integrins inhibitor, to eliminate the compensatory effect of αv-class integrins when the FN synergy site is inactivated. When cell cultures were confluent, the monolayer was scratched with a yellow pipette tip and cells were allowed to migrate to cover the gap for almost 24 h (Fig. 32A). We measured the mean velocity of cells in the migratory front and observed a significant reduction in the cell velocity of *Fn1*$^{syn/syn}$ fibroblasts (0.19 ± 0.03 μm/min) compare to FN^{wt} expressing fibroblasts (0.26 ± 0.03 μm/min) in the presence of αv-class inhibitor but with comparable cell speeds when the inhibitor is absent (Fig. 32B). Cell directionality was also analysed. At the wound edge, the directionality of cells is significantly different in the presence or absence of the αv-class inhibitor showing an increment in cell directionality when the αv-class integrins are blocked although no significant differences are observed between *Fn1*$^{syn/syn}$ fibroblasts compared to *Fn1*$^{+/+}$ in this conditions (Fig. 32C and 32D).

We then analysed the migration of single-cells that separate from the main monolayer (Fig. 32E white arrows) when there is no contribution of cell-cell interactions. We observed that

single *Fn1*$^{syn/syn}$ fibroblasts migrate at slower speeds in the presence or absence of cilengitide when they migrate individually (Fig. 32F).

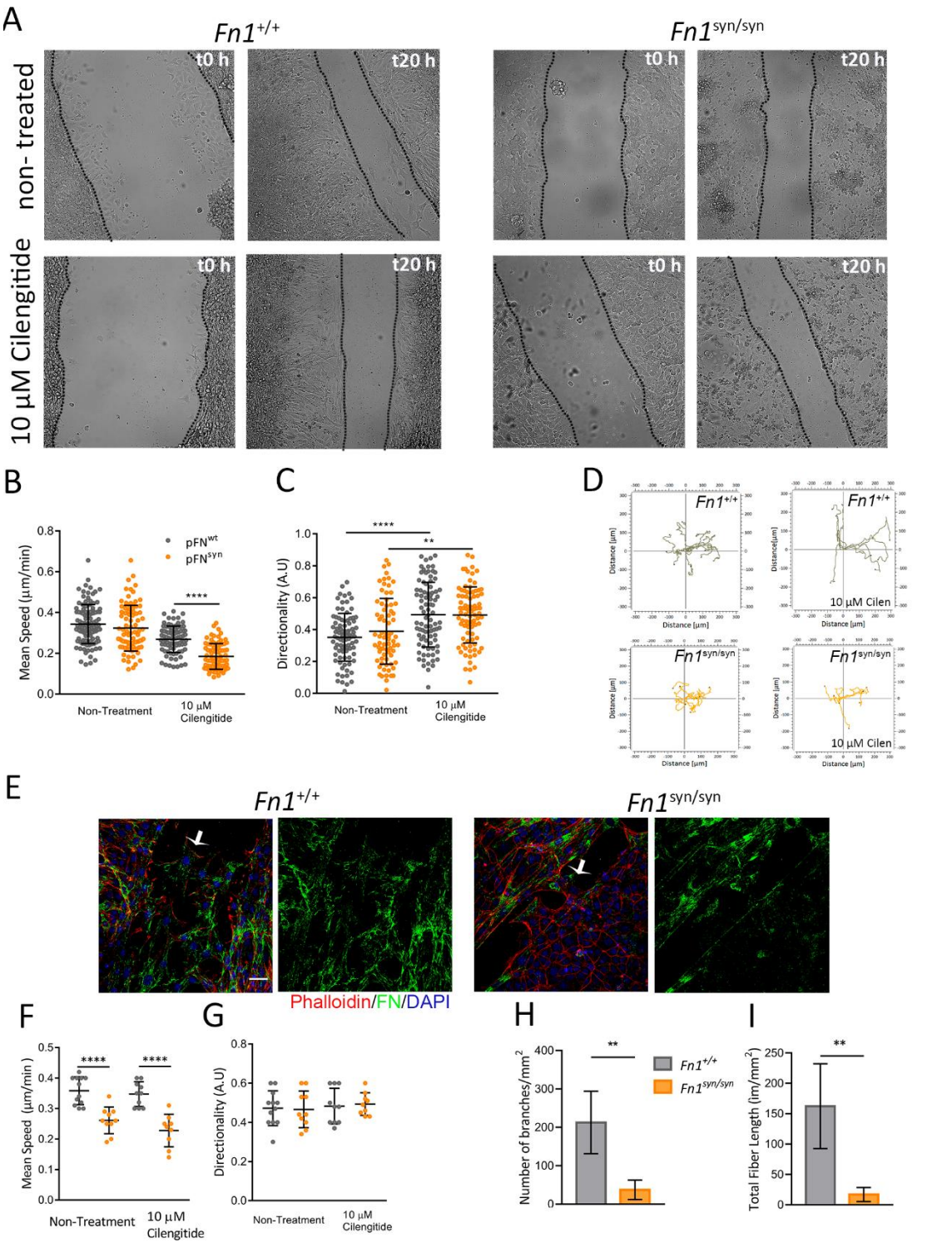

Figure 32. Scratch assay using immortalized fibroblasts derived from *Fn1*$^{+/+}$ or *Fn1*$^{syn/syn}$ mice. A) Representative images from three independent scratch assays using *Fn1*$^{+/+}$ or *Fn1*$^{syn/syn}$ fibroblasts migrating 20 h on glass. Wound edge B) mean speed and C) directionality of fibroblasts migrating after 20 h calculated in the presence or absence of cilengitide (10 µM) as a αv-class inhibitor. D) Cell tracks of representative cells migrating on FN^{wt} (grey colour) or

FN^{syn} (orange colour) substrates without (left) or with (right) αv-class inhibitor. E) Immunofluorescence of *Fn1*$^{+/+}$ or *Fn1*$^{syn/syn}$ fibroblasts after 24 h scratch assay migrating on self-secreted FN^{wt} or FN^{syn} matrices. F) Mean speed and G) directionality of leading cells at the wound edge in *Fn1*$^{+/+}$ or *Fn1*$^{syn/syn}$ fibroblasts in the presence or absence of cilengitide. H) Quantification of number of branched FN fibrils per area and I) the length of the FN fibrils. Values represent 4 images per condition. Shown values are collected from cell tracking in three independent experiments (Materials and Methods). Dots in single-cell graphs are the mean of 10 different leading cells. Statistically significance was determined using the Student t-test p-value ** p<0.01, *** p<0.001, **** p <0.0001. Scale bar 20 μm.

Despite the difference in cell migration, the directionality of the cells is not disturbed by the absence of the synergy site in the fibroblasts single-cell migration (Fig. 32G). As mentioned in the introduction, fascia dermal fibroblasts secrete and assemble a FN-collagen matrix that moves up in the dermis and contributes to the GT formation. Then, the FN fibrils assembly process was analysed in *Fn1*$^{syn/syn}$ fibroblasts and compared to *Fn1*$^{+/+}$ fibroblasts. To that purpose, we stained and characterised FN fibrils in the newly assembled ECM that migrating fibroblasts built to move along the gap (Fig. 32E). The FN^{syn} newly formed matrices are significantly less dense than matrices assembled by *Fn1*$^{+/+}$ fibroblasts, whose fibres are shorter and with significantly fewer branches (Fig. 32H and 32I). These results suggest that *Fn1*$^{syn/syn}$ fibroblasts assemble FN fibrils more slowly and form a less elaborated matrix than *Fn1*$^{+/+}$ fibroblasts, and this might be the reason limiting the migration in the absence of cell-cell contacts.

2. Study of *Fn1*$^{+/+}$ and *Fn1*$^{syn/syn}$ dermal fibroblasts differentiation to myofibroblasts

DFs were isolated from the back skin of *Fn1*$^{+/+}$ and *Fn1*$^{syn/syn}$ mice (see Materials and Methods section 2.1). To study whether the substrate stiffness affects myofibroblast conversion in the absence of the synergy site, DFs were seeded on PA gels with different stiffness (4 kPa, 50 kPa) and on glass coated with either pFN^{wt} or pFN^{syn}. After one day of culture using FN-depleted medium, cells were fixed and immunostained for α-SMA together with phalloidin to label the actin cytoskeleton (Fig. 33A). The percentage of myofibroblasts conversion was calculated as the number of α-SMA positive cells respect to the total number of cells per image. It has been described that the overall increment in ECM stiffness induces fibroblasts to myofibroblasts conversion. According to the literature, in our experiments increased stiffness induces an increment in the proportion of myofibroblast conversion in both genotypes, from 50% to 61% on pFN^{wt} and from 43% to 50% in pFN^{syn}. However, in the absence of the FN synergy site the myofibroblasts conversion is significantly reduced being more accused on softer substrates

and on glass we do not observe significant differences between *Fn1*$^{+/+}$ and *Fn1*$^{syn/syn}$ DFs (Fig. 33B). According to these results the absence of the synergy site could reduce mechanical signals transmission from the cells surroundings to the intracellular environment to activate fibroblasts into myofibroblasts.

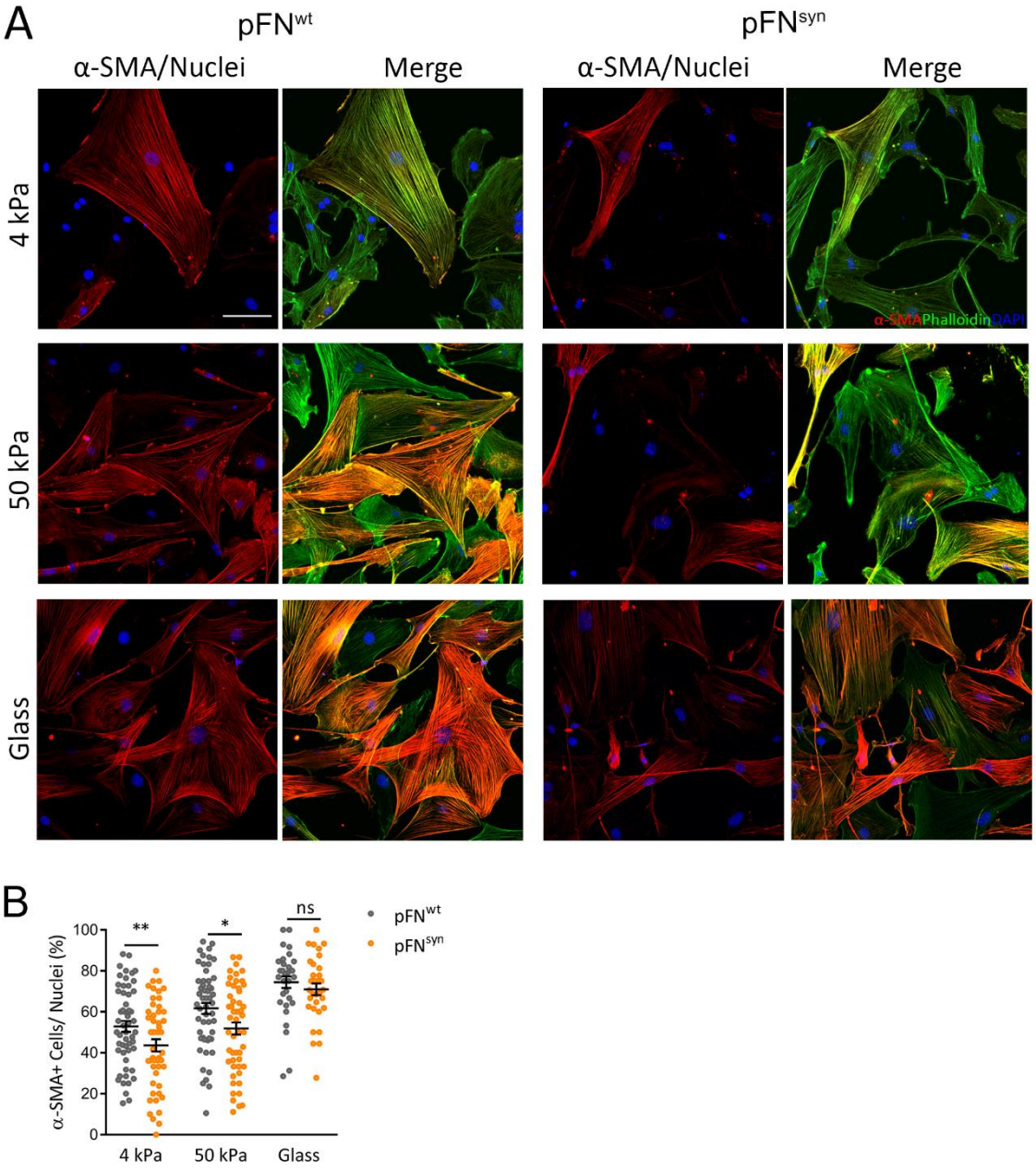

Figure 33. Dermal fibroblasts conversion to myofibroblasts on compliant surfaces. A) Representative pictures of isolated DF from *Fn1*$^{+/+}$ and *Fn1*$^{syn/syn}$ mice seeded on compliant PA gels with 4 kPa and 50 kPa, and glass coverslips (about 70 GPa) coated with pFN^{wt} or pFN^{syn}, respectively. The actin cytoskeleton is marked in green using phalloidin, nuclei is stained with DAPI in blue colour and immunostaining for α-SMA appears in red colour. Merge comprises the three stainings. B) Quantification of DF conversion to myofibroblasts calculated as the percentage of α-SMA-positive cells related to total number of cells per picture. Four different biological replicates with quantification

from 15 different pictures per assay were used for the statistical analysis. Statistically significance was determined using the Student t-test p-value * $p<0.05$ and ** $p<0.01$.

3. TGF-β bioassay in matrices from *Fn1*$^{+/+}$ and *Fn1*$^{syn/syn}$ dermal fibroblasts

Two different mechanisms could explain the role of the FN synergy site in myofibroblast conversion. On one hand, the absence of the synergy site might impair α5β1-dependent mechanosensing making cells less responsive to changes in ECM rigidity and thus, alter DF conversion to myofibroblasts. On the other hand, the FN synergy site might condition the levels of active (free) TGF-β1. TGF-β1 is secreted by cells in an inactive form bond to the latent associated protein (LAP). LAP has an RGD motif on its structure that allows binding to cells via αvβ6 integrin and to the FN through the latent binding protein (LTBP) on the opposite side (Fig. 32). Integrins play a crucial role in TGF-β1 activation as cells contract and pull from one side, induce a conformational change in LAP that liberates TGF-β1 to the surrounding media (Giacomini et al., 2012, Hinz, 2013). It has been shown that the release of TGF-β1 is directly linked to the ECM elasticity and increases either on stiffer substrates or when the pulling forces of fibroblasts are high (Wipff et al., 2007; Klingberg et al., 2014). α5β1 integrins have been directly linked to the process of force transmission through myosin-II-mediated cell contractility via RhoA and Rho kinase activation (Huveneers etal., 2008; Roca-Cusachs et al., 2009; Schiller et al., 2013) and more recently it was demonstrated the contribution of the FN synergy site to fully transmit this tension (Meckmongkol et al., 2007; Benito-Jardón et al., 2017; Miroshnikova et al., 2017).We then hypothesised that FN synergy site could control TGF-β release from fibrotic ECMs and hence mediate in myofibroblasts conversion.

To directly test the implications of the FN synergy site in TGF-β1 release bioassay was used to measure active TGF-β1 in conditioned media by *Fn1*$^{+/+}$ and *Fn1*$^{syn/syn}$ isolated DFs.

Mink lung epithelial cells (MLECs) constitutively transfected with the luciferase encoding gene under the control of a TFG-β1-dependent promoter were used to measure the presence of free TFG-β1 in conditioned media. Commercial TFG-β1 was used to test the sensibility of MLECs to different growth factor concentrations (Fig. 34A). *Fn1*$^{+/+}$ and *Fn1*$^{syn/syn}$ DFs were grown for 3-days secreting and assembling their own ECM-containing TFG-β1. After 3 days, samples of DFs conditioned media were collected and added for 14 h to MLECs. This medium will contain free active TGF-β1, released from the ECM by the activity of the cells, and inactive TGF-β1 bond to LAP secreted by cells but not bond to the ECM. Active TGF-β1 was measured from the medium directly incubating the medium with MLECs (Fig. 34B). The total amount of

TGF-β1 (Fig. 34C) secreted by cells (active and inactive) was measured as described in Materials and Methods (Section 7.2). After incubation, MLECs were lysed and the amount of synthetized luciferase was measured with a luminometer. The assay shows that the culture medium from *Fn1*$^{syn/syn}$ DFs contains more soluble TGF-β1 (free plus inactive forms) (Fig. 34C) but less free TGF-β1 (Fig. 34B), although the percentage of active (free) TFG-β1 relative to the total amount in the medium is significantly decreased compared to *Fn1*$^{+/+}$ DF cultures. This indicate both that the ECMs assembled by *Fn1*$^{syn/syn}$ DFs have a reduced capacity to trap LLC complexes and that are less efficient to release the active form of TFG-β1 compared to *Fn1*$^{+/+}$ DFs.

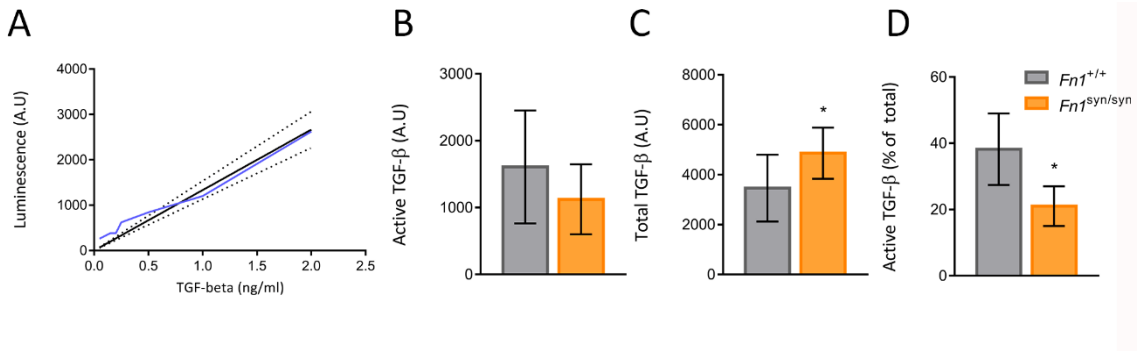

Figure 34. Measurement of active TGF-β1 bioassay in DFs conditioned media. A) MLECs luminescence measured using different concentrations of commercial TFG-β1. B) Active TFG-β1 C) Total soluble TFG-β1 D) Percentage of active TFG-β1 in conditioned media from *Fn1*$^{+/+}$ and *Fn1*$^{syn/syn}$ DFs related to the total amount. Graphics are the results from three biological assays with 2 or 3 technical replicas each one. Statistically significance was determined using the Student t-test p-value * $p<0.05$

We hypothesize in an illustration how the absence of the synergy site could be impairing the TGF-β1 release from a pre-formed ECM and hence the normal conversion from fibroblasts to myofibroblasts (Fig. 35A and 35B). In normal conditions, the full engagement between FN and α5β1 allows the complete force transmission when the cell contraction pulls the ECM from each side. On the contrary, when the FN lacks the FN synergy site, a poor engagement with α5β1 does not allow the cell machinery to fully contract the cell body and hence the TGF-β1 liberation from the ECM to the medium.

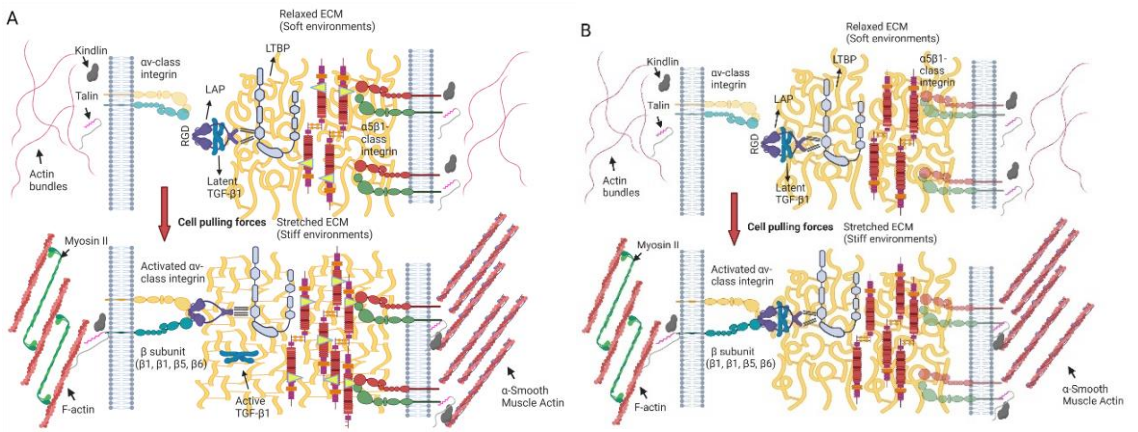

Figure 35. Illustration of possible role of FN synergy site in TGF-β1 activation. As it was previously shown in Figure 10 A) TGF-β1 is secreted bond to LAP and stored in the FN-containing (FN synergy site in yellow) ECM bond to cells on one side and the LTPB to the opposite side. As the ECM stiffness increases, cells sense the environment and change their cytoskeleton composition expressing α-smooth muscle actin. Pulling forces exerted by cells on the ECM liberate the TGF-β1 to the surroundings allowing its signalling when bind to cells receptors. B) Our results show that in the absence of the synergy site there is less presence of α-smooth muscle actin in fibroblasts cytoskeleton and hence the strength to pull the ECM and to liberate TGF-β1 to the surroundings is compromised.

VI DISCUSSION

Skin wound healing has been broadly studied in the last decades as millions of people worldwide require medical care due to pathological skin diseases every year. The new therapies are focused on achieving scarless skin regeneration with great focus in animal and human models (Monavarian et al., 2019). Scars replace the original connective tissue with dense "plugs" of matrix fibres that tighten the tissue and reduce its flexibility. Different types of fibroblasts have been shown to contribute to the formation of alternative fibrotic structures of connective tissue (Mascharak et al., 2021) and how does mechanical signals differentially drive to scar formation or regeneration remains an important question.

FN is a key protein in skin regeneration, which expression highly increases during the process of wound healing (Clark, 1990; Sakai et al., 2001). FN in skin wounds is an important component of the provisional matrix assembled during the first stages of the healing process. It is used by keratinocytes as substrate to migrate during re-epithelialization and it takes part of the FN-collagen network assembled by fibroblasts that guides cell invasion to achieve either regeneration or scar formation. The major cell adhesion motif in FN is the RGD sequence in the FNIII10 module. This motif binds α5β1/αIIbβ3 and αv-containing integrins and is essential during development (Yang et al., 1993; Leiss et al., 2008; Benito-Jardón et al., 2020). Abundant studies have shown how the FN RGD motif can differently regulate integrin class function and cell behaviour (Rocha et al., 2018; Benito-Jardón et al., 2017; Sani et al., 2021). α5β1 and αv-class integrins contribute to organise focal adhesions with distinct function, but only α5β1 integrins are responsible of fibrillar adhesions, connecting stress fibres and regulating their contractility (Bharadwaj et al., 2017). Fibroblasts engineered to express only α5β1 integrins present a more contractile phenotype compared to those only expressing αvβ3 integrins that organize bigger focal adhesions (Schiller et al., 2013). The reason of this difference is that α5β1 is directly linked to the myosin-II activity via RhoA/Rock-mediated signalling (Danen et al., 2002; Morgan et al., 2009, Gagné et al., 2020). Fully α5β1 integrin binding to FN and force development requires of a second adhesion motif, the synergy site, which engages the α5 integrin subunit and whose mutation can be partially compensated by αv-class integrins (Benito-Jardón.2017). When α5β1 binds the FN-RGD and re-enforces the bond with the synergy site motif, it follows a catch-bond behaviour (Benito et al., 2020). This implies that when force is applied to the FN-integrin bond, reinforces the union instead of breaking it, increasing its lifetime (Friedland et al., 2009; Kong et al., 2009). In this thesis our aim was to investigate the function of the FN synergy site in a process of fibrosis that involve FN overexpression and integrin-mediated force transmission. To this end, we focused on skin wound healing that includes several processes where cell adhesion to FN is highly tensioned

and whose control will determine the outcome of the healing process, repair or scar formation. We combined *in vivo* analysis of mice expressing FN with truncated synergy site together with *in vitro* studies using both keratinocytes, as the cell type responsible for re-epithelization, or fibroblasts and dermal fibroblasts that are the major producers of ECM in the dermal wound.

Upon wounding and the consequent epidermis destruction, keratinocytes at the edges of the wound are activated and acquire a migratory phenotype. The epidermal tongue moves on a provisional matrix containing FN and which includes a leading edge, whose cells up-regulate α5β1 expression, followed by a proliferative hub of basal cells. Our *in vivo* studies, do not evidence open structural differences during re-epithelialization in *Fn1*$^{syn/syn}$ mice compared to those expressing wild-type FN. The time for closing the epidermal tongue was indistinguishable between the two genotypes and, in the long term (25 daw), epidermal thickness was similar in *Fn1*$^{syn/syn}$ in wild type. Additionally, the distribution and differentiation of both basal and suprabasal keratinocytes was indistinguishable between *Fn1*$^{syn/syn}$ and wounds expressing FN^{wt}. However, we observed lower proliferation rates in *Fn1*$^{syn/syn}$ neo-epidermis at 9 daw compared to same stage *Fn1*$^{+/+}$ wounds and, accordingly, the epidermal thickness in closed wounds was significantly diminished in mutant mice (around 30%) during the 9-15 daw time-frame. Weakened adhesion to deposited FN^{syn} could be the reason for impaired keratinocytes proliferation and hence affecting epidermal thickness at 9-15 daw (Goh et al., 1997, Mittal et al., 2013). When we labelled α5β1 integrin as the major synergy site binding integrin at the epidermal tongue we observed differences in the number of α5β1-expressing basal cells at the leading edge. At the early stage of 4 daw, there were more FN^{syn} basal keratinocytes expressing α5-subunit compared to those expressing FN^{wt}.

Although it has been suggested that in the first stages after wounding keratinocytes can migrate individually, most of the epidermal tongue movement is produced by collective migration (De Pascalis and Etienne-Manneville, 2017). We studied both single and collective keratinocyte migration *in vitro*, with apparently contradictory results. When keratinocytes migrated individually, cells on pFN^{syn} moved significantly slower than keratinocytes on pFN^{wt}, being this effect more evident during the first hours of migration and on softer substrates. The reduced velocity was concomitant to reduced directionality in keratinocytes on pFN^{syn} compared to cells on pFN^{wt}. On the contrary, during collective migration keratinocyte sheets on pFN^{syn} advanced faster than on pFN^{wt}. Individual migration requires directional cell polarity involving a leading edge at the cell front and a lagging edge at the back of the cell. This motion, based in a process of contraction- elongation, implies strong traction forces generated by

integrin-based adhesions: protrusion and adhesion of the leading edge and retraction of the rear edge. Shiu et al. (2018) demonstrated that cell traction forces are larger in perinuclear regions than in the frontal cell periphery because they depend on α5β1 integrin-based fibrillar adhesions, whereas in the periphery predominates αvβ3-containing focal adhesions (Shiu et al., 2018). Perinuclear adhesions connect thick stress fibres that are necessary to retract the rear edge of the cell during migration. Our results indicate that a defective synergy site in the FN substrate might limit traction forces for cell rear retraction with its consequent chaotic directionality and reduced velocity. Collective migration, however, implies a tight balance between cell-cell junctions and cell-ECM bonds (Ladoux and Mège, 2017). According to our results, when α5β1 integrin-mediated cell-FN adhesions were weakened upon lack of the FN synergy site or by treatment with Blebbistatin, a myosin-II contractility inhibitor that disrupts transmission of traction forces to integrins but preserves cell-cell contacts, the keratinocyte sheets moved significantly faster on absent synergy site substrates than keratinocyte sheets on FN^{wt}. In our collective migration assays, we discarded a potential influence of different proliferation rates as differences were maintained in the presence of a proliferation inhibitor. Vedula et al (2012) demonstrated that in wide sheets of epithelial collective migration, cells in the middle of the sheet organize small cohorts forming transient vortices that decrease the speed to move forward. They observed that inhibiting cell-cell adhesion was lowering migration velocity but, on the contrary, under Blebbistatin treatment the formation of vortices disappeared, and the dynamics of migration was more directed and accelerated. Our results confirm that during collective migration myosin-II-induced cell contractility associated to rear retraction is dispensable and compensated by cell-cell adhesions and that the absence of the synergy site could diminish the lifetime of FN-α5β1 bonds and hence accelerate binding/unbinding rates, thus increasing collective migration speed. Our results also confirm that force transmission is sustained by cell-cell adhesion as speed differences are maintained at the cell front and inner mass. The convergence of the two effects, retarded individual migration and accelerated collective migration, could explain the apparently normal rate of re-epithelialization of *Fn1*$^{syn/syn}$ wounds suggesting that although the α5β1-expresing leading front is important to drive migration of cells, cell-cell interactions far away from the leading edge also actively contribute to the net progression of the epidermal layer. Possibly weak traction forces due to synergy mutation only influence negatively the initial hours when the epidermal tongue is not fully stablished and cells migrate individually, but might be compensated by accelerated migration in the following days.

The *in vivo* analysis of wounded dermis, evidenced that *Fn1*$^{syn/syn}$ mice depict important changes in the GT in the first 4 days after wounding, although most of them are normalised in the following days. At 4 daw, *Fn1*$^{syn/syn}$ mice form a GT half of the size of wild-type wounds. In addition, the GT contained less FN, collagen and myofibroblasts. In general, the maximal expression peak of main ECM proteins was delayed in Fn1$^{syn/syn}$ wounds. Immediately after the initial FN-fibrin matrix clot secreted by hematopoietic cells during the stage of inflammation, fibroblasts and myofibroblasts will form a provisional FN-collagen ECM that constitutes the structure of the GT that will be invaded by cells. According to the literature, this matrix is to some extent dragged by fascia-resident fibroblasts, which are mobilized towards the dermis in response to deep injuries (Harris A.K. Stopak 1981, Correa-Gallegos et al, 2019). This ECM is partially secreted and assembled by these fibroblasts, together with dermal fibroblasts migrating from the periphery of the wound (Correa-Gallegos and Rinkevich, 2021). An important proportion of the GT fibroblasts is transformed into myofibroblasts (Rinkevich et al., 2015). Myofibroblasts secrete high amounts of FN and collagen, express α-SMA and are highly contractile cells that remodel matrices into stiff structures. In our model of wound healing, we observed that at 4 daw the number of α-SMA-positive cells in the *Fn1*$^{syn/syn}$ GTs was reduced to the 30% of the observed in *Fn1*$^{+/+}$ GTs. Thus, the decrease of FN in the initial GT is possibly linked to the lower presence of myofibroblasts. Moreover, it is well demonstrated that fibrilar FN networks are a pre-requisite to assemble fibrilar collagen I matrices (Sottile 2002; Velling, 2002; Kubow et al., 2015). Therefore, the decrease of collagen in *Fn1*$^{syn/syn}$ GT could be the consequence of reduced and/or badly assembled FN matrices. Moreover, the observed defective FN fibrils assembly by *Fn1*$^{syn/syn}$ fibroblasts in our *in vitro* studies could be related with a reduced FN and collagen deposition in *Fn1*$^{syn/syn}$ wounds compare to wild type conditions.

We explored putative causes for the αSMA-positive cells decrease in early Fn1$^{syn/syn}$ wounds: i) we studied cell proliferation in the GT; ii) we analysed *in vitro* fibroblast migration; and iii) we explored fibroblast-to-myofibroblasts transformation induced by TGF-β1.

At 4 daw, we observe a reduction of cell division together with lower numbers of proliferative cells in the GT of *Fn1*$^{syn/syn}$ mice compared to *Fn1*$^{+/+}$ GTs. Then, proliferation could, at least partially, explain the presence of less fibroblasts and the reduced size of the GT. However, myofibroblasts are large cells that proliferate at a slower rate than fibroblasts. Then possibly other factors influence in the lower numbers of α-SMA-positive cells.

The GT is infiltrated by dermal fibroblasts migrating from periphery and by fibroblasts mobilized from the fascia that up-regulate N-cadherin and Connexin-43 (Jiang et al., 2020;

Wan et al. 2021), resulting in coordinated collective cell migration from wound edges toward the centre. In our model, upon wounding at 4 daw, clouds of αSMA-positive cells were visible at the lateral edges of the wound spanning all dermis. In the following days myofibroblasts at the periphery moved towards the centre by the upper layers of the dermis. At 4 daw, in *Fn1*$^{+/+}$ wounds we observe that the α-SMA-positive population enriches the upper regions, below the newly formed epidermis. In *Fn1*$^{syn/syn}$ GT, however, the αSMA-positive cloud is located in deeper levels of the dermis, suggesting a retard in their mobilization. We studied the motile behaviour of fibroblasts using an *in vitro* scratch model, which illustrates both the fibroblast velocity to secrete and assemble a migratory substrate and the velocity to migrate on this substrate. No differences in the mean speed were observed at the wound edge unless. However, we observed a reduction in the migration velocity in the presence of the αv-class integrin inhibitor, Cilengitide, confirming that αv-class integrins can compensate the absence of the synergy site (Benito-Jardón et al., 2017). Our results indicate that *Fn1*$^{syn/syn}$ fibroblasts migrating on uncoated and highly stiff surfaces exhibit slower front advance than *Fn1*$^{+/+}$ fibroblasts, possibly due to slow down capacity to assemble a FN fibrilar substrate. This was confirmed when the process of FN matrix assably was analysed by immunofluorescence in fibroblasts at the scratch gap after 24 h migration. *Fn1*$^{syn/syn}$ fibroblasts presented less amount and shorter fibres compared to *Fn1*$^{+/+}$ fibroblasts what indicated a defect in matrix remodelling and hence affecting the procces of migration.

The number of α-SMA-expressing fibroblasts at the wound site is determined by a positive feedback loop in which tension facilitates TGF-β1 production and activation. TGFβ1 signalling induces α-SMA expression and α-SMA-expressing fibroblasts, in turn, increase force production and tension development (Tomasek at al., 2002; Wipff et al., 2007). We observed that dermal fibroblasts isolated from *Fn1*$^{+/+}$ and *Fn1*$^{syn/syn}$ mice and growing on surfaces of different rigidity increase their α-SMA expression proportionally to the substrate stiffness and we evidenced that the absence of the FN synergy site reduced this rigidity cell response. In the literature, skin rigidity has been described to increase along the healing process ranging from 0.01-10 kPa in the fibrin-FN clot, to ~18 kPa in early GT and reaching levels of ~50 kPa in mature GT as the degree of organization of FN and collagen fibres increase. This would be in line with the observed decrease in myofibroblasts presence at 4 daw in GT from *Fn1*$^{syn/syn}$ wounds in the present study (Wong et al., 2011, Pensalfini et al., 2018).

LTBP-1, has been shown to be secreted independently of FN, but its fibrilar organisation in the ECMs appears to depend on the presence of FN fibrilar matrices. Consequently, integrin-mediated force application on FN fibrils induces conformational changes in LTBP-1 that lead to

the release of the active form of TGF-β1 (Klinberg et al, 2014). Thus, stiffer substrates and highly contractile myofibroblasts potentiate TGF-β1 release. Contrarily, relaxed or soft ECMs and non-contractile fibroblasts will induce poor TGF-β1 activation. Two types of integrins contribute to efficient TGF-β1 activation in stiff FN ECMs. On one hand, LAP contains a RGD motif that is engaged by αv-class integrins (Yang et al., 2007). On the other hand, cell binding to FN by α5β1 integrins generates elastic forces on the ECM that will induce conformational changes on large latent complexes (LLC) potentiating TGF-β1 release (Keski-Oja et al., 2004) (Fig. 34A). Using DFs in culture, we observed that both the ECMs assembled by *Fn1*$^{syn/syn}$ DFs have a reduced capacity to trap LLC secreted by the same cells and that *Fn1*$^{syn/syn}$ DFs are less efficient to release TFG-β1 in its active form compared to *Fn1*$^{+/+}$ DFs. The TGF-β1 release reduction was supported by our observation *in vivo* of decreased levels of p-smad2-positive cells in the granular tissue at 4 daw in *Fn1*$^{syn/syn}$ wounds, indicating lower TGF-β1 mediated cell signalling.

Our results show that the loss of FN synergy site is dispensable for *in vivo* macroscopic wound closure but deep molecular and cellular analysis shows a defect in granulation tissue formation and ECM deposition. Although *Fn1*$^{syn/syn}$ fibroblasts apparently assemble normal FN fibrilar matrices (Benito-Jardón 2017), lower traction forces due to lack of re-enforced α5β1-mediated cell adhesion will possibly limit FN fibril remodelling to achieve conformations that favour LTBP-1 storage or permit fast cell migration. In addition, the lack of FN synergy site will weaken actomyosin cell contractility and thus TGF-β1 release and activation with its consequent reduced proportion of transformed fibroblasts into myofibroblasts. Interestingly, the changes in *Fn1*$^{syn/syn}$ wounds were restricted to day 4. Our group demonstrated that αv-class integrins compensate the lack of synergy site function when external cell forces do not exceed certain threshold (Benito-Jardón et al., 2017). Effectively, we observed that *Fn1*$^{syn/syn}$ fibroblasts reduce significantly their velocity of migration when we add to the medium Cilengitide to block αvβ3 integrins. Possibly the FN synergy site is more relevant during the first stages of wound healing when the ECM is softer and FN is its major component. In the following days, as the number of α-SMA-positive cells increases and the ECM is enriched with other proteins, compensatory effects by αv-class integrins or integrins binding other ECM proteins will predominate.

However, it is important to point that the muscle *panniculus carnosus* in mice, which lies between the fascia and the skin, is well developed and plays a predominant function twitching rapidly the skin (Zomer et al., 2018). However, humans lack this twitching ability and have only a small remnant of this muscle and healing proceeds more slowly. Therefore, we cannot

exclude that the FN synergy site in human wound regeneration will be more critical than in mouse.

Another important conclusion from our data is that the absence of the FN synergy site reduces the size of the fibrosis in the earlier stages of healing. Mascharak et al., 2021 demonstrated that inhibiting Engrailed-1 (EN1) activation in wound fibroblasts promotes scarless wound repair. EN1-positive cells are the fascia mobilized fibroblasts that are mostly myofibroblasts and express α5β1 and αvβ3 integrins. They showed that Engrailed-1 expression was partially activated by mechanical tension sensing in resident fibroblasts (Mascharak et al., 2021). Lack of fascia fibroblasts drives to open wounds, but excessive fascia drives to big scars (Correa-Gallegos et al., 2019).

Molecular processes underlying mechanical signalling in wound healing have been proved to reduce the amount of granulated tissue and hence the ECM deposition (Blumbach et al., 2010; Wong et al., 2011; Werner et al., 2020). Our results show that tight mechanical conversation is needed between all healing players (cells and extracellular components) as shown that the lack of the FN synergy site impairs the normal cell behaviour in high tensional processes such as wound repair. These results have opened the revolutionary hypothesis that the outcome to postnatal wound healing, either fibrotic or regenerative, could be directed controlling myofibroblast mobilization and activation. In this context, peptides or antibodies blocking the FN synergy site might have a potential as antifibrotic tools in skin regeneration.

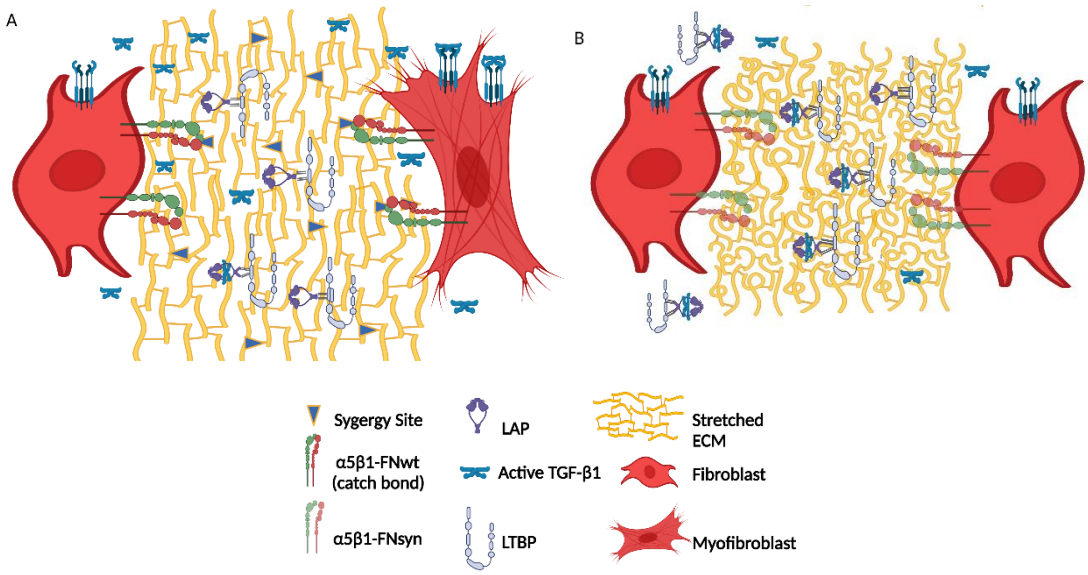

Figure 35. Non-proteolytic TGF-β1 activation in the granulation tissue of *Fn1*$^{+/+}$ (**A**) and *Fn1*$^{syn/syn}$ wounds (**B**). (A) TGF-β1 is secreted non-covalently bound to the LAP-LTBP complex and is stored on FN-containing ECMs. In *Fn1*$^{+/+}$ wounds as the ECM stiffness increases upon skin injury, FN binding cells increase traction forces on FN through

synergy site catch bond formation with α5β1 integrins. TGF-β1 is activated by its liberation from the latent complex and binds TGF-β1-receptors at the fibroblast membrane inducing myofibroblast conversion. (**B**) In *Fn1*$^{syn/syn}$ wounds ECMs are less stretched trapping less TGF-β1-LAP-LTBP latent complexes, and pulling forces mediated by FN-α5β1 bonds are reduced with the consequent decrease in TGF-β1 release and signalling.

VII CONCLUSIONS

Here we investigated the role of FN synergy site during cutaneous wound healing in mice carrying a dysfunctional FN-synergy motif (*Fn1*$^{syn/syn}$). From the present study we make the following conclusions:

1. The *Fn1*$^{syn/syn}$ mice show a delayed macroscopic wound closure at 4 days after wounding that is apparently compensated in the following days.
2. During the process of re-epithelialization in the epidermis of *Fn1*$^{syn/syn}$ wounds we observe an increment of α5β1 integrin expression in the basal layer compared to wounds from *Fn1*$^{+/+}$ mice, suggesting a compensatory effect to defective cell adhesion.
3. Our *in vitro* studies with migrating keratinocytes evidence that the absence of the synergy site develops apparently contradictory defects during single-cell and collective migration, which could explain normal timing for re-epithelialization.
4. During single-cell migration, keratinocytes migrating on FN^{syn} substrates show delayed wound closure due to lower speeds and decreased directionality.
5. During collective migration, FN^{syn} substrates accelerate the wound closure that we demonstrate to be directly linked to weakened myosin cytoskeleton contraction.
6. In the dermis, early delayed wound closure correlates with the presence of less granulation tissue in *Fn1*$^{syn/syn}$ wounds that are less fibrotic, with reduced content in myofibroblasts and collagen and FN deposition.
7. The defect in myofibroblasts conversion can derive from diminished TGF-β1-induced signaling in the granulation tissue of *Fn1*$^{syn/syn}$ wounds.
8. *In vitro* experiments using kidney fibroblasts derived from *Fn1*$^{+/+}$ and *Fn1*$^{syn/syn}$ mice reveal that the FN synergy site is important for the assembly of normal fibrillar FN matrices to withstand mechanical tensions required for cell migration.
9. *In vitro* experiments using dermal fibroblasts derived from *Fn1*$^{+/+}$ and *Fn1*$^{syn/syn}$ mice reveal that the FN synergy site is important for rigidity sensing and hence to adapt cell behavior to substrate stiffness.
10. Dermal *Fn1*$^{syn/syn}$ fibroblasts assemble FN^{syn} matrices that probably have a reduced capacity to store the Large Latent TGF-β1 Complex. This defect, together with a decreased capacity of cells to develop pulling forces on their ECM, contribute to reduce TGF-β1-induced signaling.

VIII BIBLIOGRAPHY

Abe M, Harpel JG, Metz CN, Nunes I, Loskutoff DJ, Rifkin DB (1994). An assay for transforming growth factor-beta using cells transfected with a plasminogen activator inhibitor-1 promoter-luciferase construct. Anal Biochem.Feb 1; 216(2):276-84. doi: 10.1006/abio.1994.1042. PMID: 8179182.

Abu-Hijleh, M. F., Roshier, A. L., Al-Shboul, Q., Dharap, A. S., & Harris, P. F. (2006). The membranous layer of superficial fascia: Evidence for its widespread distribution in the body. Surgical and Radiologic Anatomy, 28(6), 606–619. https://doi.org/10.1007/s00276-006-0142-8

Achterberg VF, Buscemi L, Diekmann H, Smith-Clerc J, Schwengler H, Meister JJ, Wenck H, Gallinat S, Hinz B (2014). The nano-scale mechanical properties of the extracellular matrix regulate dermal fibroblast function. J Invest Dermatol. Jul; 134(7):1862-1872. doi: 10.1038/jid.2014.90. Epub 2014 Feb 13. PMID: 24670384.

Adams, J. C., & Watt, F. M. (1991). Expression of β1, β3, β4 and β5 integrins by human epidermal keratinocytes and non-differentiating keratinocytes. Journal of Cell Biology, 115(3), 829–841. https://doi.org/10.1083/jcb.115.3.829

Aota S, Nomizu M, Yamada KM. The short amino acid sequence Pro-His-Ser-Arg-Asn in human fibronectin enhances cell-adhesive function (1994). J Biol Chem. Oct 7; 269(40):24756-61. PMID: 7929152.

Aragona, M., Dekoninck, S., Rulands, S. (2017). Defining stem cell dynamics and migration during wound healing in mouse skin epidermis. Nat Commun 8, 14684 (2017). https://doi.org/10.1038/ncomms14684

Ashcroft GS, Yang X, Glick AB, Weinstein M, Letterio JL, Mizel DE, Anzano M, Greenwell-Wild T, Wahl SM, Deng C, Roberts AB (1999). Mice lacking Smad3 show accelerated wound healing and an impaired local inflammatory response. Nat Cell Biol. Sep; 1(5):260-6. doi: 10.1038/12971. PMID: 10559937.

Astrof S, Hynes RO. Fibronectins in vascular morphogenesis (2009). Angiogenesis; 12(2):165-75. doi: 10.1007/s10456-009-9136-6. Epub 2009 Feb 14. PMID: 19219555; PMCID: PMC2716138.

Barkauskas CE, Noble PW (2014). Cellular mechanisms of tissue fibrosis. 7. New insights into the cellular mechanisms of pulmonary fibrosis. Am J Physiol Cell Physiol. Jun 1; 306(11):C987-96. doi: 10.1152/ajpcell.00321.2013. Epub 2014 Apr 16. PMID: 24740535; PMCID: PMC4422352.

Barker TH, Engler AJ (2017). The provisional matrix: setting the stage for tissue repair outcomes. Matrix Biol. Jul; 60-61:1-4. doi: 10.1016/j.matbio.2017.04.003. PMID: 28527902; PMCID: PMC5831186.

Bass, M. D., Morgan, M. R., & Humphries, M. J. (2007). Integrins and syndecan-4 make distinct, but critical, contributions to adhesion contact formation. Soft Matter, 3(3), 372–376. https://doi.org/10.1039/b614610d

Benito-Jardón, M., Klapproth, S., Gimeno-LLuch, I., Petzold, T., Bharadwaj, M., Müller, D. J., Costell, M. (2017). The fibronectin synergy site re-enforces cell adhesion and mediates a crosstalk between integrin classes. ELife, 6, 1–24. https://doi.org/10.7554/elife.22264

Benito-Jardón M, Strohmeyer N, Ortega-Sanchís S, Bharadwaj M, Moser M, Müller DJ, Fässler R, Costell M (2020). αv-Class integrin binding to fibronectin is solely mediated by RGD and unaffected by an RGE mutation. J Cell Biol. Dec 7; 219(12):e202004198. doi: 10.1083/jcb.202004198. Erratum in: J Cell Biol. 2021 Jan 4; 220(1): PMID: 33141174; PMCID: PMC7644020.

Bharadwaj, M., Strohmeyer, N., Colo, G. P., Helenius, J., Beerenwinkel, N., Schiller, H. B., Müller, D. J. (2017). αv-Class Integrins Exert Dual Roles on α5β1 Integrins To Strengthen Adhesion To Fibronectin. Nature Communications, 8. https://doi.org/10.1038/ncomms14348

Bhattacharyya S, Tamaki Z, Wang W, Hinchcliff M, Hoover P, Getsios S, White ES, Varga J (2014). Fibronectin EDA promotes chronic cutaneous fibrosis through Toll-like receptor signaling. Sci Transl Med. 2014 Apr 16; 6(232):232ra50. doi: 10.1126/scitranslmed.3008264. PMID: 24739758; PMCID: PMC4414050.

Blumbach, K., Zweers, M. C., Brunner, G., Peters, A. S., Schmitz, M., Schulz, J. N.,Eckes, B. (2010). Defective granulation tissue formation in mice with specific ablation of integrin-linked kinase in fibroblasts - Role of TGFβ1 levels and RhoA activity. Journal of Cell Science, 123(22), 3872–3883. https://doi.org/10.1242/jcs.063024

Bosnjak, M., Prosen, L., Dolinsek, T. et al (2013). Biological Properties of Melanoma and Endothelial Cells after Plasmid AMEP Gene Electrotransfer Depend on Integrin Quantity on Cells. J Membrane Biol 246, 803–819. https://doi.org/10.1007/s00232-013-9550-y

Bouvard, D., Pouwels, J., De Franceschi, N., & Ivaska, J. (2013). Integrin inactivators: Balancing cellular functions in vitro and in vivo. Nature Reviews Molecular Cell Biology, 14(7), 432–444. https://doi.org/10.1038/nrm3599

Bowditch RD, Hariharan M, Tominna EF, Smith JW, Yamada KM, Getzoff ED, Ginsberg MH (1994). Identification of a novel integrin binding site in fibronectin. Differential utilization by beta 3 integrins. J Biol Chem. Apr 8; 269(14):10856-63. PMID: 7511609.

Calderwood, D. A., Campbell, I. D., & Critchley, D. R. (2013). Talins and kindlins: Partners in integrin-mediated adhesion. Nature Reviews Molecular Cell Biology, 14(8), 503–517. https://doi.org/10.1038/nrm3624

Campbell, I. D., & Humphries, M. J. (2011). Integrin structure, activation and interactions. Cold Spring Harbor Perspectives in Biology, 3(3), 1–14. https://doi.org/10.1101/cshperspect.a004994

Case, L. B., & Waterman, C. M. (2015). Integration of actin dynamics and cell adhesion by a three-dimensional, mechanosensitive molecular clutch. Nature Cell Biology, 17(8), 955–963. https://doi.org/10.1038/ncb3191

Cavani, A., Zambruno, G., Marconi, A., Manca, V., Marchetti, M., & Giannetti, A. (1993). Distinctive Integrin Expression in the Newly Forming Epidermis During Wound Healing in Humans. Journal of Investigative Dermatology, 101(4), 600–604. https://doi.org/10.1111/1523-1747.ep12366057

Chada, D., Mather, T., & Nollert, M. U. (2006). The synergy site of fibronectin is required for strong interaction with the platelet integrin αiibβ3. Annals of Biomedical Engineering, 34(10), 1542–1552. https://doi.org/10.1007/s10439-006-9161-1

Chan, C. E., & Odde, D. J. (2008). Traction dynamics of filopodia on compliant substrates. Science, 322(5908), 1687–1691. https://doi.org/10.1126/science.1163595

Cho, S., Irianto, J., & Discher, D. E. (2017). Mechanosensing by the nucleus: From pathways to scaling relationships. Journal of Cell Biology, 216(2), 305–315. https://doi.org/10.1083/jcb.201610042

Choi CK, Vicente-Manzanares M, Zareno J, Whitmore LA, Mogilner A, Horwitz AR (2008). Actin and alpha-actinin orchestrate the assembly and maturation of nascent adhesions in a myosin II motor-independent manner. Nat Cell Biol. Sep; 10(9):1039-50. doi: 10.1038/ncb1763. PMID: 19160484; PMCID: PMC2827253.

Clark, R. A. F., Lanigan, J. M., DellaPelle, P., Manseau, E., Dvorak, H. F., & Colvin, R. B. (1982). Fibronectin and fibrin provide a provisional matrix for epidermal cell migration during wound

reepithelialization. Journal of Investigative Dermatology, 79(5), 264–269. https://doi.org/10.1111/1523-1747.ep12500075

Clark, R. a. (1990). Fibronectin matrix deposition and fibronectin receptor expression in healing and normal skin. The Journal of Investigative Dermatology. https://doi.org/10.1111/1523-1747.ep12876104

Clark K, Langeslag M, Figdor CG, van Leeuwen FN (2007). Myosin II and mechanotransduction: a balancing act. Trends Cell Biol. Apr; 17(4):178-86. doi: 10.1016/j.tcb.2007.02.002. Epub 2007 Feb 21. PMID: 17320396.

Conway, J. R. W., & Jacquemet, G. (2019). Cell matrix adhesion in cell migration. Essays in Biochemistry, 63(5), 535–551. https://doi.org/10.1042/EBC20190012

Correa-Gallegos, D., Jiang, D., Christ, S., Ramesh, P., Ye, H., Wannemacher, J.,Rinkevich, Y. (2019). Patch repair of deep wounds by mobilized fascia. Nature, 576(7786), 287–292. https://doi.org/10.1038/s41586-019-1794-y

Correa-Gallegos D, Rinkevich Y (2021). Cutting into wound repair. FEBS J. Jun 17. doi: 10.1111/febs.16078. Epub ahead of print. PMID: 34137168.

Coyer, S. R., Singh, A., Dumbauld, D. W., Calderwood, D. A., Craig, S. W., Delamarche, E., & García, A. J. (2012). Nanopatterning reveals an ECM area threshold for focal adhesion assembly and force transmission that is regulated by integrin activation and cytoskeleton tension. Journal of Cell Science, 125(21), 5110–5123. https://doi.org/10.1242/jcs.108035

Danen EH, Aota S, van Kraats AA, Yamada KM, Ruiter DJ, van Muijen GN. Requirement for the synergy site for cell adhesion to fibronectin depends on the activation state of integrin alpha 5 beta 1 (1995). J Biol Chem. Sep 15; 270(37):21612-8. doi: 10.1074/jbc.270.37.21612. PMID: 7545166.

Danen EH, Sonneveld P, Brakebusch C, Fassler R, Sonnenberg A. The fibronectin-binding integrins alpha5beta1 and alphavbeta3 differentially modulate RhoA-GTP loading, organization of cell matrix adhesions, and fibronectin fibrillogenesis (2002). J Cell Biol. Dec 23; 159(6):1071-86. doi: 10.1083/jcb.200205014. Epub 2002 Dec 16. PMID: 12486108; PMCID: PMC2173988.

De Pascalis C, Etienne-Manneville S (2017). Single and collective cell migration: the mechanics of adhesions. Mol Biol Cell. Jul 7;28(14):1833-1846. doi: 10.1091/mbc.E17-03-0134. PMID: 28684609; PMCID: PMC5541834.

Denis, C. V., & Wagner, D. D. (2007). Platelet adhesion receptors and their ligands in mouse models of thrombosis. Arteriosclerosis, Thrombosis, and Vascular Biology, 27(4), 728–739. https://doi.org/10.1161/01.ATV.0000259359.52265.62

Desmoulière, A., Geinoz, A., Gabbiani, F., & Gabbiani, G. (1993). Transforming growth factor-β1 induces α-smooth muscle actin expression in granulation tissue myofibroblasts and in quiescent and growing cultured fibroblasts. Journal of Cell Biology, 122(1), 103–111. https://doi.org/10.1083/jcb.122.1.103

Desmoulière A, Redard M, Darby I, Gabbiani G (1995). Apoptosis mediates the decrease in cellularity during the transition between granulation tissue and scar. Am J Pathol. 1995 Jan; 146(1):56-66. PMID: 7856739; PMCID: PMC1870783.

Driskell, R. R., Lichtenberger, B. M., Hoste, E., Kretzschmar, K., Simons, B. D., Charalambous, M., Watt, F. M. (2013). Distinct fibroblast lineages determine dermal architecture in skin development and repair. Nature, 504(7479), 277–281. https://doi.org/10.1038/nature12783

Duffield JS (2014). Cellular and molecular mechanisms in kidney fibrosis. J Clin Invest. Jun; 124(6):2299-306. doi: 10.1172/JCI72267. Epub 2014 Jun 2. PMID: 24892703; PMCID: PMC4038570.

Duperret, E. K., Dahal, A., & Ridky, T. W. (2015). Focal-adhesion-independent integrin-av regulation of FAK and c-Myc is necessary for 3D skin formation and tumor invasion. Journal of Cell Science, 128(21), 3997–4013. https://doi.org/10.1242/jcs.175539

Elosegui-Artola, A., Bazellières, E., Allen, M. D., Andreu, I., Oria, R., Sunyer, R., Roca-Cusachs, P. (2014). Rigidity sensing and adaptation through regulation of integrin types. Nature Materials, 13(6), 631–637. https://doi.org/10.1038/nmat3960

Elosegui-Artola, A., & Oria, R. (2020). Cell Migration: Deconstructing the Matrix. Current Biology, 30(20), R1266–R1268. https://doi.org/10.1016/j.cub.2020.08.013

Elosegui-Artola, A., Oria, R., Chen, Y., Kosmalska, A., Pérez-González, C., Castro, N., Roca-Cusachs, P. (2016). Mechanical regulation of a molecular clutch defines force transmission and transduction in response to matrix rigidity. Nature Cell Biology, 18(5), 540–548. https://doi.org/10.1038/ncb3336

Elosegui-Artola, A., Trepat, X., & Roca-Cusachs, P. (2018). Control of Mechanotransduction by Molecular Clutch Dynamics. Trends in Cell Biology, 28(5), 356–367. https://doi.org/10.1016/j.tcb.2018.01.008

El Ayadi A, Jay JW, Prasai A (2020). Current Approaches Targeting the Wound Healing Phases to Attenuate Fibrosis and Scarring. Int J Mol Sci. Feb 7; 21(3):1105. doi: 10.3390/ijms21031105. PMID: 32046094; PMCID: PMC7037118.

Eming SA, Koch M, Krieger A, Brachvogel B, Kreft S, Bruckner-Tuderman L, Krieg T, Shannon JD, Fox JW (2010). Differential proteomic analysis distinguishes tissue repair biomarker signatures in wound exudates obtained from normal healing and chronic wounds. J Proteome Res. Sep 3; 9(9):4758-66. doi: 10.1021/pr100456d. PMID: 20666496.

Eming SA, Wynn TA, Martin P. Inflammation and metabolism in tissue repair and regeneration (2017). Science. Jun 9; 356(6342):1026-1030. doi: 10.1126/science.aam7928. Epub 2017 Jun 8. PMID: 28596335.

Engler AJ, Sen S, Sweeney HL, Discher DE (2006). Matrix elasticity directs stem cell lineage specification. Cell. Aug 25; 126(4):677-89. doi: 10.1016/j.cell.2006.06.044. PMID: 16923388.

Erickson JR, Echeverri K. Learning from regeneration research organisms: The circuitous road to scar free wound healing (2018). Dev Biol. Jan 15; 433(2):144-154. doi: 10.1016/j.ydbio.2017.09.025. Epub 2017 Nov 24. PMID: 29179946; PMCID: PMC5914521

Evans RA, Tian YC, Steadman R, Phillips AO (2003). TGF-beta1-mediated fibroblast-myofibroblast terminal differentiation-the role of Smad proteins. Exp Cell Res.Jan 15; 282(2):90-100. doi: 10.1016/s0014-4827(02)00015-0. PMID: 12531695.

Fang RC, Mustoe TA. (2008) Animal models of wound healing: utility in transgenic mice. J Biomater Sci Polym Ed.; 19(8):989-1005. doi: 10.1163/156856208784909327. PMID: 18644226.

Fässler R, Meyer M (1995). Consequences of lack of beta 1 integrin gene expression in mice. Genes Dev. Aug 1; 9(15):1896-908. doi: 10.1101/gad.9.15.1896. PMID: 7544313.

Ffrench-Constant, C., Van De Water, L., Dvorak, H. F., & Hynes, R. O. (1989). Reappearance of an embryonic pattern of fibronectin splicing during wound healing in the adult rat. Journal of Cell Biology, 109(2), 903–914. https://doi.org/10.1083/jcb.109.2.903

Freedberg IM, Tomic-Canic M, Komine M, Blumenberg M (2001). Keratins and the keratinocyte activation cycle. J Invest Dermatol. 2001 May; 116(5):633-40. doi: 10.1046/j.1523-1747.2001.01327.x. PMID: 11348449.

Friedland, J. C., Lee, M. H., & Boettiger, D. (2009). Mechanically activated integrin switch controls alpha5beta1 function. Science (New York, N.Y.), 323(5914), 642–644.

https://doi.org/10.1126/science.1168441https://www.ncbi.nlm.nih.gov/pmc/articles/PMC3624763/pdf/nihms412728.pdf

Gadelkarim M, Abushouk AI, Ghanem E, Hamaad AM, Saad AM, Abdel-Daim MM (2018). Adipose-derived stem cells: Effectiveness and advances in delivery in diabetic wound healing. Biomed Pharmacother. Nov; 107:625-633. doi: 10.1016/j.biopha.2018.08.013. Epub 2018 Aug 14. PMID: 30118878.

Gaggioli, C., Hooper, S., Hidalgo-Carcedo, C., Grosse, R., Marshall, J. F., Harrington, K., & Sahai, E. (2007). Fibroblast-led collective invasion of carcinoma cells with differing roles for RhoGTPases in leading and following cells. Nature Cell Biology, 9(12), 1392–1400. https://doi.org/10.1038/ncb1658

Gagné, D., Benoit, Y. D., Groulx, J. F., Vachon, P. H., & Beaulieu, J. F. (2020). ILK supports RhoA/ROCK-mediated contractility of human intestinal epithelial crypt cells by inducing the fibrillogenesis of endogenous soluble fibronectin during the spreading process. BMC Molecular and Cell Biology, 21(1), 1–19. https://doi.org/10.1186/s12860-020-00259-0

Gailit, J., Welch, M. P., & Clark, R. A. F. (1994). TGF-β1 stimulates expression of keratinocyte integrins during re-epithelialization of cutaneous wounds. Journal of Investigative Dermatology, 103(2), 221–227. https://doi.org/10.1111/1523-1747.ep12393176

Gantwerker, E. A., & Hom, D. B. (2012). Skin: Histology and physiology of wound healing. Clinics in Plastic Surgery, 39(1), 85–97. https://doi.org/10.1016/j.cps.2011.09.005

Garmy-Susini B, Jin H, Zhu Y, Sung RJ, Hwang R, Varner J. Integrin alpha4beta1-VCAM-1-mediated adhesion between endothelial and mural cells is required for blood vessel maturation. J Clin Invest. 2005 Jun; 115(6):1542-51. doi: 10.1172/JCI23445. Epub 2005 May 2. PMID: 15902308; PMCID: PMC1088016.

Geiger, B., Spatz, J. P., & Bershadsky, A. D. (2009). Environmental sensing through focal adhesions. Nature Reviews Molecular Cell Biology, 10(1), 21–33. https://doi.org/10.1038/nrm2593

George, E. L., Georges-Labouesse, E. N., Patel-King, R. S., Rayburn, H., & Hynes, R. O. (1993). Defects in mesoderm, neural tube and vascular development in mouse embryos lacking fibronectin. Development (Cambridge, England), 119(4), 1079–1091.

Giacomini MM, Travis MA, Kudo M, Sheppard D. Epithelial cells utilize cortical actin/myosin to activate latent TGF-β through integrin α(v)β(6)-dependent physical force (2012). Exp Cell Res.

2012 Apr 1; 318(6):716-22. doi: 10.1016/j.yexcr.2012.01.020. Epub 2012 Jan 28. PMID: 22309779; PMCID: PMC3294033.

Girós, A., Grgur, K., Gossler, A., & Costell, M. (2011). A5B1 Integrin-Mediated Adhesion To Fibronectin Is Required for Axis Elongation and Somitogenesis in Mice. PLoS ONE, 6(7). https://doi.org/10.1371/journal.pone.0022002

Goh KL, Yang JT, Hynes RO (1997). Mesodermal defects and cranial neural crest apoptosis in alpha5 integrin-null embryos. Development. Nov; 124(21):4309-19. doi: 10.1242/dev.124.21.4309. PMID: 9334279.

Gahmberg CG, Fagerholm SC, Nurmi SM, Chavakis T, Marchesan S, Grönholm M (2009). Regulation of integrin activity and signalling. Biochim Biophys Acta. 2009 Jun; 1790(6):431-44. doi: 10.1016/j.bbagen.03.007. Epub 2009 Mar 14. PMID: 19289150; PMCID: PMC2734279.

Graham, J., Raghunath, M., & Vogel, V. (2019). Fibrillar fibronectin plays a key role as nucleator of collagen i polymerization during macromolecular crowding-enhanced matrix assembly. Biomaterials Science, 7(11), 4519–4535. https://doi.org/10.1039/c9bm00868c

Grose, R., Hutter, C., Bloch, W., Thorey, I., Watt, F. M., Fässler, R., Werner, S. (2002). A crucial role of β1 integrins for keratinocyte migration in vitro and during cutaneous wound repair. Development, 129(9), 2303–2315. https://doi.org/10.1242/dev.129.9.2303

Guan JL, Hynes RO. Lymphoid cells recognize an alternatively spliced segment of fibronectin via the integrin receptor alpha 4 beta 1. Cell. 1990 Jan 12; 60(1):53-61. doi: 10.1016/0092-8674(90)90715-q. PMID: 2295088.

Guo WH, Frey MT, Burnham NA, Wang YL. Substrate rigidity regulates the formation and maintenance of tissues (2006). Biophys J. Mar 15; 90(6):2213-20. doi: 10.1529/biophysj.105.070144. Epub 2005 Dec 30. PMID: 16387786; PMCID: PMC1386800.

Gurtner, G. C., Werner, S., Barrandon, Y., & Longaker, M. T. (2008). Wound repair and regeneration. Nature, 453(7193), 314–321. https://doi.org/10.1038/nature07039

Hamidi, H., & Ivaska, J. (2018). Every step of the way: integrins in cancer progression and metastasis. Nature Reviews Cancer, 18(9), 1–16. https://doi.org/10.1038/s41568-018-0038-z

Harris AK, Stopak D, Wild P (1981). Fibroblast traction as a mechanism for collagen morphogenesis. Nature. Mar 19; 290(5803):249-51. doi: 10.1038/290249a0. PMID: 7207616.

Heldin, C. H., Landström, M., & Moustakas, A. (2009). Mechanism of TGF-β signaling to growth arrest, apoptosis, and epithelial-mesenchymal transition. Current Opinion in Cell Biology, 21(2), 166–176. https://doi.org/10.1016/j.ceb.2009.01.021

Henderson NC, Sheppard D (2013). Integrin-mediated regulation of TGFβ in fibrosis. Biochim Biophys Acta. 2013 Jul; 1832(7):891-6. doi: 10.1016/j.bbadis.2012.10.005. Epub 2012 Oct 6. PMID: 23046811; PMCID: PMC3573259.

Hinz B, Celetta G, Tomasek JJ, Gabbiani G, Chaponnier C (2001a). Alpha-smooth muscle actin expression upregulates fibroblast contractile activity. Mol Biol Cell. Sep; 12(9):2730-41. doi: 10.1091/mbc.12.9.2730. PMID: 11553712; PMCID: PMC59708.

Hinz B, Mastrangelo D, Iselin CE, Chaponnier C, Gabbiani G (2001b). Mechanical tension controls granulation tissue contractile activity and myofibroblast differentiation. Am J Pathol. Sep; 159(3):1009-20. doi: 10.1016/S0002-9440(10)61776-2. PMID: 11549593; PMCID: PMC1850455.

Hinz B, Phan SH, Thannickal VJ, Prunotto M, Desmoulière A, Varga J, De Wever O, Mareel M, Gabbiani G. Recent developments in myofibroblast biology: paradigms for connective tissue remodeling. Am J Pathol. 2012 Apr; 180(4):1340-55. doi: 10.1016/j.ajpath.2012.02.004. Epub 2012 Mar 2. PMID: 22387320; PMCID: PMC3640252.

Hinz B. It has to be the αv: myofibroblast integrins activate latent TGF-β1. Nat Med. 2013 Dec; 19(12):1567-8. doi: 10.1038/nm.3421. PMID: 24309651.

Hinz B (2016). The role of myofibroblasts in wound healing. Curr Res Transl Med. Oct-Dec; 64(4):171-177. doi: 10.1016/j.retram.2016.09.003. Epub 2016 Nov 4. PMID: 27939455.

Horiguchi M, Ota M, Rifkin DB (2012). Matrix control of transforming growth factor-β function. J Biochem. Oct; 152(4):321-9. doi: 10.1093/jb/mvs089. Epub 2012 Aug 24. PMID: 22923731; PMCID: PMC3529568.

Horton, E. R., Humphries, J. D., James, J., Jones, M. C., Askari, J. A., & Humphries, M. J. (2016). The integrin adhesome network at a glance. Journal of Cell Science, 129(22), 4159–4163. https://doi.org/10.1242/jcs.192054

Humphrey, J. D., Dufresne, E. R., & Schwartz, M. A. (2014). Mechanotransduction and extracellular matrix homeostasis. Nature Reviews Molecular Cell Biology, 15(12), 802–812. https://doi.org/10.1038/nrm3896

Humphries, J. D., Byron, A., & J. Humphries, M. (2006). Inegrin Ligands. Journal of Cell Science, 119(19), 3901–3903. https://doi.org/10.1242/jcs.03098.INTEGRIN

Humphries, J. D., Chastney, M. R., Askari, J. A., & Humphries, M. J. (2019). Signal transduction via integrin adhesion complexes. Current Opinion in Cell Biology, 56, 14–21. https://doi.org/10.1016/j.ceb.2018.08.004

Huveneers, S., Truong, H., Fässler, R., Sonnenberg, A., & Danen, E. H. J. (2008). Binding of soluble fibronectin to integrin alpha5 beta1 - link to focal adhesion redistribution and contractile shape. Journal of Cell Science, 121(Pt 15), 2452–2462. https://doi.org/10.1242/jcs.033001

Hynes RO (2002). Integrins: bidirectional, allosteric signaling machines. Cell. Sep 20; 110(6):673-87. doi: 10.1016/s0092-8674(02)00971-6. PMID: 12297042.

Jiang, D., Correa-Gallegos, D., Christ, S., Stefanska, A., Liu, J., Ramesh, P., Rinkevich, Y. (2018). Two succeeding fibroblastic lineages drive dermal development and the transition from regeneration to scarring. Nature Cell Biology, 20(4), 422–431. https://doi.org/10.1038/s41556-018-0073-8

Headon, D (2017). Reversing stratification during wound healing. Nat Cell Biol 19, 595–597. https://doi.org/10.1038/ncb3545

Hosokawa R, Urata MM, Ito Y, Bringas P Jr, Chai Y (2005). Functional significance of Smad2 in regulating basal keratinocyte migration during wound healing. J Invest Dermatol. Dec; 125(6):1302-9. doi: 10.1111/j.0022-202X.2005.23963.x. PMID: 16354202.

Kechagia, J. Z., Ivaska, J., & Roca-Cusachs, P. (2019). Integrins as biomechanical sensors of the microenvironment. Nature Reviews Molecular Cell Biology, 20(8), 457–473. https://doi.org/10.1038/s41580-019-0134-2

Keski-Oja J, Koli K, von Melchner H (2004). TGF-beta activation by traction? Trends Cell Biol. Dec;14(12):657-9. doi: 10.1016/j.tcb.2004.10.003. PMID: 15564041.

Kim, C., Ye, F., Hu, X., & Ginsberg, M. H. (2012). Talin activates integrins by altering the topology of the β transmembrane domain. Journal of Cell Biology, 197(5), 605–611. https://doi.org/10.1083/jcb.201112141

Kisseleva T (2017). The origin of fibrogenic myofibroblasts in fibrotic liver. Hepatology. Mar;65(3):1039-1043. doi: 10.1002/hep.28948. Epub 2017 Jan 11. PMID: 27859502; PMCID: PMC5476301.

Klingberg, F., Chow, M. L., Koehler, A., Boo, S., Buscemi, L., Quinn, T. M., Hinz, B. (2014). Prestress in the extracellular matrix sensitizes latent TGF-β1 for activation. Journal of Cell Biology, 207(2), 283–297. https://doi.org/10.1083/jcb.201402006

Koivisto, L., Heino, J., Häkkinen, L., & Larjava, H. (2014). Integrins in Wound Healing. Advances in Wound Care, 3(12), 762–783. https://doi.org/10.1089/wound.2013.0436

Kong F, García AJ, Mould AP, Humphries MJ, Zhu C (2009). Demonstration of catch bonds between an integrin and its ligand. J Cell Biol. Jun 29;185(7):1275-84. doi: 10.1083/jcb.200810002. PMID: 19564406; PMCID: PMC2712956.

Krammer, A., Craig, D., Thomas, W. E., Schulten, K., & Vogel, V. (2002). A structural model for force regulated integrin binding to fibronectin's RGD-synergy site. Matrix Biology, 21(2), 139–147. https://doi.org/10.1016/S0945-053X(01)00197-4

Kubow, K. E., Vukmirovic, R., Zhe, L., Klotzsch, E., Smith, M. L., Gourdon, D., Vogel, V. (2015). Mechanical forces regulate the interactions of fibronectin and collagen i in extracellular matrix. Nature Communications, 6. https://doi.org/10.1038/ncomms9026

Ladoux, B., & Mège, R. M. (2017). Mechanobiology of collective cell behaviours. Nature Reviews Molecular Cell Biology, 18(12), 743–757. https://doi.org/10.1038/nrm.2017.98

Landén NX, Li D, Ståhle M. Transition from inflammation to proliferation: a critical step during wound healing (2016). Cell Mol Life Sci. Oct;73(20):3861-85. doi: 10.1007/s00018-016-2268-0. Epub 2016 May 14. PMID: 27180275; PMCID: PMC5021733.

Larjava, H., Salo, T., Haapasalmi, K., Kramer, R. H., & Heino, J. (1993). Expression of integrins and basement membrane components by wound keratinocytes. Journal of Clinical Investigation, 92(3), 1425–1435. https://doi.org/10.1172/JCI116719

Lawson, C. D., & Burridge, K. (2014). The on-off relationship of Rho and Rac during integrin-mediated adhesion and cell migration. Small GTPases, 5(MAR). https://doi.org/10.4161/sgtp.27958

Leahy, D. J., Aukhil, I., & Erickson, H. P. (1996). 2.0 Å crystal structure of a four-domain segment of human fibronectin encompassing the RGD loop and synergy region. Cell, 84(1), 155–164. https://doi.org/10.1016/S0092-8674(00)81002-8

LeBert DC, Huttenlocher A. Inflammation and wound repair (2014). Semin Immunol. Aug; 26(4):315-20. doi: 10.1016/j.smim.2014.04.007. Epub 2014 May 19. PMID: 24853879; PMCID: PMC6801000.

LeBert, D. C., Squirrell, J. M., Rindy, J., Broadbridge, E., Lui, Y., Zakrzewska, A., Huttenlocher, A. (2015). Matrix metalloproteinase 9 modulates collagen matrices and wound repair. Development (Cambridge), 142(12), 2136–2146. https://doi.org/10.1242/dev.121160

Leiss, M., Beckmann, K., Girós, A., Costell, M., & Fässler, R. (2008). The role of integrin binding sites in fibronectin matrix assembly in vivo. Current Opinion in Cell Biology, 20(5), 502–507. https://doi.org/10.1016/j.ceb.2008.06.001

Liao, Y. F., Gotwals, P. J., Koteliansky, V. E., Sheppard, D. and Van De Water, L. (2002). The EIIIA segment of fibronectin is a ligand for integrins α9β1 andα 4β1 providing a novel mechanism for regulating cell adhesion by alternative splicing. J. Biol. Chem. 277, 14467-14474.

Liu, S., Shi-wen, X., Blumbach, K., Eastwood, M., Denton, C. P., Eckes, B.,Leask, A. (2010). Expression of integrin β1 by fibroblasts is required for tissue repair in vivo. Journal of Cell Science, 123(21), 3674–3682. https://doi.org/10.1242/jcs.070672

Lu, P., Takai, K., Weaver, V. M., & Werb, Z. (2011). Extracellular Matrix degradation and remodeling in development and disease. Cold Spring Harbor Perspectives in Biology, 3(12), 1–24. https://doi.org/10.1101/cshperspect.a005058

Lukjanenko, L., Jung, M. J., Hegde, N., Perruisseau-Carrier, C., Migliavacca, E., Rozo, M., … Bentzinger, C. F. (2016). Loss of fibronectin from the aged stem cell niche affects the regenerative capacity of skeletal muscle in mice. Nature Medicine, 22(8), 897–905. https://doi.org/10.1038/nm.4126

Luo, B. H., Carman, C. V., & Springer, T. A. (2007). Structural basis of integrin regulation and signaling. Annual Review of Immunology, 25(July 2014), 619–647. https://doi.org/10.1146/annurev.immunol.25.022106.141618

Maden, M. (2018). The evolution of regeneration – Where does that leave mammals? International Journal of Developmental Biology, 62(6–8), 369–372. https://doi.org/10.1387/ijdb.180031mm

Mao, Y., & Schwarzbauer, J. E. (2005). Fibronectin fibrillogenesis, a cell-mediated matrix assembly process. Matrix Biology. https://doi.org/10.1016/j.matbio.2005.06.008

Mardon HJ, Grant KE. The role of the ninth and tenth type III domains of human fibronectin in cell adhesion (1994). FEBS Lett. 1994 Mar 7; 340(3):197-201. doi: 10.1016/0014-5793(94)80137-1. PMID: 8131845.

Martinez-Ferrer, M., Afshar-Sherif, A. R., Uwamariya, C., De Crombrugghe, B., Davidson, J. M., & Bhowmick, N. A. (2010). Dermal transforming growth factor-β responsiveness mediates wound contraction and epithelial closure. American Journal of Pathology, 176(1), 98–107. https://doi.org/10.2353/ajpath.2010.090283

Mascharak S, desJardins-Park HE, Davitt MF, Griffin M, Borrelli MR, Moore AL, Chen K, Duoto B, Chinta M, Foster DS, Shen AH, Januszyk M, Kwon SH, Wernig G, Wan DC, Lorenz HP, Gurtner GC, Longaker MT (2021). Preventing Engrailed-1 activation in fibroblasts yields wound regeneration without scarring. Science. Apr 23; 372(6540):eaba2374. doi: 10.1126/science.aba2374. PMID: 33888614; PMCID: PMC9008875.

Meckmongkol TT, Harmon R, McKeown-Longo P, Van De Water L (2007). The fibronectin synergy site modulates TGF-beta-dependent fibroblast contraction. Biochem Biophys Res Commun. 2007 Sep 7; 360(4):709-14. doi: 10.1016/j.bbrc.2007.06.121. Epub 2007 Jul 3. PMID: 17631278; PMCID: PMC2034296.

Mezu-Ndubuisi, O. J., & Maheshwari, A. (2021). The role of integrins in inflammation and angiogenesis. Pediatric Research, 89(7), 1619–1626. https://doi.org/10.1038/s41390-020-01177-9

Miroshnikova, Y. A., Rozenberg, G. I., Cassereau, L., Pickup, M., Mouw, J. K., Ou, G., Weaver, V. M. (2017). α5β1-Integrin promotes tension-dependent mammary epithelial cell invasion by engaging the fibronectin synergy site. Molecular Biology of the Cell, 28(22), 2958–2977. https://doi.org/10.1091/mbc.E17-02-0126

Mitchison T, Kirschner M (1984). Dynamic instability of microtubule growth. Nature. Nov 15-21; 312(5991):237-42. doi: 10.1038/312237a0. PMID: 6504138.

Mittal A, Pulina M, Hou SY, Astrof S (2013). Fibronectin and integrin alpha 5 play requisite roles in cardiac morphogenesis. Dev Biol.Sep 1; 381(1):73-82.doi: 10.1016/j.ydbio.2013.06.010. Epub 2013 Jun 17. PMID: 23791818; PMCID: PMC3833817.

Monavarian, M., Kader, S., Moeinzadeh, S., & Jabbari, E. (2019). Regenerative Scar-Free Skin Wound Healing. Tissue Engineering - Part B: Reviews, 25(4), 294–311. https://doi.org/10.1089/ten.teb.2018.0350

Morgan, M. R., Humphries, M. J., & Bass, M. D. (2007). Synergistic control of cell adhesion by integrins and syndecans. Nature Reviews Molecular Cell Biology, 8(12), 957–969. https://doi.org/10.1038/nrm2289

Morgan, M. R., Byron, A., Humphries, M. J., & Bass, M. D. (2009). Giving off mixed signals - Distinct functions of α5β 1 and αvβ3 integrins in regulating cell behaviour. IUBMB Life, 61(7), 731–738. https://doi.org/10.1002/iub.200

Moser, M., Legate, K. R., Zent, R., & Fässler, R. (2009). The tail of integrins, talin, and kindlins. Science, 324(5929), 895–899. https://doi.org/10.1126/science.1163865

Mould, A. P., Askari, J. A., Aota, S. I., Yamada, K. M., Irie, A., Takada, Y., Humphries, M. J. (1997). Defining the topology of integrin α5β1-fibronectin interactions using inhibitory anti-α5 and anti-β1 monoclonal antibodies: Evidence that the synergy sequence of fibronectin is recognized by the amino-terminal repeats of the α5 subunit. Journal of Biological Chemistry, 272(28), 17283–17292. https://doi.org/10.1074/jbc.272.28.17283

Mui KL, Chen CS, Assoian RK (2016). The mechanical regulation of integrin-cadherin crosstalk organizes cells, signaling and forces. J Cell Sci. Mar 15; 129(6):1093-100. doi: 10.1242/jcs.183699. Epub 2016 Feb 26. PMID: 26919980; PMCID: PMC4813297.

Muro, A. F., Moretti, F. A., Moore, B. B., Yan, M., Atrasz, R. G., Wilke, C. A., White, E. S. (2008). An essential role for fibronectin extra type III domain A in pulmonary fibrosis. American Journal of Respiratory and Critical Care Medicine, 177(6), 638‑645. https://doi.org/10.1164/rccm.200708-1291OC

Murray IR, Gonzalez ZN, Baily J, Dobie R, Wallace RJ, Mackinnon AC, Smith JR, Greenhalgh SN, Thompson AI, Conroy KP, Griggs DW, Ruminski PG, Gray GA, Singh M, Campbell MA, Kendall TJ, Dai J, Li Y, Iredale JP, Simpson H, Huard J, Péault B, Henderson NC (2017). αv integrins on mesenchymal cells regulate skeletal and cardiac muscle fibrosis. Nat Commun. 2017 Oct 24; 8(1):1118. doi: 10.1038/s41467-017-01097-z. PMID: 29061963; PMCID: PMC5653645.

Nagae, M., Re, S., Mihara, E., Nogi, T., Sugita, Y., & Takagi, J. (2012). Crystal structure of α5β1 integrin ectodomain: Atomic details of the fibronectin receptor. Journal of Cell Biology, 197(1), 131–140. https://doi.org/10.1083/jcb.201111077

Nagai, T., Yamakawa, N., Aota, S., Yamada, S. S., Akiyama, S. K., Olden, K., & Yamada, K. M. (1991). Monoclonal antibody characterization of two distant sites required for function of the central cell-binding domain of fibronectin in cell adhesion, cell migration, and matrix assembly. Journal of Cell Biology, 114(6), 1295–1305. https://doi.org/10.1083/jcb.114.6.1295

Nunan R, Campbell J, Mori R, Pitulescu ME, Jiang WG, Harding KG, Adams RH, Nobes CD, Martin P (2015). Ephrin-Bs Drive Junctional Downregulation and Actin Stress Fiber Disassembly

to Enable Wound Re-epithelialization. Cell Rep. Nov 17; 13(7):1380-1395. doi: 10.1016/j.celrep.2015.09.085. Epub 2015 Nov 5. PMID: 26549443; PMCID: PMC4660216.

Ogawa R (2017). Keloid and Hypertrophic Scars Are the Result of Chronic Inflammation in the Reticular Dermis. Int J Mol Sci. Mar 10; 18(3):606. doi: 10.3390/ijms18030606. PMID: 28287424; PMCID: PMC5372622.

Paladini RD, Takahashi K, Bravo NS, Coulombe PA (1996). Onset of re-epithelialization after skin injury correlates with a reorganization of keratin filaments in wound edge keratinocytes: defining a potential role for keratin 16. J Cell Biol. Feb; 132(3):381-97. doi: 10.1083/jcb.132.3.381. PMID: 8636216; PMCID: PMC2120730.

Pandya, P., Orgaz, J. L., & Sanz-Moreno, V. (2017). Actomyosin contractility and collective migration: may the force be with you. Current Opinion in Cell Biology, 48, 87–96. https://doi.org/10.1016/j.ceb.2017.06.006

Park, S., Gonzalez, D. G., Guirao, B., Boucher, J. D., Marsh, E. D., Mesa, K. R., Greco, V. (2017). Epidermal Wound Repair in Live Mice, 19(2), 155–163. https://doi.org/10.1038/ncb3472.Tissue-scale

Petrie, R. J., Doyle, A. D., & Yamada, K. M. (2009). Random versus directionally persistent cell migration. Nature Reviews Molecular Cell Biology, 10(8), 538–549. https://doi.org/10.1038/nrm2729

Pensalfini M, Haertel E, Hopf R, Wietecha M, Werner S, Mazza E (2018). The mechanical fingerprint of murine excisional wounds. Acta Biomater.Jan; 65:226-236. doi: 10.1016/j.actbio.2017.10.021. Epub 2017 Oct 12. PMID: 29031511.

Penke LR, Peters-Golden M (2019). Molecular determinants of mesenchymal cell activation in fibroproliferative diseases. Cell Mol Life Sci. Nov; 76(21):4179-4201. doi: 10.1007/s00018-019-03212-3. Epub 2019 Sep 28. PMID: 31563998; PMCID: PMC6858579.

Pierschbacher MD, Ruoslahti E. Cell attachment activity of fibronectin can be duplicated by small synthetic fragments of the molecule. Nature. 1984 May 3-9; 309(5963):30-3. doi: 10.1038/309030a0. PMID: 6325925.

Plikus, M. V., Wang, X., Sinha, S., Forte, E., Thompson, S. M., Herzog, E. L., Horsley, V. (2021). Fibroblasts: Origins, definitions, and functions in health and disease. Cell, 184(15), 3852–3872. https://doi.org/10.1016/j.cell.2021.06.024

Plotnikov SV, Pasapera AM, Sabass B, Waterman CM. Force fluctuations within focal adhesions mediate ECM-rigidity sensing to guide directed cell migration. Cell. 2012 Dec 21; 151(7):1513-27. doi: 10.1016/j.cell.2012.11.034. PMID: 23260139; PMCID: PMC3821979.

Prabhu SD, Frangogiannis NG (2016). The Biological Basis for Cardiac Repair After Myocardial Infarction: From Inflammation to Fibrosis. Circ Res. Jun 24; 119(1):91-112. doi: 10.1161/CIRCRESAHA.116.303577. PMID: 27340270; PMCID: PMC4922528.

Ramakrishnan V, Bhaskar V, Law DA, Wong MH, DuBridge RB, Breinberg D, O'Hara C, Powers DB, Liu G, Grove J, Hevezi P, Cass KM, Watson S, Evangelista F, Powers RA, Finck B, Wills M, Caras I, Fang Y, McDonald D, Johnson D, Murray R, Jeffry U (2006). Preclinical evaluation of an anti-alpha5beta1 integrin antibody as a novel anti-angiogenic agent. J Exp Ther Oncol. 5(4):273-86. PMID: 17024968.

Redick SD, Settles DL, Briscoe G, Erickson HP. Defining fibronectin's cell adhesion synergy site by site-directed mutagenesis (2000). J Cell Biol Apr 17;149(2):521-7. doi: 10.1083/jcb.149.2.521. PMID: 10769040; PMCID: PMC2175162.

Reffay M, Parrini MC, Cochet-Escartin O, Ladoux B, Buguin A, Coscoy S, Amblard F, Camonis J, Silberzan P (2014). Interplay of RhoA and mechanical forces in collective cell migration driven by leader cells. Nat Cell Biol. Mar; 16(3):217-23. doi: 10.1038/ncb2917. Erratum in: Nat Cell Biol. 2014 Apr; 16(4):382. PMID: 24561621.

Reynolds, L. E., Conti, F. J., Lucas, M., Grose, R., Robinson, S., Stone, M., Hodivala-Dilke, K. (2005). Accelerated re-epithelialization in β3-integrin-deficient mice is associated with enhanced TGF-β1 signaling. Nature Medicine, 11(2), 167–174. https://doi.org/10.1038/nm1165

Richard A F Clark (1990). Fibronectin Matrix Deposition and Fibronectin Receptor Expression in Healing and Normal Skin, Journal of Investigative Dermatology, Volume 94, Issue 6, Supplement, Pages s128-s134, ISSN 0022-202X, https://doi.org/10.1111/1523-1747.ep12876104.

Rinkevich Y, Walmsley GG, Hu MS, Maan ZN, Newman AM, Drukker M, Januszyk M, Krampitz GW, Gurtner GC, Lorenz HP, Weissman IL, Longaker MT (2015). Skin fibrosis. Identification and isolation of a dermal lineage with intrinsic fibrogenic potential. Science. Apr 17; 348(6232):aaa2151. doi: 10.1126/science.aaa2151. PMID: 25883361; PMCID: PMC5088503.

Rippa, A. L., Kalabusheva, E. P., & Vorotelyak, E. A. (2019). Regeneration of Dermis: Scarring and Cells Involved. Cells, 8(6), 607. https://doi.org/10.3390/cells8060607

Roca-Cusachs P, Gauthier NC, Del Rio A, Sheetz MP. Clustering of alpha(5)beta(1) integrins determines adhesion strength whereas alpha(v)beta(3) and talin enable mechanotransduction. Proc Natl Acad Sci U S A. 2009 Sep 22;106(38):16245-50. doi: 10.1073/pnas.0902818106. Epub 2009 Sep 3. PMID: 19805288; PMCID: PMC2752568.

Rocha LA, Learmonth DA, Sousa RA, Salgado AJ (2018). αvβ3 and α5β1 integrin-specific ligands: From tumor angiogenesis inhibitors to vascularization promoters in regenerative medicine? Biotechnol Adv. Jan-Feb;36(1):208-227. doi: 10.1016/j.biotechadv.2017.11.004. Epub 2017 Nov 15. PMID: 29155160.

Rognoni, E., Pisco, A. O., Hiratsuka, T., Sipilä, K. H., Belmonte, J. M., Mobasseri, S. A., Watt, F. M. (2018). Fibroblast state switching orchestrates dermal maturation and wound healing. Molecular Systems Biology, 14(8), 1–20. https://doi.org/10.15252/msb.20178174

Rognoni, E., Widmaier, M., Jakobson, M., Ruppert, R., Katsougkri, D., Böttcher, R. T., Rifkin, D. B. (2014). Europe PMC Funders Group Kindlin-1 controls Wnt and TGF- β availability to regulate cutaneous epithelial stem cell proliferation, 20(4), 350–359. https://doi.org/10.1038/nm.3490.Kindlin-1

Rosique, R. G., Rosique, M. J., & Farina Junior, J. A. (2015). Curbing inflammation in skin wound healing: A review. International Journal of Inflammation, 2015(iv). https://doi.org/10.1155/2015/316235

Ross, T. D., Coon, B. G., Yun, S., Baeyens, N., Tanaka, K., Ouyang, M., & Schwartz, M. A. (2013). Integrins in mechanotransduction. Current Opinion in Cell Biology, 25(5), 613–618. https://doi.org/10.1016/j.ceb.2013.05.006

Rozario, T., & Desimone, D. W. (2011). Dynamic View. Regenerative Medicine, 341(1), 126–140. https://doi.org/10.1016/j.ydbio.2009.10.026.

Sakai T, Johnson KJ, Murozono M, Sakai K, Magnuson MA, Wieloch T, Cronberg T, Isshiki A, Erickson HP, Fässler R. (2001) Plasma fibronectin supports neuronal survival and reduces brain injury following transient focal cerebral ischemia but is not essential for skin-wound healing and hemostasis. Nat Med. Mar; 7(3):324-30. doi: 10.1038/85471. PMID: 11231631.

Sanchis, A., Alba, L., Latorre, V., Sevilla, L. M., & Pérez, P. (2012). Keratinocyte-targeted overexpression of the glucocorticoid receptor delays cutaneous wound healing. PLoS ONE, 7(1). https://doi.org/10.1371/journal.pone.0029701

Sani S, Messe M, Fuchs Q, Pierrevelcin M, Laquerriere P, Entz-Werle N, Reita D, Etienne-Selloum N, Bruban V, Choulier L, Martin S, Dontenwill M (2021). Biological Relevance of RGD-Integrin Subtype-Specific Ligands in Cancer. Chembiochem. Apr 6; 22(7):1151-1160. doi: 10.1002/cbic.202000626. Epub 2020 Nov 27. PMID: 33140906.

Sasse, P., Malan, D., Fleischmann, M., Roell, W., Gustafsson, E., Bostani, T., Fleischmann, B. K. (2008). Perlecan is critical for heart stability. Cardiovascular Research, 80(3), 435–444. https://doi.org/10.1093/cvr/cvn225

Schiller, H. B., Hermann, M. R., Polleux, J., Vignaud, T., Zanivan, S., Friedel, C. C., Fässler, R. (2013). β 1 - And α v -class integrins cooperate to regulate myosin II during rigidity sensing of fibronectin-based microenvironments. Nature Cell Biology, 15(6), 625–636. https://doi.org/10.1038/ncb2747

Schnittert J, Bansal R, Storm G, Prakash J. Integrins in wound healing, fibrosis and tumor stroma: High potential targets for therapeutics and drug delivery. Adv Drug Deliv Rev. 2018 Apr;129:37-53. doi: 10.1016/j.addr.2018.01.020. Epub 2018 Feb 4. PMID: 29414674.

Shinde AV, Kelsh R, Peters JH, Sekiguchi K, Van De Water L, McKeown-Longo PJ (2015). The α4β1 integrin and the EDA domain of fibronectin regulate a profibrotic phenotype in dermal fibroblasts. Matrix Biol. Jan;41:26-35. doi: 10.1016/j.matbio.2014.11.004. Epub 2014 Nov 26. PMID: 25433338; PMCID: PMC4657864.

Schwarzbauer, J. E., & Sechler, J. L. (1999). Fibronectin fibrillogenesis: A paradigm for extracellular matrix assembly. Current Opinion in Cell Biology, 11(5), 622–627. https://doi.org/10.1016/S0955-0674(99)00017-4

Shams, H., Hoffman, B. D., & Mofrad, M. R. K. (2018). The “stressful” Life of Cell Adhesion Molecules: On the Mechanosensitivity of Integrin Adhesome. Journal of Biomechanical Engineering, 140(2). https://doi.org/10.1115/1.4038812

Shi Q, Boettiger D. A novel mode for integrin-mediated signaling: tethering is required for phosphorylation of FAK Y397 (2003). Mol Biol Cell. Oct;14(10):4306-15. doi: 10.1091/mbc.e03-01-0046. Epub 2003 Sep 5. PMID: 12960434; PMCID: PMC207021.

Shiu, J. Y., Aires, L., Lin, Z., & Vogel, V. (2018). Nanopillar force measurements reveal actin-cap-mediated YAP mechanotransduction. Nature Cell Biology, 20(3), 262–271. https://doi.org/10.1038/s41556-017-0030-y

Sottile, J., & Hocking, D. C. (2002). Fibronectin polymerization regulates the composition and stability of extracellular matrix fibrils and cell-matrix adhesions. Molecular Biology of the Cell, 13(10), 3546–3559. https://doi.org/10.1091/mbc.E02-01-0048

Sottile, J., Shi, F., Rublyevska, I., Chiang, H. Y., Lust, J., & Chandler, J. (2007). Fibronectin-dependent collagen I deposition modulates the cell response to fibronectin. American Journal of Physiology - Cell Physiology, 293(6), 1934–1946. https://doi.org/10.1152/ajpcell.00130.2007

Strohmeyer, N., Bharadwaj, M., Costell, M., Fässler, R., & Müller, D. J. (2017). Fibronectin-bound α5β1 integrins sense load and signal to reinforce adhesion in less than a second. Nature Materials, 16(12), 1262–1270. https://doi.org/10.1038/nmat5023

Suga H, Rennert RC, Rodrigues M, Sorkin M, Glotzbach JP, Januszyk M, Fujiwara T, Longaker MT, Gurtner GC (2014). Tracking the elusive fibrocyte: identification and characterization of collagen-producing hematopoietic lineage cells during murine wound healing. Stem Cells. May;32(5):1347-60. doi: 10.1002/stem.1648. PMID: 24446236; PMCID: PMC4096488.

Sun Z, Guo S, Reinhard Fässler R (2016). Integrin-mediated mechanotransduction. J Cell Biol 21 November; 215 (4): 445–456. doi: https://doi.org/10.1083/jcb.201609037

Sun, Z., Costell, M., & Fässler, R. (2019). Integrin activation by talin, kindlin and mechanical forces. Nature Cell Biology, 21(1), 25–31. https://doi.org/10.1038/s41556-018-0234-9

Sunyer R, Conte V, Escribano J, Elosegui-Artola A, Labernadie A, Valon L, Navajas D, García-Aznar JM, Muñoz JJ, Roca-Cusachs P, Trepat X (2016). Collective cell durotaxis emerges from long-range intercellular force transmission. Science. Sep 9;353(6304):1157-61. doi: 10.1126/science.aaf7119. PMID: 27609894.

Swaminathan V, Waterman CM (2016). The molecular clutch model for mechanotransduction evolves. Nat Cell Biol. Apr 27;18(5):459-61. doi: 10.1038/ncb3350. PMID: 27117328; PMCID: PMC6792288.

Takagi, J., Petre, B. M., Walz, T., & Springer, T. A. (2002). Global conformational earrangements in integrin extracellular domains in outside-in and inside-out signaling. Cell, 110(5), 599–611. https://doi.org/10.1016/S0092-8674(02)00935-2

Takagi, J., Strokovich, K., Springer, T. A., & Walz, T. (2003). Structure of integrin α5β1 in complex with fibronectin. EMBO Journal, 22(18), 4607–4615. https://doi.org/10.1093/emboj/cdg445

Takahashi, S., Leiss, M., Moser, M., Ohashi, T., Kitao, T., Heckmann, D., Fässler, R. (2007). The RGD motif in fibronectin is essential for development but dispensable for fibril assembly. Journal of Cell Biology, 178(1), 167–178. https://doi.org/10.1083/jcb.200703021

Tambe DT, Hardin CC, Angelini TE, Rajendran K, Park CY, Serra-Picamal X, Zhou EH, Zaman MH, Butler JP, Weitz DA, Fredberg JJ, Trepat X. Collective cell guidance by cooperative intercellular forces. Nat Mater. 2011 Jun;10(6):469-75. doi: 10.1038/nmat3025. PMID: 21602808; PMCID: PMC3135682.

Theodosiou, M., Widmaier, M., Böttcher, R. T., Rognoni, E., Veelders, M., Bharadwaj, M., Fässler, R. (2016). Kindlin-2 cooperates with talin to activate integrins and induces cell spreading by directly binding paxillin. ELife, 5(JANUARY2016), 1–24. https://doi.org/10.7554/eLife.10130

Thievessen I, Thompson PM, Berlemont S, Plevock KM, Plotnikov SV, Zemljic-Harpf A, Ross RS, Davidson MW, Danuser G, Campbell SL, Waterman CM (2013). Vinculin-actin interaction couples actin retrograde flow to focal adhesions, but is dispensable for focal adhesion growth. J Cell Biol.Jul 8;202(1):163-77. doi: 10.1083/jcb.201303129. PMID: 23836933; PMCID: PMC3704983.

To WS, Midwood KS (2011). Plasma and cellular fibronectin: distinct and independent functions during tissue repair. Fibrogenesis Tissue Repair. Sep 16;4:21. doi: 10.1186/1755-1536-4-21. PMID: 21923916; PMCID: PMC3182887.

Tomasek, J. J., Gabbiani, G., Hinz, B., Chaponnier, C., & Brown, R. A. (2002). Myofibroblasts and mechano: Regulation of connective tissue remodelling. Nature Reviews Molecular Cell Biology, 3(5), 349–363. https://doi.org/10.1038/nrm809

Trappmann, B., Gautrot, J. E., Connelly, J. T., Strange, D. G. T., Li, Y., Oyen, M. L., … Huck, W. T. S. (2012). Extracellular-matrix tethering regulates stem-cell fate. Nature Materials, 11(7), 642–649. https://doi.org/10.1038/nmat3339

Trepat, X., Wasserman, M., Angelini, T. et al. Physical forces during collective cell migration. Nature Phys 5, 426–430 (2009). https://doi.org/10.1038/nphys1269

Tzavlaki, K., & Moustakas, A. (2020). TGF-B signaling. Biomolecules, 10(3), 1–38. https://doi.org/10.3390/biom10030487

Vadasz B, Chen P, Yougbaré I, Zdravic D, Li J, Li C, Carrim N, Ni H (2015). Platelets and platelet alloantigens: Lessons from human patients and animal models of fetal and neonatal alloimmune thrombocytopenia. Genes Dis. Jun 1;2(2):173-185. doi: 10.1016/j.gendis.2015.02.003. PMID: 28345015; PMCID: PMC5362271.

Vanden Oever, M., Twaroski, K., Osborn, M. J., Wagner, J. E., & Tolar, J. (2018). Inside out: Regenerative medicine for recessive dystrophic epidermolysis bullosa. Pediatric Research, 83(1–2), 318–324. https://doi.org/10.1038/pr.2017.244

Vedula, S. R. K., Leong, M. C., Lai, T. L., Hersen, P., Kabla, A. J., Lim, C. T., & Ladoux, B. (2012). Emerging modes of collective cell migration induced by geometrical constraints. Proceedings of the National Academy of Sciences of the United States of America, 109(32), 12974–12979. https://doi.org/10.1073/pnas.1119313109

Velling T, Risteli J, Wennerberg K, Mosher DF, Johansson S (2002). Polymerization of type I and III collagens is dependent on fibronectin and enhanced by integrins alpha 11beta 1 and alpha 2beta 1. J Biol Chem. 2002 Oct 4;277(40):37377-81. doi: 10.1074/jbc.M206286200. Epub Jul 26. PMID: 12145303.

Wan L, Jiang D, Correa-Gallegos D, Ramesh P, Zhao J, Ye H, Zhu S, Wannemacher J, Volz T, Rinkevich Y (2021). Connexin43 gap junction drives fascia mobilization and repair of deep skin wounds. Matrix Biol. Mar;97:58-71. doi: 10.1016/j.matbio.2021.01.005. Epub 2021 Jan 27. PMID: 33508427.

Wang, Y., & Wang, X. (2016). Integrins outside focal adhesions transmit tensions during stable cell adhesion. Scientific Reports, 6(July), 1–9. https://doi.org/10.1038/srep36959

Watt FM (2002). Role of integrins in regulating epidermal adhesion, growth and differentiation. EMBO J. Aug 1;21(15):3919-26. doi: 10.1093/emboj/cdf399. PMID: 12145193; PMCID: PMC126145.

Wells RG (2013). Tissue mechanics and fibrosis. Biochim Biophys Acta. Jul; 1832(7):884-90. doi: 10.1016/j.bbadis.2013.02.007. Epub 2013 Feb 20. PMID: 23434892; PMCID: PMC3641165.

Wells AR, Leung KP (2020). Pirfenidone attenuates the profibrotic contractile phenotype of differentiated human dermal myofibroblasts. Biochem Biophys Res Commun. Jan 15;521(3):646-651. doi: 10.1016/j.bbrc.2019.10.177. Epub 2019 Nov 1. PMID: 31679692.

Werner S, Grose R (2003). Regulation of wound healing by growth factors and cytokines. Physiol Rev. Jul;83(3):835-70. doi: 10.1152/physrev.2003.83.3.835. PMID: 12843410.

White ES, Baralle FE, Muro AF. New insights into form and function of fibronectin splice variants. J Pathol. 2008 Sep;216(1):1-14. doi: 10.1002/path.2388. PMID: 18680111; PMCID: PMC4630009.

Wierzbicka-Patynowski I, Schwarzbauer JE (2003). The ins and outs of fibronectin matrix assembly. J Cell Sci.Aug 15; 116(Pt 16):3269-76. doi: 10.1242/jcs.00670. PMID: 12857786.

Wietecha, M. S., Pensalfini, M., Cangkrama, M., Müller, B., Jin, J., Brinckmann, J., Werner, S. (2020). Activin-mediated alterations of the fibroblast transcriptome and matrisome control the biomechanical properties of skin wounds. Nature Communications, 11(1). https://doi.org/10.1038/s41467-020-16409-z

Wipff, P. J., Rifkin, D. B., Meister, J. J., & Hinz, B. (2007). Myofibroblast contraction activates latent TGF-β1 from the extracellular matrix. Journal of Cell Biology, 179(6), 1311–1323. https://doi.org/10.1083/jcb.200704042

Wojcik, S. M., Bundman, D. S., & Roop, D. R. (2000). Delayed Wound Healing in Keratin 6a Knockout Mice. Molecular and Cellular Biology, 20(14), 5248–5255. https://doi.org/10.1128/mcb.20.14.5248-5255.2000

Wong VW, Akaishi S, Longaker MT, Gurtner GC (2011). Pushing back: wound mechanotransduction in repair and regeneration. J Invest Dermatol. Nov;131(11):2186-96. doi: 10.1038/jid.2011.212. Epub 2011 Jul 21. PMID: 21776006.

Xu XR, Zhang D, Oswald BE, Carrim N, Wang X, Hou Y, Zhang Q, Lavalle C, McKeown T, Marshall AH, Ni H (2016). Platelets are versatile cells: New discoveries in hemostasis, thrombosis, immune responses, tumor metastasis and beyond. Crit Rev Clin Lab Sci. Dec;53(6):409-30. doi: 10.1080/10408363.2016.1200008. Epub 2016 Jul 22. PMID: 27282765.

Yang JT, Rayburn H, Hynes RO (1993). Embryonic mesodermal defects in α5 integrin-deficient mice. Development. 1993 Dec; 119(4):1093-105. PMID: 7508365.

Yang, J. T., & Hynes, R. O. (1996). Fibronectin receptor functions in embryonic cells deficient in α5β1 integrin can be replaced by α(v) integrins. Molecular Biology of the Cell, 7(11), 1737–1748. https://doi.org/10.1091/mbc.7.11.1737

Yang, J. T., Bader, B. L., Kreidberg, J. A., Ullman-Culleré, M., Trevithick, J. E., & Hynes, R. O. (1999). Overlapping and independent functions of fibronectin receptor integrins in early

mesodermal development. Developmental Biology, 215(2), 264–277. https://doi.org/10.1006/dbio.1999.9451

Yang Z, Mu Z, Dabovic B, Jurukovski V, Yu D, Sung J, Xiong X, Munger JS (2007). Absence of integrin-mediated TGFbeta1 activation in vivo recapitulates the phenotype of TGFbeta1-null mice. J Cell Biol. Mar 12; 176(6):787-93. doi: 10.1083/jcb.200611044. PMID: 17353357; PMCID: PMC2064053.

Yano H, Mazaki Y, Kurokawa K, Hanks SK, Matsuda M, Sabe H (2004). Roles played by a subset of integrin signaling molecules in cadherin-based cell-cell adhesion. J Cell Biol. Jul 19; 166(2):283-95. doi: 10.1083/jcb.200312013. PMID: 15263022; PMCID: PMC2172299.

Yoshinaga K, Obata H, Jurukovski V, Mazzieri R, Chen Y, Zilberberg L, Huso D, Melamed J, Prijatelj P, Todorovic V, Dabovic B, Rifkin DB (2008). Perturbation of transforming growth factor (TGF)-beta1 association with latent TGF-beta binding protein yields inflammation and tumors. Proc Natl Acad Sci U S A. Dec 2; 105(48):18758-63. doi: 10.1073/pnas.0805411105. Epub 2008 Nov 20. PMID: 19022904; PMCID: PMC2596235.

Zhang Y, Xu G, Lee RM, Zhu Z, Wu J, Liao S, Zhang G, Sun Y, Mogilner A, Losert W, Pan T, Lin F, Xu Z, Zhao M (2017). Collective cell migration has distinct directionality and speed dynamics. Cell Mol Life Sci. Oct; 74(20):3841-3850. doi: 10.1007/s00018-017-2553-6. Epub 2017 Jun 13. PMID: 28612218; PMCID: PMC5709186.

Yonemura S, Wada Y, Watanabe T, Nagafuchi A, Shibata M. alpha-Catenin as a tension transducer that induces adherens junction development. Nat Cell Biol. 2010 Jun;12(6):533-42. doi: 10.1038/ncb2055. Epub 2010 May 9. PMID: 20453849.

Zaidel-Bar, R., Milo, R., Kam, Z., & Geiger, B. (2007). A paxillin tyrosine phosphorylation switch regulates the assembly and form of cell-matrix adhesions. Journal of Cell Science, 120(1), 137–148. https://doi.org/10.1242/jcs.03314

Zhong, C., Chrzanowska-Wodnicka, M., Brown, J., Shaub, A., Belkin, A. M., & Burridge, K. (1998). Rho-mediated contractility exposes a cryptic site in fibronectin and induces fibronectin matrix assembly. Journal of Cell Biology, 141(2), 539–551. https://doi.org/10.1083/jcb.141.2.539

Zomer, H. D., & Trentin, A. G. (2018). Skin wound healing in humans and mice: Challenges in translational research. Journal of Dermatological Science, 90(1), 3–12. https://doi.org/10.1016/j.jdermsci.2017.12.009

IX RESUMEN

INTRODUCCIÓN

La piel es el órgano del cuerpo que actúa como barrera contra infecciones, lesiones y pérdida de agua por termorregulación. Cuando se produce una herida cutánea, se activan respuestas a nivel celular y molecular en el lugar de la herida, cuyo último objetivo es la recuperación de la integridad del tejido dañado. En adultos, el resultado de este proceso reemplaza la estructura original por un tejido fibrótico también conocido como cicatriz. Se ha visto que en estadios fetales en mamíferos u organismos inferiores tanto vertebrados como invertebrados, se suele producir una regeneración completa del tejido. A pesar de la aparición en los últimos años de abundante literatura relativa a los factores y mecanismos que determinan la resolución de las heridas cutáneas, este proceso todavía no se conoce completamente.

La fibronectina (FN) es una proteína de la matriz extracelular (MEC) que se ensambla en forma de red tridimensional en un proceso complejo dirigido por las propias células. A la red fibrilar de FN se van ensamblando otras proteínas como colágenos o proteoglicanos permitiendo la maduración de la MEC. Esta red tridimensional no conforma únicamente una estructura de andamiaje, sino que al estarle unidas las células genera señales mecánicas que condicionan el destino y comportamiento celular. Se ha observado que, a consecuencia de una herida cutánea, la FN es ensamblada en fibrillas que estarán presentes en todas las fases de reparación hasta finalizar el cierre del tejido. La FN es extravasada desde los capilares dañados hasta la zona de la herida lo que permite, junto con el fibrinógeno, formar la primera matriz provisional que sirve de sustrato a las células en la formación del tejido granular (TG). Durante las horas siguientes esta matriz provisional es enriquecida y remodelada con células hematopoyéticas y fibroblastos, tanto dérmicos como provenientes de la fascia. Esta nueva MEC da soporte estructural a nuevas células migrantes que llegan a la zona dañada y que, en última instancia, determinan la resolución de la herida como cicatriz fibrótica o, por el contrario, como tejido regenerado. Mientras tanto, en la epidermis, la FN sirve como proteína de adhesión de los queratinocitos para favorecer la reepitelización de la herida.

El principal motivo de unión de las células a la FN es una secuencia arginina-glicina-aspartato (RGD) que se localiza en el décimo módulo de tipo III de la FN (FNIII10) y que une las integrinas α5β1, αIIbβ3 (exclusiva de plaquetas) y las integrinas de clase αv. En el módulo adyacente al del sitio RGD de la FN (FNIII9) se encuentra una secuencia denominada sitio sinérgico que une las subunidades α de las integrinas α5β1 y αIIbβ3 pero no une las integrinas αv. Esta secuencia favorece la formación de uniones FN-α5β1 reforzadas (en inglés, *catch bonds).* La inactivación del sitio sinérgico en ratones genéticamente modificados (knock-In, KI) desveló la importancia

de este motivo cuando las células tienen que soportar fuerzas de tensión muy elevadas. Sin embargo, las integrinas de tipo αv compensan la ausencia del sitio sinérgico cuando estas tensiones no superan cierto umbral.

Durante la cicatrización de heridas cutáneas en adultos, se producen varios procesos que están dirigidos por señales mecánicas y que, por ende, dependen de la fuerza de unión entre las integrinas de las células y la FN. Estos procesos mecano-dependientes incluyen: i) la migración de la población de queratinocitos durante la reepitelización, marcada por la expresión y activación de integrinas α5β1 que permiten la adhesión a un sustrato que contiene FN del que tiran para avanzar de forma colectiva; ii) la formación del tejido granular en la dermis, fomentada por la infiltración de fibroblastos dérmicos con capacidad migrante que, además, secretan y ensamblan nuevas fibras de FN y de fibroblastos de la fascia que mueven su propia MEC hacia la superficie de la herida; iii) la conversión en el tejido de granulación de fibroblastos a miofibroblastos, orquestada por un aumento de TGF-β1 liberado desde la MEC al ambiente; y iv) la liberación de TGF-β1 que está asociada a cambios de tensión de la MEC donde este factor de crecimiento se encuentra almacenado en su forma latente.

En la presente tesis he investigado el papel del sitio sinérgico de la FN durante la cicatrización de heridas cutáneas. Para ello, he utilizado ratones KI que expresan FN con el sitio sinérgico disfuncional (*Fn1*$^{syn/syn}$). Los resultados demuestran que los ratones *Fn1*$^{syn/syn}$ cierran las heridas cutáneas de forma comparable a ratones sin la mutación pero con un retraso en los primeros días de cierre. Esta diferencia se ve reflejada en una disminución de tejido de granulación acompañada de reducción de proteínas de la MEC, como FN y colágeno en las primeras etapas del cierre dérmico. Mediante experimentos de migración de queratinocitos *in vitro* que simulan el cierre epidérmico, junto con experimentos de migración de fibroblastos sobre FN purificada a partir del plasma sanguíneo de los ratones genéticamente modificados, he demostrado el papel del sitio sinérgico de la FN como refuerzo de adhesión cuando las células deben soportar tensiones elevadas en los puntos de adhesión durante procesos de migración y de liberación de factores de crecimiento de la MEC como el TGF-β1.

OBJETIVOS

Publicaciones anteriores de nuestro laboratorio demostraron la relevancia del sitio sinérgico en el refuerzo de la unión entre α5β1/αIIbβ3-FN y los efectos compensatorios de las integrinas de tipo αvβ3 cuando el sitio sinérgico estaba ausente (Benito-Jardón et al., 2017). El principal objetivo de esta tesis fue profundizar en el papel del sitio sinérgico de la FN en procesos

fibróticos, donde las células están sujetas a una tensión elevada. Por ese motivo se decidió estudiar:

La importancia *in vivo* del sitio sinérgico de la FN en la cicatrización de heridas cutáneas, utilizando para ello ratones que expresan FN con esta región inactivada (*Fn1*$^{syn/syn}$) y comparar el proceso con ratones que expresan FN silvestre *Fn1*$^{+/+}$. Para ello, se analizó:

- El cierre macroscópico de heridas en la piel de ratones *Fn1*$^{+/+}$ y *Fn1*$^{syn/syn}$ a tiempos cortos y largos del proceso de cicatrización.
- La formación de nuevo tejido epidérmico utilizando marcadores de activación, proliferación y migración celular en muestras de tejido de ratones *Fn1*$^{+/+}$ y *Fn1*$^{syn/syn}$ recogidos a distintos tiempos del proceso de cierre.
- La formación del tejido de granulación en la dermis, analizando parámetros indicadores de proliferación, migración y conversión de miofibroblastos en muestras de tejido de ratones *Fn1*$^{+/+}$ y *Fn1*$^{syn/syn}$ recogidos a distintos tiempos del proceso de cierre.
- La formación de nuevos vasos sanguíneos en el tejido de granulación en heridas de ratones *Fn1*$^{+/+}$ y *Fn1*$^{syn/syn}$ a tiempos largos del proceso de cicatrización.

La relevancia *in vitro* del sitio sinérgico de la FN en los procesos de cierre de la herida y regeneración cutánea, utilizando para ello distintos tipos celulares involucrados en el proceso *in vivo*, y FN purificada del plasma (pFN) de ratones *Fn1*$^{+/+}$ (pFN^{wt}) y *Fn1*$^{syn/syn}$ (pFN^{syn}) como sustrato de migración. Para ello analizamos:

- La migración individual de queratinocitos sobre plástico o geles de distintas rigideces recubiertos con pFN^{wt} o pFN^{syn}.
- La migración colectiva de queratinocitos, utilizando pFN^{wt} o pFN^{syn} como sustrato para la migración.
- La migración y ensamblado de un sustrato por fibroblastos aislados de ratones *Fn1*$^{+/+}$ y *Fn1*$^{syn/syn}$ tras la rotura de la monocapa celular.
- La conversión de fibroblastos a miofibroblastos utilizando sustratos, recubiertos con pFN^{wt} o pFN^{syn}, de distintas rigideces que simulan el entorno de la herida.
- El estudio mediante ensayos de bio-luminiscencia de la liberación de TGF-β1 en fibroblastos dérmicos derivados de ratones *Fn1*$^{+/+}$ o *Fn1*$^{syn/syn}$.

METODOLOGÍA

1. Animales de experimentación

Los ratones genéticamente modificados que expresan FN con el sitio sinérgico inactivado fueron generados previamente a este trabajo mediante la técnica de diana genética (Benito-Jardón et al., 2017). La función del sitio sinérgico (D**R**VPPS**R**N) fue eliminada por la sustitución de dos argininas de su secuencia por dos alaninas (R1374A and R1379A). Estos ratones *Fn1*$^{syn/syn}$ son viables y fértiles. Los ratones utilizados en este estudio (*Fn1*$^{+/+}$ o *Fn1*$^{syn/syn}$) procedían de cruces entre ratones heterocigotos para la mutación (*Fn1*$^{+/syn}$).

Para los experimentos de heridas cutáneas, se utilizaron hembras de 10 semanas de edad. Dos días antes del procedimiento se afeitó el pelo de los ratones para sincronizar el ciclo. A los ratones se les administró analgesia unas horas antes del procedimiento. A continuación, fueron anestesiados con Isofluorano y se practicaron 4 heridas de 6 mm de diámetro (Biopsi Punch) en la espalda de los mismos. Las heridas se fotografiaron justo después de realizarse (t0) y en los días posteriores para calcular la velocidad de cierre de la herida.

Los animales utilizados en este estudio se mantuvieron en espacios libres de patógenos y se trasladaron a áreas convencionales de trabajo para realizar las heridas y seguir el proceso de cierre de la herida. Todo el trabajo realizado en ratones está de acuerdo con la normativa vigente del Gobierno de la Comunidad Valenciana (número de permiso 2016/VSC/PEA/00070).

2. Líneas celulares

En el presente estudio se emplearon las siguientes líneas celulares de ratón:

La línea de queratinocitos utilizada en los experimentos de migración fue donada por el departamento de Medicina Molecular del Instituto Max Planck de Bioquímica dirigido por el Prof. Reinhar Fässler (Rognoni et al., 2014). Esta línea se mantuvo en medio KGM en placas recubiertas con colágeno I y en bajas concentraciones de calcio (0.45 µM CaCl2) para evitar su diferenciación.

Las líneas de fibroblastos utilizadas para la técnica de migración con rotura de monocapa habían sido derivadas de riñón de ratones *Fn1*$^{+/+}$ y *Fn1*$^{syn/syn}$ e inmortalizadas (Benito-Jardón et al., 2017). Estas células se mantuvieron en medio DMEM con 10% de FCS y 1% (v:v) de penicilina-estreptomicina.

La línea celular permanentemente transfectada con un vector que contiene el gen de la luciferasa controlado por un promotor dependiente de TGF-β1 (MLECs) fue una donación del laboratorio del Dr. Daniel Rifkin y se utilizó para los experimentos de bioluminiscencia. Estas células se mantuvieron en medio DMEM con 10% de FCS y 1% de penicilina-estreptomicina.

Los fibroblastos dérmicos son cultivos primarios derivados de biopsias de piel de la espalda de ratones *Fn1*$^{+/+}$ y *Fn1*$^{syn/syn}$ según el siguiente protocolo: los ratones se sacrificaron previamente y la piel de la espalda afeitada, desinfectada y separada de otros tejidos. La piel se cortó en trozos de aproximadamente 1 cm^2 de tamaño que se depositaron en placas multipocillo de plástico, para dejar adherir durante 5 minutos. Una vez adheridos los trozos, se añadió a la placa la cantidad suficiente de medio DMEM con 10% de FCS y 1% de penicilina-estreptomicina sin llegar a cubrir los trozos para evitar su separación de la placa. El tiempo de migración de los fibroblastos dérmicos de la piel era de entre 3-10 días. Una vez alcanzada una cantidad suficiente de células, se despegaron de la placa con tripsina y se cultivaron en placas más grandes.

3. Procesado de muestras y análisis histológico

A los 4, 7, 9, 15 y 25 días post-lesión (dpl) los ratones se sacrificaron y la piel con la herida aislada y fijada 48 horas en etanol al 70%. Las heridas se diseccionaron por la mitad y se embebieron en parafina después de realizarles un proceso de deshidratación. Para las tinciones histológicas de Hematoxilina-Eosina, tinción de colágeno por la triple tinción de Masson y las immunofluorescencias, la parafina se eliminó de la siguiente forma: las muestras se sometieron a dos pases consecutivos por xileno y se rehidrataron en concentraciones decrecientes de etanol (100 I, 100 II, 90, 80, 70, 50%) con una duración de 5 minutos cada uno. Para finalizar, las muestras se sumergieron en agua destilada y mantuvieron en PBS hasta su tinción.

Para las tinciones histológicas se utilizaron protocolos estándar de Hematoxilina-Eosina y el protocolo del kit de Sigma para la triple tinción de Masson. Para las immnunofluorescencias, las muestras se permeabilizaron durante 20 minutos con Triton-X-100 al 0.1% y las uniones inespecíficas se bloquearon durante 30 minutos usando BSA al 3% en PBS. Las muestras se incubaron con anticuerpo primario disuelto en solución de bloqueo durante la noche a 4°C. Después de eliminar el exceso de anticuerpo primario con lavados consecutivos de PBS las muestras se incubaron con el anticuerpo secundario disuelto en solución de bloqueo durante 1 hora y 30 minutos. El exceso de anticuerpo secundario se eliminó con lavados de PBS antes de

incubar con Hoechst en PBS para teñir el núcleo durante 5 minutos. Las muestras se prepararon para microscopía con Gelvatol como medio de montaje.

4. Purificación de fibronectina a partir de plasma sanguíneo

El plasma se aisló a partir de la sangre de ratones *Fn1*$^{+/+}$ y *Fn1*$^{syn/syn}$, empleando EDTA como anticoagulante. Para la purificación de la proteína se utilizaron columnas de cromatografía de afinidad (gelatina-Sefarosa), que se incubaron durante toda la noche a 4°C con el plasma recogido. La FN unida a la columna se lavó con tampones de tris-base con pH de 7.4 para eliminar proteínas unidas a la misma y a continuación, se recogió la FN utilizando urea 4M. La urea se eliminó de la FN mediante diálisis en TBS. La proteína purificada se analizó por electroforesis en SDS-PAGE y se tiñó con el colorante azul Coomasie para comprobar su pureza. A continuación, se cuantificó por la técnica de western blot, comparando la intensidad de banda con una cantidad conocida de FN comercial.

5. Experimentos con fibroblastos dérmicos

Los fibroblastos dérmicos aislados de ratones *Fn1*$^{+/+}$ y *Fn1*$^{syn/syn}$, se emplearon para los siguientes experimentos:

- Conversión a miofibroblastos sobre geles de distintas rigideces. Los fibroblastos dérmicos aislados se sembraron durante 24 horas en geles de poliacrilamida de distintas rigideces (4, 50 kPa) y sobre cristal previamente recubiertos con proteína purificada de plasma de ratón (pFN^{wt} o pFN^{syn}). Las células se tiñeron por imnunofluorescencia con phalloidin que marca el citoesqueleto de actina y anticuerpos contra la α-actina de musculo liso que tiñen solo miofibroblastos. A continuación, se calculó el porcentaje de conversión a miofibroblastos sobre las distintas rigideces y sobre los dos tipos de FN.
- Liberación de TGF-β1 de matrices de fibroblastos dérmicos. Los fibroblastos dérmicos aislados se sembraron durante 3 días sobre placas multi-pocillo recubiertas previamente con proteína purificada (pFN^{wt} o pFN^{syn}), para dejar que formaran una MEC madura. Los medios de cultivo de las células se recogieron pasados los tres días y se incubaron con las MLECs durante 14 horas. Las células se lisaron y utilizando un kit de bioluminiscencia se midió la cantidad de luciferasa que era proporcional a la cantidad de TFG-β1 liberado de la MEC en los medios acondicionados por los fibroblastos dérmicos.

6. Experimentos de migración

Para los experimentos de migración se utilizaron las líneas celulares de queratinocitos y de fibroblastos inmortalizados aislados de ratones *Fn1*$^{+/+}$ y *Fn1*$^{syn/syn}$.

- Experimentos de migración de célula aislada o migración colectiva. Los queratinocitos se sembraron sobre placas multi-pocillo de plástico previamente recubiertas con proteína purificada (pFN^{wt} o pFN^{syn}), en presencia (migración colectiva) o ausencia (migración célula aislada) de 1.5 mM de $CaCl_2$. Para formar un espacio libre de células hacia el que las células pudieran migrar, se utilizaron dispositivos de inserción propia (Ibidi) generando un espacio entre las dos siembras de células. Al quitar el dispositivo las células podían migrar libremente hacia el centro. La migración se grabó por microscopía de time-lapse, realizando posteriormente el análisis de diversos parámetros de migración.
- Experimentos de migración por la técnica de rotura de monocapa. Para estos experimentos se sembraron los fibroblastos sobre cubres de cristal previamente recubiertos con laminina. Una vez formada una monocapa de células, se generó una brecha mediante la punta de una pipeta que simulaba una herida. Los fibroblastos tenían que secretar y ensamblar una matriz que les sirviera de sustrato para migrar hacia delante. La migración se grabó por microscopía de time-lapse, realizando posteriormente el análisis de diversos parámetros de migración.

RESULTADOS Y DISCUSIÓN

La importancia de estudios sobre los mecanismos implicados en la reparación de heridas cutáneas se ha puesto de manifiesto en las últimas décadas, debido a la cantidad de personas que requieren de cuidados médicos por alteración en los procesos de cicatrización. Las nuevas terapias que se utilizan hoy en día tienen como objetivo potenciar aquellos procesos que conducen a la completa regeneración del tejido, evitando la formación de cicatrices por deposición masiva de colágeno y que derivan ocasionalmente en estructuras queloides con ausencia de función. Las cicatrices son el resultado de la acción de ciertos linajes de fibroblastos cuya secreción de grandes cantidades de MEC y elevadas fuerzas mecánicas facilitan el rápido cierre de la herida. En la actualidad se conocen todavía muy poco los mecanismos que determinan que ciertas señales mecánicas condicionen el cierre de una herida por completa regeneración o, en cambio, deriven en la formación de una cicatriz.

Análisis de la reepitelización de heridas en ratones mutantes para el sitio sinérgico de la FN.

Tras una lesión cutánea, la FN es una de las primeras proteínas de la MEC que se deposita en abundancia en el lugar del daño. Los resultados de este estudio demuestran la presencia de un retraso en el cierre macroscópico en ratones *Fn1*$^{syn/syn}$ durante las primeras etapas, en comparación con ratones *Fn1*$^{+/+}$, y que luego parece compensarse en las etapas finales del cierre. Observamos diferencias en el grosor de la epidermis en heridas de 9 y 15 dpl, siendo de un grosor significativamente menor en las heridas de ratones *Fn1*$^{syn/syn}$. La distribución de los distintos tipos de queratinocitos activados durante una herida cutánea (marcados con K6 y K14), no mostraba diferencias entre ambos genotipos a ninguno de los tiempos evaluados. Sin embargo, la proporción de queratinocitos basales positivos para la integrina α5β1 a 4 dpl estaba significantemente aumentada en heridas *Fn1*$^{syn/syn}$ comparada con muestras de ratones *Fn1*$^{+/+}$ al mismo tiempo de cierre. Para entender mejor el proceso de reepitelización, se estudió la migración de queratinocitos en cultivo sobre sustratos recubiertos con pFN^{syn}. Aunque durante los primeros momentos de la reepitelización los queratinocitos migran como células aisladas, el cierre completo de la herida se produce con la ayuda de las interacciones célula-célula en el tejido epidérmico en forma de migración colectiva. Por esa razón, en el presente estudio se estudiaron las migraciones de queratinocitos, tanto como células aisladas como en forma colectiva, utilizando sustratos de FN con o sin la mutación en el sitio sinérgico. La migración de queratinocitos en forma aislada sobre sustratos pFN^{syn} resultó ser más lenta comparada con la migración sobre sustratos pFN^{wt} y también se producía una disminución en la direccionalidad de las células sobre pFN^{syn}. Sorprendentemente, cuando estos experimentos se realizaron en forma de migración colectiva, dejando previamente a las células formar adhesiones célula-célula observamos el efecto opuesto. Cuando las células migraban sobre pFN^{syn} el cierre se realizaba a una velocidad mayor que en aquellas sobre pFN^{wt}. La migración individual requiere de la polarización de las células en el sentido del avance, involucrando un avance de parte delantera que guía el movimiento y la retracción de la parte trasera de la célula. El movimiento depende de una fuerte fuerza de tracción en la que intervienen las interacciones de las integrinas con el sustrato. Se ha visto que las fuerzas de tracción son más fuertes en la parte perinuclear de la célula comparadas con el frente de las células. La diferencia de esta fuerza se piensa que reside, en parte, por la distribución de los distintos tipos de integrinas. Así, las integrinas α5β1 están presentes en las adhesiones fibrilares que se forman en la segunda mitad de la célula y que retraen la parte trasera, mientras que las integrinas αvβ3 predominan en las adhesiones focales que producen en el frente celular.

Nuestros resultados *in vitro*, sugieren que la pérdida del sitio sinérgico de la FN podrían limitar la formación de fuerzas de retracción trasera en las células que migran de forma aislada, con la consecuente reducción en la direccionalidad y velocidad de migración. La migración colectiva, por el contrario, depende de una estrecha colaboración entre las interacciones célula-célula y célula-MEC. De acuerdo con nuestros resultados, la debilidad de las adhesiones entre la integrina α5β1 y la FN por la pérdida del sitio sinérgico o a causa de tratamientos con inhibidores de la contracción de miosina, como la Blebbistatina, aumentó la velocidad del movimiento colectivo. Estos resultados están en consonancia con estudios en los que se ha demostrado que la falta de impulso por la contracción de la miosina-II es compensada por las interacciones célula-célula durante la migración colectiva (Vedula et al., 2012). Estos resultados sugieren que al disminuir la vida media de las uniones de α5β1-FNsyn aumenta la velocidad de movimiento. Esta contraposición de resultados entre el movimiento individual y el colectivo de los queratinocitos sobre sustratos de FN con ausencia del sitio sinérgico, pondrían dar lugar a un cierre de la epidermis aparentemente normal en heridas cutáneas de ratones *Fn1*$^{syn/syn}$. Posiblemente, la debilidad de las fuerzas de tracción causada por la ausencia de sitio sinérgico, podría enlentecer el cierre de la herida cuando la manta de queratinocitos no está completamente establecida. Este problema, al comienzo de la migración, se vería compensado por el aumento de la velocidad de migración conforme aumentan las uniones célula-célula durante los días siguientes del proceso de reepitelización. Este resultado estaría apoyado además por el aumento que observamos en la proporción de queratinocitos que expresan la integrina α5β1 en los 4 días posteriores a la lesión, aumento que podría compensar las adhesiones debilitadas a la FN carente del sitio sinérgico.

Análisis del cierre dérmico en heridas de ratones mutantes para el sitio sinérgico de la FN.

En el análisis de la dermis a los 4 días dpl, las heridas de ratones *Fn1*$^{syn/syn}$ presentaban una reducción a la mitad del TG, comparado con las heridas en ratones *Fn1*$^{+/+}$. A su vez, este TG contenía menos cantidad de FN, colágeno y miofibroblastos. Estos resultados están en línea con los estudios hechos en ratones con ausencia de la kinasa de las adhesiones focales FAK. Esta proteína es la encargada de transmitir señales de fuerza mecánica del exterior al interior de las células gracias a su interacción con la cara intracelular de las integrinas y al mismo tiempo con el citoesqueleto celular. Durante el cierre de la herida, una importante cantidad de fibroblastos se diferencian en miofibroblastos como consecuencia de un aumento de la tensión en el tejido seguida de un aumento de la cantidad de TFG-β1 liberado al medio por las

células. En nuestro modelo de estudio, observamos que a 4 dpl el número de células positivas para la proteína α-SMA en el TG de ratones *Fn1*$^{syn/syn}$ se reducía en un 30% comparado con el TG de ratones *Fn1*$^{+/+}$. Exploramos las posibles causas que podrían estar detrás de esta reducción y para ello se midió la proliferación celular, apareciendo disminuida para dos marcadores distintos en heridas de ratones *Fn1*$^{syn/syn}$ a tiempos tempranos del cierre. La proliferación podía explicar parcialmente una disminución de la cantidad de miofibroblastos. Otro aspecto que estudiamos fue la capacidad migratoria de fibroblastos en estas condiciones. Para ello, utilizamos fibroblastos que expresaban FN con la mutación en el sitio sinérgico y observamos su comportamiento tras la rotura de la monocapa ("Scratch Assay") comparándola con fibroblastos que expresan FN silvestre y en presencia o ausencia del inhibidor de integrinas αv, Cilengitide. En el presente estudio se observaron diferencias en el avance de los fibroblastos en presencia de Cilengitide en el frente de migración, que se caracteriza por la combinación de interacciones célula-célula y célula-sustrato para el avance de la monocapa. En cambio, cuando se analizaron las células individuales que escapaban a la monocapa, estas diferencias en la velocidad de migración se observaron tanto en presencia como ausencia del inhibidor de integrinas αv. Estos resultados pondrían de manifiesto la importancia del sitio sinérgico en el avance de los fibroblastos durante el cierre dérmico posiblemente debido a menor interacción entre la FN y la integrina α5β1 por la ausencia del sitio sinérgico que se ve parcialmente compensada por la presencia de las integrinas de tipo αv y de las interacciones célula-célula.

La rigidez de la dermis aumenta a lo largo del proceso de cierre de una herida cutánea. Se ha observado que en las primeras fases del proceso la rigidez disminuye a valores de entre 0.01-10 kPa, pero luego aumenta hasta los 18 kPa en las primeras etapas de formación del TG, llegando a valores de unos 50 kPa cuando la FN y el colágeno ocupan gran parte del espacio y se alinean con las propias células de la dermis. La conversión de fibroblastos a miofibroblastos en el TG es el resultado de una retroalimentación positiva en la que el aumento de la tensión extracelular potencia la liberación del factor de crecimiento TFG-β1 de la MEC y, a su vez, señaliza los fibroblastos dérmicos activando la expresión de la proteína α-SMA y favoreciendo su conversión a miofibroblastos. El aumento de la cantidad de miofibroblastos incrementa a su vez las fuerzas de tensión al contraer el tejido, ayudando así al propio cierre de la herida. En nuestros experimentos in vitro observamos que los miofibroblastos adheridos a FN^{syn} respondían peor a la rigidez del sustrato. La conversión a miofibroblastos en sustratos menos rígidos era menor en ausencia del sitio sinérgico, eliminándose esta diferencia cuando las células estaban sembradas sobre cristal. El factor de crecimiento TFG-β1 se almacena unido no

covalentemente a la proteína LAP que, a su vez, está unida a la proteína LTBP-1 que se une a las fibrillas de FN y de fibrilina. Su liberación de la MEC depende de la acción de metaloproteasas o de la contracción de la MEC debida a fuerzas de tensión mecánica ejercida por las células. Nuestros experimentos mostraban que matrices construidas a partir de FN con ausencia del sitio sinérgico eran menos eficientes para liberar el factor de crecimiento al medio extracelular y por tanto pudiendo ser esto una causa de la menor conversión de fibroblastos a miofibroblastos. Esta menor eficacia se podría explicar por la débil interacción entre la FN mutante y la integrina α5β1, que se ha visto que es importante para la transmisión de fuerzas contráctiles desde la célula. Para comprobar si en las heridas cutáneas a 4 dpl había una menor señalización por TFG-β1 que pudiera estar afectando la conversión a miofibroblastos, se analizó uno de los principales intermediarios de la vía de señalización intracelular por TFG-β1, como es el factor nuclear Smad-2 fosforilado. Efectivamente, pudimos comprobar la diminución de la fosforilación de Smad-2 en el TG de heridas cutáneas de ratones *Fn1*$^{syn/syn}$ en comparación con heridas de ratones que expresan FN silvestre. Estos resultados señalan la importancia del sitio sinérgico en la transmisión de fuerza durante la formación del TG durante los primeros días del cierre de heridas cutáneas.

En resumen, nuestros resultados muestran que la pérdida del sitio sinérgico de la FN no impide el cierre de heridas cutáneas debido a dos alteraciones contrapuestas en el proceso de migración de queratinocitos durante la reepitelización. Por otra parte, observamos una reducción del proceso fibrótico en la dermis. En el contexto de una búsqueda terapéutica para reducir los procesos fibróticos, moléculas que consigan bloquear el sitio sinérgico de la FN supondrían un campo de investigación como potencial herramienta antifibrótica.

CONCLUSIONES

En el presente trabajo se estudiaron las posibles funciones del sitio sinérgico de la FN durante la cicatrización de heridas cutáneas en ratones con una mutación disfuncional en el propio motivo del sitio sinérgico (*Fn1*$^{syn/syn}$) y del que se pueden asumir las siguientes conclusiones:

1. Los ratones *Fn1*$^{syn/syn}$ muestran un retraso en el cierre macroscópico de las heridas cutáneas a los 4 días y que parece quedar compensado en las etapas posteriores.
2. Durante el proceso de reepitelización de la epidermis en heridas *Fn1*$^{syn/syn}$ se obseva un incremento de la expresión de la integrina α5β1 en queratinocitos basales comparado con heridas de ratones *Fn1*$^{+/+}$, lo que sugiere un efecto compensatorio a un defecto en la adhesión.

3. Los experimentos de migración *in vitro* utilizando queratinocitos evidencian que la mutación del sitio sinérgico desencadena comportamientos aparentemente contradictorios, durante la migración de célula única y la migración colectiva, lo que podría explicar la aparente normalidad en el cierre epidérmico de las heridas mutantes.
4. Durante la migración de célula única, los queratinocitos migrando sobre sustratos FN^{syn} muestran un cierre tardío de la herida debido a un enlentecimiento de la velocidad de movimiento y disminución de la direccionalidad comparado con sustratos FN^{wt}.
5. Durante la migración colectiva, los sustratos FN^{syn} favorecen un aceleramiento en el cierre de la herida que se ha demostrado que está directamente ligado con una disminución de la fuerza de contracción del citoesqueleto de miosina.
6. En la dermis, el enlentecimiento del cierre macroscópico durante los primeros días se relaciona con la presencia de menos cantidad de tejido fibrótico en las heridas *Fn1*$^{syn/syn}$ con una reducción del contenido en miofibroblastos y una menor deposición de colageno y FN.
7. El fallo en la conversión a miofibroblastos puede derivar de una disminución en la señalización por TGF-β1 en el tejido granular de herida *Fn1*$^{syn/syn}$.
8. Los experimentos *in vitro* utilizando fibroblastos renales derivados de ratones *Fn1*$^{+/+}$ and *Fn1*$^{syn/syn}$ revelan que el sitio sinérgico de la FN es importante para el ensamblado de una red fibrilar normal de FN, y que se requiere para soportar la tensión derivada de la migración celular.
9. Los experimentos *in vitro* utilizando fibroblastos dérmicos derivados de ratones *Fn1*$^{+/+}$ y *Fn1*$^{syn/syn}$ revelan que el sitio sinérgico de la FN es importante para sentir los cambios en la rigidez de la matriz y a consecuencia, para adaptar el comportamiento de las células a la rigidez del sustrato.
10. Los fibroblastos dérmicos *Fn1*$^{syn/syn}$ ensamblan matrices con, posiblemente, una menor capacidad de almacenar el LLC que, unido a una disminución en su facultad de generar tensión hacia la matriz, disminuye la señalización por TGF-β1.